Modelling One-Dimensional Non-Uniform Growth with Applications to Cylindrical Yeast Colonies

Anthony Gallo

April 19, 2020

Thesis submitted for the degree of
Master of Philosophy
in
Applied Mathematics
at The University of Adelaide
Faculty of Engineering, Computer and Mathematical Sciences
School of Mathematical Sciences

THE UNIVERSITY
of ADELAIDE

Contents

Signed Statement

I certify that this work contains no material which has been accepted for the award of any other degree or diploma in my name, in any university or other tertiary institution and, to the best of my knowledge and belief, contains no material previously published or written by another person, except where due reference has been made in the text. In addition, I certify that no part of this work will, in the future, be used in a submission in my name, for any other degree or diploma in any university or other tertiary institution without the prior approval of the University of Adelaide and where applicable, any partner institution responsible for the joint-award of this degree.

I give permission for the digital version of my thesis to be made available on the web, via the University's digital research repository, the Library Search and also through web search engines, unless permission has been granted by the University to restrict access for a period of time.

I acknowledge the support I have received for my research through the provision of an Australian Government Research Training Program Scholarship.

Signed: .. .. Date: 19/04/2020 .....

Acknowledgements

I would like to thank my supervisors, Ben Binder, Ed Green and Hayden Tronnolone for all the support and assistance throughout my journey from a naïve second year undergraduate to a confident HDR student. Thank you for always being approachable and friendly. You were always happy to answer any questions I had and helped me to understand the technical mathematical concepts in my work. I was very lucky to have you three as supervisors. If you are a prospective student that has, for some unknown reason, chosen to read the acknowledgement section of my thesis, I would strongly recommend all three to you.

I'd also like to give a special acknowledgement to fellow students, Matt Hopwood, Alex Tam and Phill Brown. As PhD students with your own work to worry about, you were always happy to answer any technical questions about math bio and I am very thankful. I would also like to give a special thanks to my 'desk buddy' Sarah James for being supportive throughout the long days in the office and for giving me FruChocs on multiple occasions.

I'd also like to thank all my friends and fellow students at the University of Adelaide. I'd like to thank Matt Ryan for all the casual banter, life tips and always having a stupidly large amount of chocolate you were willing to share. I'd like to thank Andrew Tasker for getting through all the difficult coursework with me. I'd like to thank Big Dave, Aline Kunnel, Rose Crocker, Kym Wilkins, James Walker, Haripriya Sridharan and Jack Mac for the many great conversations over tea and mutual appreciation for hummus. I'd also like to thank Tyson Klingner for the many lunches and wrestling banter and I'd like to thank Tetsuya Naito for teaching me to be 'Tranquilo'. Lastly, I'd like to thank Tobin South, Max Wurm, Isabelle Greco and the rest of the AUMS committee over the years for creating a great social environment for the maths students and for implementing the 48 hour rule.

Most importantly, I'd like to thank my girlfriend, Sophie Schiller. Your love and support has helped me get through my M.Phil and given me direction for the future. My achievements are far more meaningful knowing I have you to celebrate them with. I'd also like to thank my family. I am truly appreciative of everything you have done for me.

Abstract

Biologists have shown that yeast can be restricted to grow vertically upwards from an agar plate to form cylindrical colonies. It is known that cell proliferation within the cylindrical yeast colonies is nutrient driven. However, the cell behaviour within the colony is not fully understood. Yeast colonies are not well mixed cultures and the cells throughout the colony will not have equal access to nutrient. This results in non-uniform domain growth within the colonies. Furthermore, the height of the cylindrical yeast colonies was found to grow linearly in time. We present a discrete cellular automaton and a continuous partial differential equation model to predict the cellular behaviour and cell growth within the cylindrical yeast colonies. We provide a general method for determining the average trajectories of initial cells in a non-uniformly growing domain using cellular automata and obtain closed form solutions for some particular cases of interest. Furthermore, we provide a numerical approximation to the pathlines of individual cells using a reaction–diffusion–advection PDE model that couples domain length, nutrient concentration and cell density on a non-uniformly growing domain. We compare our numerical approximation to the experimental results of Vulin et al. (2014) to predict the cell behaviour within the cylindrical yeast colonies. It was found that only a fixed number of cells at the base of the colony can proliferate. The cylindrical yeast colonies grow linearly as a result of this.

Chapter 1

Introduction

Yeasts are unicellular microorganisms and are classified as part of the fungi kingdom (Rosa & Peter 2006). They are a eukaryotic fungus and thus have organelles, such a cell nuclei and mitochondria, within their cells. This is different to prokaryotic microorganisms, such as bacteria, that do not have organelles. There are currently over 1500 recognised species of yeast (Rosa & Peter 2006). The yeast species *Saccharomyces cerevisiae* was the first eukaryotic cell to have its genome fully sequenced (Williams 1996) and is used as a model organism for other eukaryotic cells (Botstein 2011). Thus yeast experiments have applications in cell biology and can be used to investigate the genetic traits of diseases such as cancer. Furthermore, yeast is used for brewing beverages, such as beer (Priest et al. 2006) and Kombucha (Teoh et al. 2004), and used as a leavening agent when baking bread (Moore-Landecker 1996).

Saccharomyces cerevisiae, like many other yeasts, typically reproduce asexually via mitosis in the presence of a nutrient. Yeast cells cannot proliferate if they do not have access to nutrient. As a result, yeast grows by consuming nutrient and the behaviour of cells within yeasts can be modified by adjusting the nutrient supply (Palkova 2004). In experiments, this nutrient typically comes from an agar medium within a Petri dish. Many yeast experiments, and mathematical models describing them, examine growth in the radial direction along the surface of the dish (Pirt 1967, Reynolds & Fink 2001, Reynolds et al. 2008, Chen et al. 2014, Tronnolone et al. 2017, Tam et al. 2018, Tam 2019). Figure 1.1 contains photographs of one of these experiments for *Saccharomyces cerevisiae* that resulted in a floral pattern formation (Tam et al. 2018).

However, the remarkable experiments conducted by Vulin et al. (2014) showed that *Saccharomyces cerevisiae* can be restricted to grow vertically upwards from an agar plate to form a cylindrical colony. A schematic of the cylindrical yeast colony experiment is shown in Figure 1.2. Vulin et al. (2014) designed a culture system to control nutrient delivery.

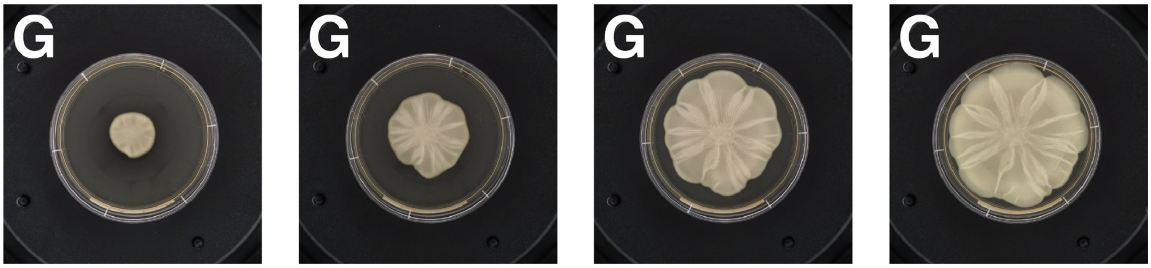

(a) (b) (c) (d)

Figure 1.1: Time lapse images for a *Saccharomyces cerevisiae* mat formation experiment displaying a floral pattern formation. The photographs are taken after approximately (a) 68 hrs, (b) 117 hrs, (c) 164 hrs and (d) 237 hrs of incubation. Images from Tam et al. (2018).

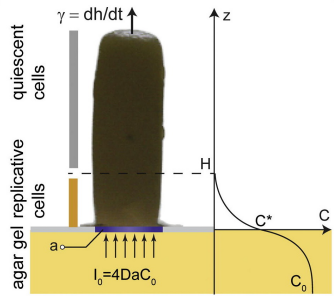

Figure 1.2: Sketch of the cylindrical yeast colonies growing vertically upwards from an agar plate (image from Vulin et al. (2014)). The nutrient concentration (given on the right) will be monotonically decreasing up the colony until it reaches 0 mM. We use the variable H to refer to the height that nutrient can reach. The cells below H are known as replicative cells as they have access to local nutrient and can proliferate and the cells above H are known as quiescent cells as they have do not access to local nutrient and cannot proliferate.

This was designed to allow the experimentalists to grow yeast colonies into desired geometries — including the letters of the alphabet (Vulin et al. 2014). The versatile culture system ensured nutrient was delivered into the agar gel directly beneath the colony. As a result, there was a monotonically decreasing nutrient concentration from the base to the top of the colony with both a replicative and quiescent region within the tower (see Figure 1.2). In the replicative region there is sufficient nutrient for the cells to proliferate. However, in the quiescent region there is insufficient nutrient for the cells to proliferate. This is due to the nutrient being consumed in the lower region of the colony at a greater rate than it can diffuse into the upper region. The distance in which nutrient can reach up the colony depends on the nutrient consumption rate of the yeast, the amount of nutrient delivered and its diffusivity (Nguyen et al. 2004).

Time lapse images of a cylindrical yeast colony grown by Vulin et al. (2014) are shown in

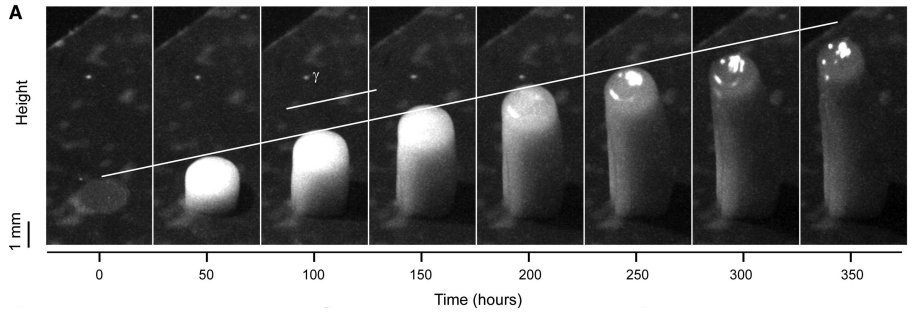

Figure 1.3: Growth of a cylindrical yeast colony over time (image from Vulin et al. (2014)). The radius of this yeast colony is 1.5 mm and the constant flux of nutrient into the agar gel is 111 mM. The height of the colony is growing linearly in time and appears to be growing in the order of 1 mm per 50 hours.

Figure 1.3. The growth is uniaxial and the height of the tower is growing linearly. It was hypothesised by Vulin et al. (2014) that this linear increase in the number of cells is due to the fact that nutrient can only reach a certain distance up the colony. As yeast is a model organism, this observation of uniaxial growth is applicable to other biological systems. It is therefore important to understand the relationship between nutrient concentration and the spatial properties within the colony.

The non-constant nutrient concentration within the colony results in spatially dependent growth (Minarikova et al. 2001, Vachova et al. 2009). As both quantities are difficult to measure during an experiment, little is known of their relationship and how this influences the colony height. We address this by developing mathematical models of cylindrical colony growth that provide new insights into the influence of the nutrient distribution on the cell growth rates and colony morphology. We explore the growth rates by tracking the average trajectories of the initial cells within a colony. We may equivalently refer to the average trajectory of a cell as the pathline of a cell. We consider two different one-dimensional models to predict cell growth rates in the cylindrical yeast colonies.

Generally speaking, the growth of yeast colonies on agar gel is a problem in three spatial dimensions. Yeast colonies may grow into various different shapes and can experience radial growth. However, Vulin et al. (2014) prevented radial growth by controlling the nutrient delivery. We observe in Figure 1.3 that the diameter of the colony is fixed to 1.5 mm throughout the duration of the experiment. As there is no radial growth, the cells will remain in a fixed radial and azimuthal position. Hence, we assume that cells may only travel upwards in one spatial dimension. Furthermore, Figure 1.2 suggests that the nutrient concentration is only changing in one spatial dimension — it is decreasing up the colony. Thus, it is plausible to assume that two cells at the same height will have the same amount of access to nutrient. As cell proliferation, and hence cell displacement, is nutrient driven, we expect two cells at the same height to have the same proliferation

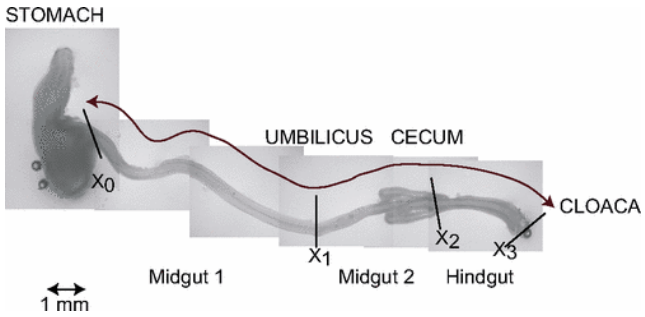

Figure 1.4: Image of an E6 quail embryo. The gut tissue has been split into three sections to illustrate non-uniform growth dynamics. Image from Binder et al. (2008).

rate. Hence, the vertical growth rate of a cell depends only on the vertical position of a cell. As a result, it is a reasonable assumption to model the non-uniform growth in cylindrical yeast colonies in one spatial dimension.

The first of the two models we develop is an agent based cellular automaton (CA). These models have previously been used to model proliferative tissue growth in biology (Binder & Landman 2009*a*,*b*, Hywood et al. 2013, Ross et al. 2016). CA models can also be used to model proliferative tissue growth with cell motility or other intercellular interactions (Codling et al. 2008, Ross & Binder 2014, Yates et al. 2015, Ross et al. 2015). Some previous applications of CA models include tumour growth (Kansal et al. 2000, Monteagudo & Santos 2015), embryonic tissue growth (Binder et al. 2008), bone growth (Czarnecki et al. 2014), fungal colonies (Matsuura 2000) and yeast colonies (Tronnolone et al. 2017).

Binder et al. (2008) developed a CA model for uniaxial growth in the gut tissue of an embryonic quail. They found that unbiased cell proliferation (implying that all cells have equal access to nutrient) results in uniform uniaxial growth. They also showed that the length of the tissue grew exponentially in time. Binder et al. (2008) also considered a uniaxial growth model where the tissue was split up into three sections with three different uniform growth rates (see Figure 1.4). This adds a bias into the CA model and results in non-uniform growth of the tissue.

A major limitation of this piecewise uniform model developed by Binder et al. (2008) is that the non-uniform growth rate cannot be continuous across the domain. Lai De Oliveira & Binder (2019) overcame this limitation by introducing a continuous probability distribution that assigned a bias to cell proliferation. This biased cell proliferation can account for a non-constant nutrient concentration and results in non-uniform growth. Lai De Oliveira & Binder (2019) took a combinatorial approach to numerically compute the average trajectories of the cells. The numerical approximation limits the potential for further analysis and thus we wish to find a closed form solution for the average trajectories of cells, if possible.

The CA models we use allow for some randomness of the spatial positions and times of proliferation events. They are microscopic models that encapsulate the proliferation at an individual cell level. However, the average cell trajectories are a macroscopic property of cylindrical yeast colonies. A challenge in developing our model is deriving a solution for macroscopic behaviour using microscopic properties.

An alternative approach is to use a partial differential equation (PDE) model for macro scale behaviour (Deroulers et al. 2009, Baker et al. 2010, Yates et al. 2012, Davies et al. 2014, Davies 2016). Vulin et al. (2014) used a PDE model to predict the evolution of the nutrient concentration and colony height (resulting curve can be found in Figure 1.2). However, their model does not couple nutrient concentration and colony height. In this work we develop a PDE model that couples nutrient concentration with yeast growth.

One widely used PDE model for analysis of macroscopic properties is the Keller–Segel Model (Keller & Segel 1970, Horstmann 2003). The Keller–Segel model is used for continuous models in chemotaxis (Painter 2009). The model can be derived by taking the continuous limit of the cellular Potts model with chemotactic interactions of the form of a Fokker–Planck PDE (Turner et al. 2004, Alber et al. 2006, Yates 2014). It has also been shown that an advection–diffusion equation for nutrient transport can be derived by taking the continuous limits of a discrete stochastic process (Penington et al. 2011).

Our PDE model is derived by considering the conservation of mass (nutrient concentration and cell production). Specifically, we develop a model using reaction–diffusion theory. Reaction–diffusion theory has been used to model a wide range of biological phenomena (Britton 2003, Murray 2003, K. Maini et al. 1997). It was first proposed by Turing (1952) to model spatial patterns in biological systems. Since then, many mathematicians have used reaction–diffusion theory to develop models for tissue growth (Ward & King 1997, 1999, Byrne & Chaplain 1995, Chaplain 1996, McGillen et al. 2014). The models are particularly interesting to us as they incorporate domain growth into the model. Reaction–diffusion models incorporating domain growth have also been applied to predict skin patterns in certain species of fish (Kondo & Asai n.d., Varea et al. 1997, Painter et al. 1999). We note, however, that domain growth is usually specified (Crampin et al. 1999, Simpson 2015). The common specifications in the literature for domain growth are linear growth (Chaplain et al. 2001) and exponential growth (Mulesa et al. 1996). We also note that models typically make the constitutive assumption that cell density is constant (Ward & King 1997, Neville et al. 2006).

Although the cylindrical yeast colonies have been observed to grow linearly, it is not appropriate to specify linear domain growth. This is because domain growth is dependent on nutrient concentration. Furthermore, the spatial distribution of nutrient will depend on the length of the colony. Thus, we wish to create a model that couples domain growth with nutrient concentration. Neville et al. (2006) have previously created a reaction–

diffusion model that couples domain growth with concentrations of two chemicals to analyse spatial patterns in one dimension. We wish to adapt the techniques used by Neville et al. (2006), Simpson (2015) and Crampin et al. (1999) to derive a reaction–diffusion model that couples domain growth with nutrient concentration. Furthermore, we wish to incorporate cell compressibility into our model.

1.1 A Brief Summary of this Thesis

In Chapter 2, we develop our CA model and algorithm. We carefully define the proliferation mechanism and how this can be used to determine the average trajectories of the initial cells. We also explain the importance of differentiating between quiescent cell (cells that cannot proliferate) and replicative cells (cells that can proliferate).

In Chapter 3, we run simulations of our CA model to obtain results for both biased and unbiased proliferation. We find that, on average, unbiased proliferation leads to uniform growth and biased proliferation leads to non-uniform growth within the colony. We also find that the colony growth is exponential if all cells in the colony are replicative (all cells can proliferate) or if a fraction of the cells are replicative. However, if there is only a fixed number of replicative cells at the base of the colony (and all remaining cells are quiescent) then the colony grows linearly. This is an important result as it helps to explain why the cylindrical yeast colonies are growing linearly. We also show that the continuum approximation is accurate for predicting the discrete cell positions as time evolves.

In Chapter 4, we derive a continuous reaction–diffusion model for non–uniform growth and explore model parameters and their biological applications. The model we develop is an improvement on the model suggested by Vulin et al. (2014) as we have coupled nutrient concentration with domain growth. Furthermore, we allow for cell compressibility in our model. We compute numerical solutions to the system in Chapters 5 and 6.

In Chapter 5, we obtain numerical solutions to a system where cells are incompressible. In our PDE model, we do not specify the length of the colony or nutrient concentration but instead simulate nutrient consumption coupled with colony growth from an initial condition. We use known physical measurements from Vulin et al. (2014) to parameterise the model. Our results predict that there is a fixed number of replicative cells at the base of the colony and thus the colony grows linearly for the known parameters. Hence our model is able to predict the linear growth of the cylindrical yeast colony observed in the experiments of Vulin et al. (2014).

As yeast is a model organism for other eukaryotic cells, our model is applicable to compressible systems in cell biology. Hence, we also obtain numerical solutions to the system when cells are compressible in Chapter 6. We find that increasing cell compressibility increases the cell density at the base of the colony. This is because a majority of cell

proliferation occurs near the base of the colony. Lastly, we suggest some extensions to the model — including alternate pressure laws.

Chapter 2

Development of the CA model and Algorithm

In this chapter, we present a one-dimensional cellular automaton (CA) to model the microscopic stochastic behaviour of individual cells that are proliferating in the colony. The CA model we develop can be also be generalised to model other biological systems that exhibit proliferative cell growth. As the CA is a stochastic model, any single simulation will result in a non-uniform spatial distribution for the initial cells. However, Binder et al. (2008) showed that the ensemble average of many CA simulations can lead to a uniform spatial distribution for the initial cells if proliferation is unbiased. We wish to extend their CA model to include biased cell proliferation based on the nutrient availability in the colony. If cell proliferation is biased, we expect the ensemble average of many CA simulations to result in a non–uniform spatial distribution for initial cells.

2.1 Framework

To model one-dimensional non-uniform growth using CA, we first define a one–dimensional array of discrete cells as illustrated in Figure 2.1. Each of the discrete cells in the array represent one biological cell. We assume that all the cells are the same size and are evenly spread across the array. This is equivalent to assuming the cells are incompressible. Each of the cells in the array may proliferate to give birth to daughter cells. We use the term daughter cell to refer to the new cell and parent cell to refer to the original cell. Furthermore, we assume that there will be no cell motility and no cell death. These are reasonable assumptions as yeast cells are sessile and cell death is negligible for the time-scale of the experiments (Tam et al. 2018). Hence, the number of cells in the array, and length, will be increasing with time. We will use CA models to predict uniform and non-uniform growth in one-dimensional biological systems and focus on the cylindrical

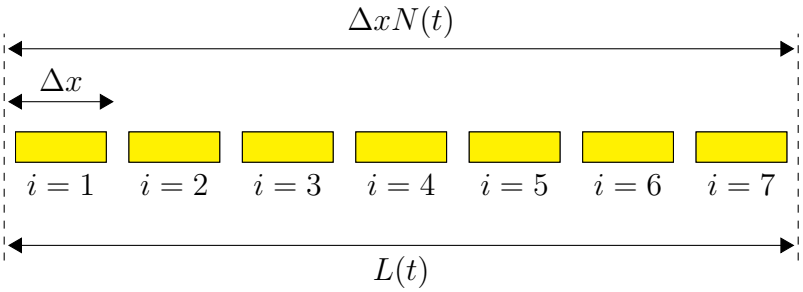

Figure 2.1: Our one-dimensional CA model is built from a simple array of cells. We note that the array has been drawn such that are spaces between adjacent cells. This is purely for illustrative purpose and emphasise that there are no empty spaces between adjacent cells. Each of the cells within the colony is labelled by a dimensionless variable $i = 1, 2, \ldots, N(t)$, where $N(t)$ is the total number of cells at time t. Each of the N cells in the colony will have width Δx units. Hence if we define a physical length $L(t)$, we observe that $L(t) = \Delta x N(t)$.

yeast colonies experimentally grown by Vulin et al. (2014).

We first introduce the nomenclature of our model. We denote the width of a cell as Δx. At time t, each cell in the colony is labelled with the index i such that the physical position of the cell is given by $x = i\Delta x$. The leftmost cell is indexed as $i = 1$ and the second cell from the left is indexed $i = 2$ until the rightmost cell. The physical position x can be interpreted as the distance from the base of the colony. The length of the colony at time t will be given by $L(t) = \Delta x N(t)$ where $N(t)$ is the total number of cells in the colony at time t. In setting this length, we have assumed that there are no gaps between adjacent cells in the colony. A simple CA is illustrated in Figure 2.1. We impose that the initial number of cells in the colony is $N(0) = N_0$ and initial length of the colony is $L(0) = L_0$.

We choose to split up time into discrete time steps of size Δt. We also define τ as the number of time steps since the start of the simulation. Hence our temporal variable can be written as $t = \tau\Delta t$. The temporal variable t will be continuous in the limit $\Delta t \to 0$. In each time step of length Δt, each of the cells will have the opportunity to proliferate. We introduce a proliferation probability p^i defined as the probability that the cell located at position i proliferates in a given time step. It is important to note that this probability p^i will depend on the size of the time step. We also define a proliferation rate $\hat{p}^i$ as the rate in which a cell located at position i proliferates. As the proliferation rate is a physical quantity, $\hat{p}^i$ will not change as the size of the time step Δt varies. The relationship between the proliferation probability and proliferation rate is given by $p^i = \hat{p}^i \Delta t$.

We now define the cell proliferation rule for our model. As aforementioned, each of the cells may proliferate to produce a daughter cell in one time step of length Δt. If a cell in position i proliferates, the parent cell is displaced to the right, to position $i + 1$,

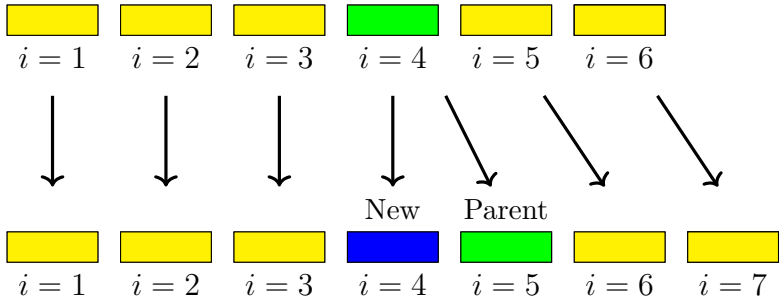

Figure 2.2: This is an illustrative example of the 'proliferation to the left' mechanism within the CA model. We again note that the empty spaces between adjacent cells are purely for illustrative purposes. In this case, the parent cell located at position $i = 4$ (green cell) is proliferating so moves to $i = 5$ and the daughter cell (blue cell) has been birthed to position $i = 4$. We note that the cells originally to the left of the proliferating cell (the three cells located at $i = 1, 2, 3$) have stayed in their original position. Furthermore, the cells originally to the right of the green proliferating cell have gone from locations $i = 5$ and $i = 6$, respectively, to $i = 6$ and $i = 7$. Hence we can see that a cell will be displaced one position to the right if a proliferation event occurs to the left of it.

and a daughter cell is inserted in the parent cell's original position i. We refer to this proliferation mechanism as cells 'proliferating to the left' as is depicted in Figure 2.2. The cells to the left of the proliferating cell remain in the same position while the cells right of the proliferating cell are displaced one position to the right. This displacement occurs because of the insertion of the daughter cell.

We also introduce the notation N_τ to refer to the number of cells after τ time steps. We define this mathematically by $N_\tau = N(\tau\Delta t)$. Furthermore, we note the physical length after τ time steps will be $L_\tau = L(\tau\Delta t)$. As before, we have the relationship $L_\tau = \Delta x N_\tau$.

It is important to note that in one time step, we can have multiple proliferation events. Although unlikely, it is possible that every cell in the colony proliferates in one time step. Similarly, it is also possible that no cell in the colony proliferates in one time step. Suppose the number of cells in the colony at some point in time is N_τ. Hence, after one time step of length Δt, the total number of cells in the colony will satisfy $N_\tau \leq N_{\tau+1} \leq 2N_\tau$. This is because each of the N_τ cells may proliferate and add one more cell to the colony.

We now consider the displacement of a cell when multiple proliferation events have occurred in one time step. This situation is illustrated in Figure 2.3. We impose that each of the proliferation events occur due to the previously defined 'proliferation to the left' mechanism (see Figure 2.2). We recall that when a proliferation event occurs, the proliferating parent cell will be displaced one position to the right. We also recall that all cells to the right of that proliferating parent cell will be displaced one position to the right.

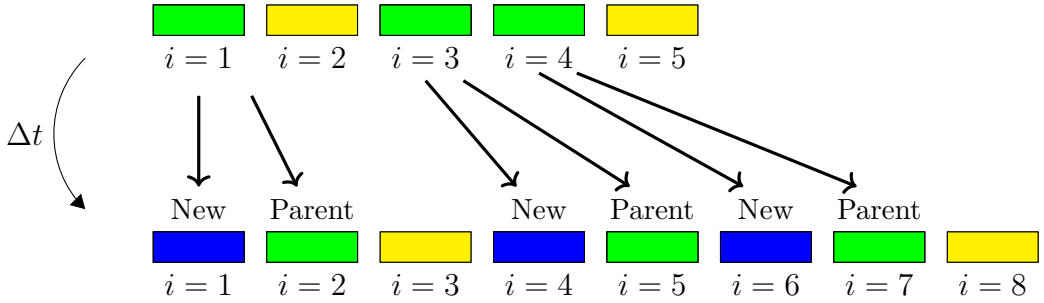

Figure 2.3: One time step of the CA model where multiple proliferation events have occurred. During the second time step three proliferation events have occurred at positions $i = 1, 3, 4$. One proliferation event has occurred to the left of the cell at $i = 2$ so it is displaced one position to the right to $i = 3$ and three proliferation events have occurred to the left of the cell at $i = 5$ so it is displaced three positions to the right to $i = 8$. Two proliferation events have occurring to the left of the parent cell at $i = 4$. Thus the daughter cell is birthed at position $i = 6$ and the parent cell is displaced three positions to the right to position $i = 7$.

Thus we conclude that a specific cell will be displaced one position to the right if one proliferation event has occurred to the left of that specific cell. We can extend this idea to say that a cell will be displaced n positions to the right if n proliferation events have occurred to the left of it. Furthermore, if a cell is chosen to the proliferate, its daughter cell will be birthed n positions to the right and the parent cell will be displaced $n + 1$ positions to the right if n proliferation events have occurred to the left fo the parent cell. An example of multiple proliferations in one time step is illustrated in Figure 2.3. As we have defined all the key parameters and mechanisms for the CA model, we can now specify the algorithm for simulating growth with cellular automata. This is outlined in Algorithm 1.

We choose to label the proliferation probabilities and proliferation rates at the time step τ with p_τ^i and $\hat{p}_\tau^i$, respectively. We know that the proliferation probabilities will depend on the size of the time step and proliferation rate such that $p_\tau^i = \Delta t \hat{p}_\tau^i$. We specify the size of the time step Δt in Algorithm 1 as a sufficiently small value in the order of around 10^{-2}. We also specify the value $\mathcal{T}$ as the total number of time steps. Lastly, we must specify the proliferation rate. This is a physical parameter that will depend on the biology of the system.

One of the main biological factors used to determine the proliferation rate is the nutrient concentration within the colony. Suppose we define the nutrient concentration within the colony $C(x, t)$ as a function of space and time. In our CA model, the concentration will have support on the spatial domain $x = \Delta x, 2\Delta x, \ldots, L_\tau$ and the temporal domain $t = \Delta t, 2\Delta t, \ldots, \mathcal{T}\Delta t$. Recall that $L_\tau = \Delta x N_\tau$ and $\mathcal{T}$ is the total number of time steps. Thus we can define the nutrient concentration of the i-th cell after τ time steps by

Algorithm 1: Simulating One–Dimensional Growth with Cellular Automata

```
1  Set initial number of cells to N_0;
2  Initialise a fixed number of time steps as T;
3  for τ = 1 to T do
4  |  Set proliferation probabilities for each cell in colony;
   |  // used to determine whether a cell proliferates
5  |  for i = 1 to N_{τ-1} do
6  |  |  Determine whether cell i is proliferating;
7  |  |  Set n_i as the number of cells proliferating to the left of i;
   |  |  // used to determine cell displacement
8  |  |  if Cell i proliferates then
9  |  |  |  Cell i will be displaced to position i + n_i + 1;
10 |  |  |  New cell inserted at position i + n_i;
11 |  |  else
12 |  |  |  Cell i will be displaced to position i + n_i
13 |  |  end
14 |  end
15 |  Determine total number of cell proliferations in the timestep;
   |  // used to determine total number of cells in the colony after time
   |     step
16 |  Set N_τ as the new total number of cells in the colony
17 end
```

$C_\tau^i = C(j\Delta x, \tau\Delta t)$.

We expect a cell to have a higher proliferation rate if it has access to more nutrient. Thus a higher nutrient concentration at a cell leads to a higher proliferation rate and hence higher proliferation probability. Hence we assume $\hat{p}_\tau^i = kC_\tau^i$ where k is a constant. It is important that k is selected appropriately such that the resulting probabilities $p_\tau^i = \Delta t k C_\tau^i$ are between zero and one.

2.2 Trajectories of Initial Cells

We can use the CA algorithm to track the trajectories of cells within the colony. The cell trajectories can be defined as the path of an individual cell as the colony grows. We may also refer to the cell trajectories as the pathlines of the cells. These trajectories depend on the number of cell proliferation events and their positions. Thus they depend on the proliferation probabilities and are stochastic. Hence we expect the trajectories to be different each simulation and are thus interested in the average trajectories. Furthermore, we are particularly interested in the average trajectories of the N_0 initial cells. The average trajectories of the initial cells allow us to analyse the spatial distribution of the cells, infer where in the colony the proliferation events are occurring and how this evolves over time. From these average trajectories, we can determine whether uniform or non–uniform growth has occurred.

As aforementioned, the average trajectories of the initial cells depend on the proliferation probabilities. We also recall that the proliferation probabilities depend on the nutrient concentration in the colony. Thus the average trajectories will depend on the nutrient concentration. Hence we expect to see different trajectories for different nutrient concentrations. In particular, a constant nutrient concentration will lead to uniform growth on average (Binder et al. 2008). We confirm this result in Chapter 3 and show that a non–constant nutrient concentration leads to non–uniform growth on average.

As we are interested in the initial cells, we track N_0 cells in each simulation. Suppose we label the trajectory $\tilde{X}_\tau^j$ where τ is the number of time steps and j is the initial position of the tracked cell. Thus at $t = 0$, we have $\tilde{X}_0^j = j\Delta x$ for $j = 1, 2, \ldots, N_0$. We note that $\tilde{X}_\tau^j$ is the dimensional position in terms of physical length. We also observe that the trajectory $\tilde{X}_\tau^j = \tilde{L}_\tau$ due to the proliferation rule, where $\tilde{L}_\tau$ is the length of one simulation. An example of tracking cells and cell trajectories is illustrated in Figure 2.4.

A naïve method of calculating the average behaviour would be to run multiple simulations of Algorithm 1 and calculate an ensemble average for the trajectory. Using this method, we expect the average value to be more accurate as the we increase the number of simulations. However, this will be computationally expensive. Thus we explore another method for obtaining the average trajectories of the initial cells.

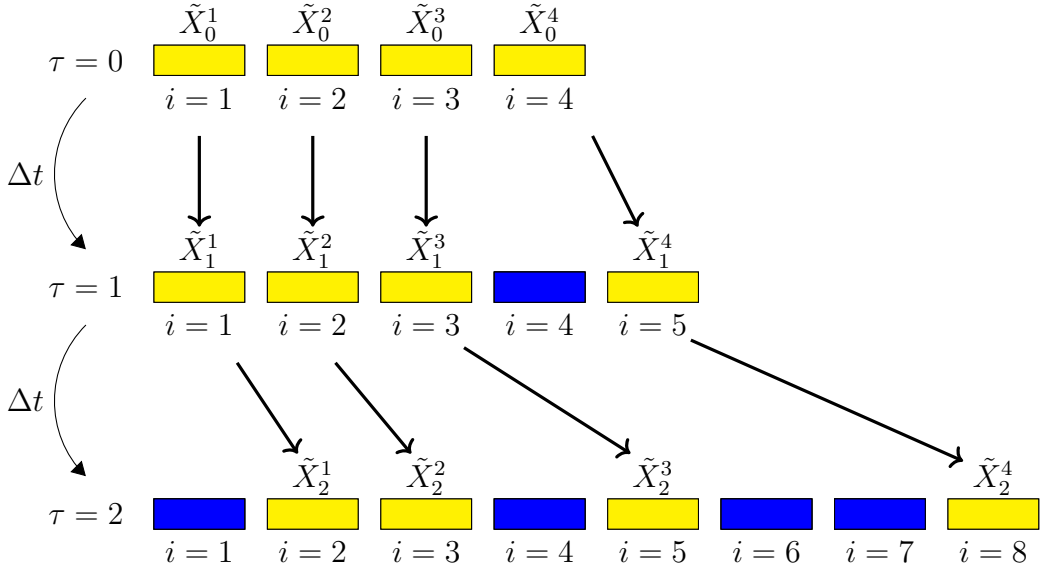

Figure 2.4: Tracking $N_0 = 4$ initial cells after two time steps. The four trajectories are labelled $\tilde{X}_\tau^1$, $\tilde{X}_\tau^2$, $\tilde{X}_\tau^3$ and $\tilde{X}_\tau^4$. We observe that the cell trajectories will not crossover and that $\tilde{X}_\tau^4 = \tilde{L}_\tau$.

We wish to derive an expression for the evolution of the average trajectories over time. Recall our proliferation rule and our illustrations of the CA model in Figures 2.2, 2.3, 2.4. Any given cell can either stay in the same position or move to the right. Thus the average trajectories for each of the initial cells will be increasing functions. Furthermore, we recall that the cell displacement depends on the number of cell proliferations to the left of it. Specifically, the cell displacement will be $n\Delta x$, where n is the number of cell proliferations to the left of, and including, the specific cell. Thus we need to determine the value of n for each of the initial cells at each time step. Recall that $\tilde{X}_\tau^j$ is the trajectory of the cell initially in position j. Suppose we define n_τ^j as the number of cells proliferating to the left of, and including, $\tilde{X}_\tau^j$ during time step τ. Hence we can derive the difference equation for one simulation to be

$$\underbrace{\tilde{X}_{\tau+1}^j}_{\substack{\text{Location of cell at}\\ \text{next time step}}} = \underbrace{\tilde{X}_\tau^j}_{\substack{\text{Location of cell at}\\ \text{current time Sstep}}} + \underbrace{n_\tau^j \Delta x.}_{\substack{\text{Displacement during}\\ \text{time step } \tau}} \tag{2.1}$$

However, we note we that we are interested in finding average trajectories of the initial cells. We recall the CA model is a stochastic model and the cell proliferations depend on probabilities. Thus n_τ^j is a random variable. Hence we can derive the average trajectories by using the expected value of n_τ^j. We label the expected value $\mathbb{E}[n_\tau^j]$. Thus the difference equation for the average trajectories of the initial cells will be

$$X_{\tau+1}^j = X_\tau^j + \Delta x \mathbb{E}\left[n_\tau^j\right], \tag{2.2}$$

where $X_\tau^j = \mathbb{E}\left[\tilde{X}_\tau^j\right]$ is defined as the average trajectory of the cell initially in position j after τ time steps. We note that $\tilde{X}_\tau^j$ can only be a multiple of Δx but the average trajectory X_τ^j can be any real positive number. Intuitively, $\mathbb{E}\left[n_\tau^j\right]$ will depend on the proliferation probabilities p_τ^i. We recall that for the proliferation probabilities p_τ^i, the i refers to the dimensionless index of the cell. Suppose we refer to a cell proliferating as a success and a cell not proliferating as a failure. Furthermore, we assign the value 1 to a success and 0 to a failure. We assign these values as we are counting the number of cell proliferations and thus one cell proliferation event is equal to 1. Hence we can view a cell proliferation as a Boolean outcome with success probability p_τ^i. This is known as a Bernoulli trial and has expected value that is equal to the probability of success. Hence the expected value of cell proliferation for a cell with proliferation probability p_τ^i is simply p_τ^i. We also note that each of the cells proliferate independently of each other. Thus we can view the n_τ^j as a sum of independent Bernoulli trials. Hence the expected value for n_τ^j will be the cumulative sum of the proliferation probabilities up to, and including, the cell X_τ^j,

$$\mathbb{E}\left[n_\tau^j\right] = \sum_{i=1}^{X_\tau^j/\Delta x} p_\tau^i. \tag{2.3}$$

It is important to note that the i in the expression for the proliferation probabilities refers to the dimensionless index of the cell. As X_τ^j is the dimensional position of the cell, we need to convert it to a nondimensional value. This is why we divide X_τ^j by Δx in Equation (2.3). Hence, we can simplify the difference equation for the average trajectories of the initial cells to be

$$X_{\tau+1}^j = X_\tau^j + \Delta x \sum_{i=1}^{X_\tau^j/\Delta x} p_\tau^i. \tag{2.4}$$

2.3 Quiescent and Replicative Cells

We now introduce the concept of quiescent and replicative cells. A quiescent cell is defined as one that cannot proliferate and a replicative cell is one that can. As proliferation is nutrient driven, a quiescent cell can also be defined as one that does not have access to nutrient. We can define a cell as quiescent in our model by setting its proliferation probability $p_\tau^i = 0$. We recall that the proliferation probability is related to the nutrient

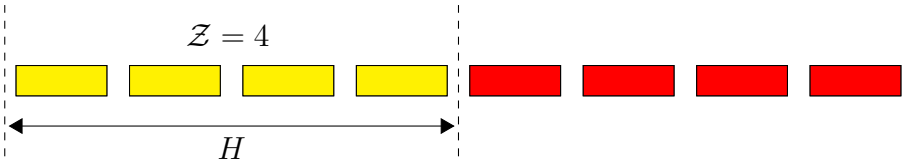

Figure 2.5: An example of a CA with $N = 8$ cells with quiescent and replicative cells. The yellow cells are replicative and the red cells are quiescent. The quiescent region is always assumed to be at the top of the colony. We note that the number of cells in the replicative region is $\mathcal{Z} = 4$. Hence the the length of the replicative region is $H = 4\Delta x$.

concentration such that $p_\tau^i = k\Delta t C_\tau^i$, where Δt is the size of the time step and k is a proportionality constant. As both Δt and k are nonzero, $p_\tau^i = 0$ implies that $C_\tau^i = 0$. This confirms that quiescent cells will not have any access to nutrient. It is not physically meaningful to have quiescent cells arbitrarily scattered throughout the colony. Hence quiescent cells will usually appear in regions. We refer to these regions of quiescent cells as quiescent regions. Similarly, replicative cells will appear in regions and we refer to these as replicative regions.

In the cylindrical yeast colonies experimentally grown by Vulin et al. (2014), the nutrient was injected into the colony from the base (the left). It is also suggested that this nutrient does not diffuse the whole way through the colony (see Figure 1.2). Thus we assume that there is a quiescent region at the top of the colony. This also implies that there is a replicative region at the base of the colony. An example of this is depicted in Figure 2.5. Recall that we may refer to colony size as the dimensionless number of cells or the dimensional length. When defining the size of the replicative region, we use the dimensionless variable $\mathcal{Z}$ to represent the number of cells in the region. Equivalently, we use the dimensional variable H to represent the physical length of the replicative region. As before, we have $H = \mathcal{Z}\Delta x$, where Δx is the width of a cell.

We now consider changes to the size of the replicative region over time. In the model, there is no restriction on how the size of the replicative region changes. Suppose we define $\mathcal{Z}_\tau$ as the number of cells in the replicative region at time step τ. Similarly, we may also define $H_\tau = \mathcal{Z}_\tau \Delta x$ as the length of replicative region at time step τ. Intuitively, we require $\mathcal{Z}_\tau \leq N_\tau$ (and equivalently $H_\tau \leq L_\tau$) for all time steps τ. Other than this inequality, we may arbitrarily define $\mathcal{Z}_\tau$. However, we choose to focus on two separate specifications for $\mathcal{Z}_\tau$.

The first specification is to say that the number of cells in the replicative region is constant at all times. Thus we set $\mathcal{Z}_\tau = \mathcal{Z}$, for all time steps τ. This would correspond to a physical system in which the nutrient can only diffuse a specific length up the colony. An example of the evolution a colony with a fixed number of replicative cells is illustrated in Figure 2.6

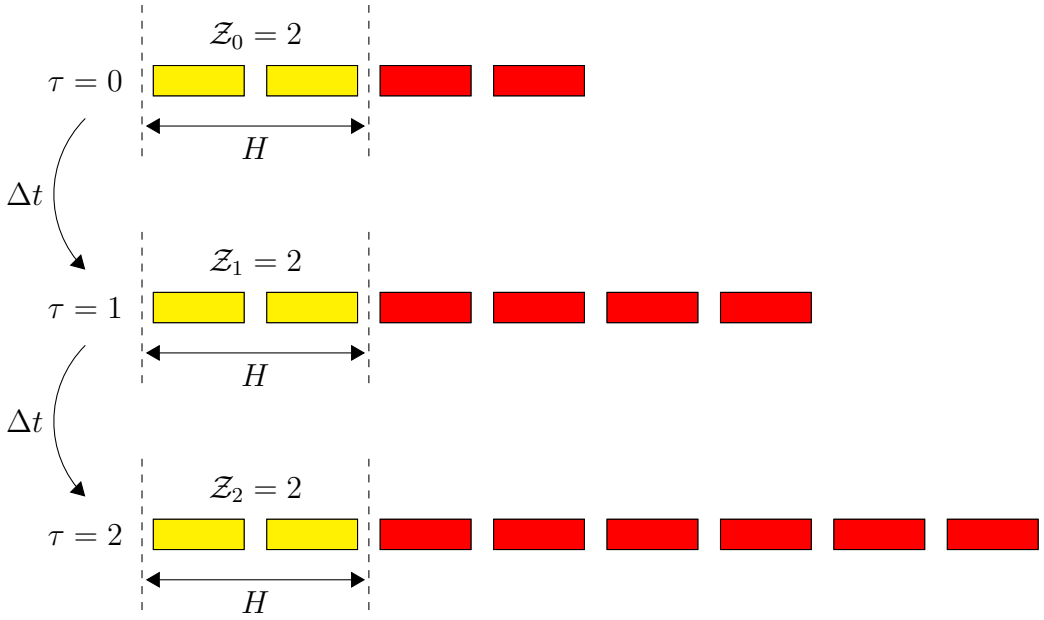

Figure 2.6: An example of the evolution of a CA model with quiescent cells. Similarly to Figure 2.5, the yellow cells are replicative and the red cells are quiescent. We observe that $\mathcal{Z}_\tau = 2$ for all time steps τ. Hence this is an example of a system with a fixed number of replicative cells.

The second specification is to say that the number of cell in the replicative region is some scale of the length of the colony. We set $\mathcal{Z}_\tau = hN_\tau$, where h is a scale between zero and one. We can also interpret h as the proportion of replicative cells in the colony. If $h = 0$, then there will be no replicative cells and thus no growth. If $h = 1$, then there will be no quiescent cells. Depending upon the choice of the scale h, we may find that $\mathcal{Z}_\tau$ has a non integer value. If this is the case we simply round to the nearest integer. Thus we set $\mathcal{Z}_\tau = \text{round}\,(hN_\tau)$. An example of the evolution a colony with a scaled number of replicative cells is illustrated in Figure 2.7. In Chapter 3, we explore simulations of the CA model for both of the two specifications for $\mathcal{Z}_\tau$ and well as CA models without any quiescent cells.

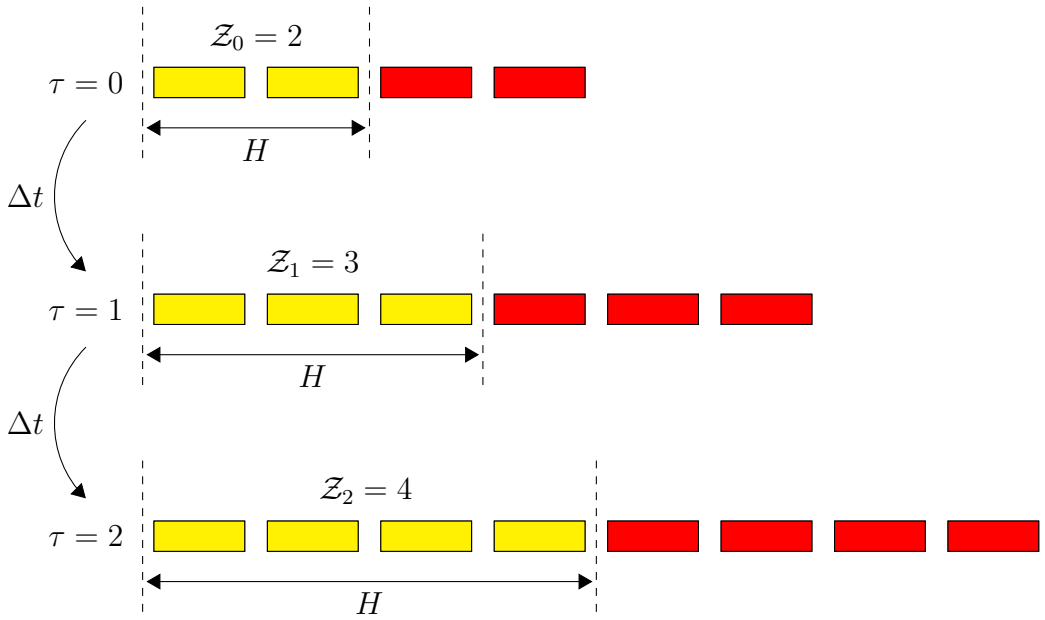

Figure 2.7: An example of the evolution of a CA model with quiescent cells with $h = 0.5$ so that $\mathcal{Z}_\tau = 0.5N_\tau$. Thus 50% of the cells in the colony are replicative cells. Similarly to Figure 2.5 and 2.6, the yellow cells are replicative and the red cells are quiescent.

Chapter 3

Results for the CA Model

In this chapter, we run simulations of our CA model for cases of constant and non–constant nutrient concentration. A constant nutrient implies that all the cells in the colony have equal access to nutrient. This results in unbiased (or spatially invariant) cell proliferation and, on average, uniform growth across the colony. Conversely, a non–constant nutrient concentration implies that cells do not have equal access to nutrient and thus cell proliferation is biased (or spatially varying). Due to the uneven nutrient distribution within the cylindrical yeast colonies (see Figure 1.2), cell proliferation will be biased and thus we expect them to exhibit non–uniform growth.

The main input into the CA model is the cell proliferation probabilities. There are an endless number of distributions we can have for the proliferation probabilities. As discussed in Chapter 2, these proliferation probability distributions are derived from the nutrient concentration. Some potential probability distributions include a unifrom distribution or an exponential distribution. Thesewould correspong to a constant nutrient concentration or an exponentially decreasing nutrient concentration, respectively. Although we may choose more complicated probability distributions to represent the nutrient concentrations, it is best to use simpler distributions to approximate concentration.

In this chapter, we explore results for a constant nutrient concentration across the colony (corresponding to a well mixed culture) and a linearly decreasing nutrient concentration (an approximation for the cylindrical yeast colonies). For both of these nutrient concentration specifications, we explore results for colonies with unlimited and limited nutrient supplies and colonies with and without quiescent cells. The models we consider are summarised in Table 3.1

	Constant Nutrient Concentration	Linearly Decreasing Nutrient Concentration
No Quiescent Cells	**CNCA**	**LNCA**
Fixed Number of Replicative Cells	**CNCA-Q1**	**LNCA-Q1**
Increasing Number of Replicative Cells	**CNCA-Q2**	**LNCA-Q2**
Limited Nutrient Supply	**DCNCA**	**DLNCA**

Table 3.1: List of CA models

3.1 Uniform Growth

3.1.1 Constant Nutrient Cellular Automaton (CNCA) Model

We first consider a CA with constant nutrient across the entire colony. This problem was previously considered by Binder et al. (2008) and enables us to validate the results of our model. This nutrient concentration corresponds to a physical system where the nutrient has diffused evenly throughout the colony. Furthermore, as the colony grows, suppose the nutrient concentration remains at the same constant value across the colony. Thus as t gets large and the colony grows, the nutrient concentration will remain at a constant value $C_\tau^j = C$. This corresponds to a physical system with a constant flux of nutrient and an unlimited supply of nutrient. We assume the nutrient quickly diffuses throughout the colony. We will refer to this model as the Constant Nutrient Cellular Automaton (CNCA) model.

As there is a constant nutrient concentration in the CNCA model we may assume that the proliferation rate is also constant such that $\hat{p}_\tau^i = \hat{p}$. Thus, as the size of the time step Δt is fixed, the proliferation probabilities will also be constant such that $p_\tau^i = p$.

Using Algorithm 1 (as defined in Chapter 2), we run 1000 simulations of the CNCA model. We use a CA with $N_0 = 100$ initial cells and a uniform proliferation probability, $p = 0.05$. The average positions of the initial cells are plotted in Figure 3.1. We observe that the distance between adjacent initial cells is approximately equal on average for any fixed time. We also note that this distance between adjacent cells is growing as we increase the number of time steps. This is evidence that cell proliferation events are occurring evenly across the domain. We may use this uniformly increasing distance between adjacent cells as a way of classifying uniform growth. We now wish to solve the difference equation (2.4) and compare its result to the simulations.

For the CNCA model, we recall that $p_\tau^i = p$ for all values of i and τ. Thus (2.4) becomes

$$X_{\tau+1}^{j} = X_{\tau}^{j} + \Delta x \sum_{i=1}^{X_{\tau}^{j}/\Delta x} p. \tag{3.1}$$

Simplifying, we find that

$$X_{\tau+1}^{j} = X_{\tau}^{j} + pX_{\tau}^{j} = (1+p)\, X_{\tau}^{j}. \tag{3.2}$$

Hence, we may solve Equation (3.2) to find that

$$X_{\tau}^{j} = X_{0}^{j}\,(1+p)^{\tau}\,. \tag{3.3}$$

We also note that

$$L_{\tau} = L_{0}\,(1+p)^{\tau}\,, \tag{3.4}$$

as $X_{\tau}^{N_0} = L_{\tau}$. The average positions derived from the difference equation, as defined in Equation (3.3), coincide with the average positions calculated from the 1000 simulations of Algorithm 1. Thus validating the accuracy of the difference equation method for determining the average cell positions. Notably, it takes much less computation time than running 1000 simulations.

We note that the solution to the difference equation is discrete in time. Furthermore, it is in terms of the uniform proliferation probability, p. Suppose we now wish to express this in terms of continuous time and uniform proliferation rate, $\hat{p}$. We recall that our continuous time will be given by $t = \Delta t\tau$ and that $p = \hat{p}\Delta t$. We can obtain a continuum path for the average cell position by taking the limit as the time step $\Delta t \to 0$. Hence, the continuum path will be given by $X^{j}(t) = \lim_{\Delta t\to 0} X_{\tau}^{j}$. We find that

$$X^{j}(t) = \lim_{\Delta t\to 0} X_{0}^{j}\,(1+\hat{p}\Delta t)^{t/\Delta t}\,. \tag{3.5}$$

Noting the identity

$$\exp(x) = \lim_{h\to 0}(1+xh)^{1/h}\,, \tag{3.6}$$

we get the solution

$$X^{j}(t) = X_{0}^{j} e^{\hat{p}t}. \tag{3.7}$$

We observe that the average length of the colony can be approximated by

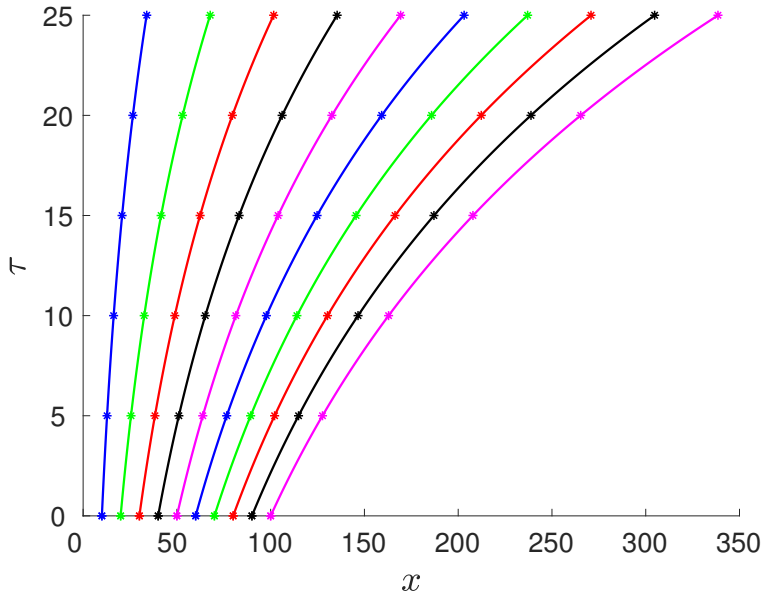

Figure 3.1: Average positions of tracked initial cells for the CNCA model from 1000 simulations and $\mathcal{T} = 25$ time steps with cell proliferation probability $p = 0.05$. The initial number of cells in the model is $N_0 = 1000$ and the cell width is $\Delta x = 0.1$. We have chosen to plot the the positions of 10 initials cells (asterisks) at $j = 100, 200, \ldots, 1000$ with the corresponding continuum paths $X^j(t)$ as defined in Equation (3.7).

$$L(t) = L_0 e^{\hat{p}t}. \tag{3.8}$$

We refer to $X^j(t)$, given in Equation (3.7), as the continuum paths for the average position of the initial cells. As shown by Binder et al. (2008), the continuum paths are exponential. Furthermore, we note that the exponential growth rate is the uniform proliferation rate of the cells. This makes intuitive sense as the total number of cells in the colony is increasing at every time step and thus the number of cells that can proliferate is also increasing. This exponential growth with cell proliferation rate as a growth rate can be used to describe the continuum paths for a well mixed yeast culture.

From Figure 3.1, we can see that the there is a strong agreement between the average discrete positions simulated using Algorithm 1 and the continuum approximations for the average cell behaviour (Equation (3.7)). The discrete difference equation (Equation (3.3)) also gives similar results for the average cell locations. This is very useful as we have derived an accurate closed form solution for the evolution of the cell positions in time.

It is important to note that the dependent variable $X^j(t)$ is a continuous variable so the continuum paths are defined over a continuous spatial domain. Hence there is no longer a discrete array of cells and the cell length Δx is now zero. Hence, the continuum paths will give the best agreement with their discrete equivalent when the change in length for each proliferation event (Δx) is small compared to X^j_τ. This is equivalent to the limit $X/\Delta x \to \infty$ and will occur when there is a large number of cells in the colony. We note that taking the limit $\Delta x \to 0$ implies that $X/\Delta x \to \infty$.

3.1.2 CNCA models with quiescent cells (CNCA-Q Models)

We now consider the CNCA model with the addition of quiescent cells. We refer to this model as the CNCA-Q model. Recall that quiescent cells do not proliferate as they have no access to nutrient. We first explore the case where there are a fixed number of replicative cells so that $\mathcal{Z}_\tau = \mathcal{Z}$. We refer to the this as the CNCA-Q1 model. As aforementioned, the fixed number of replicative cells corresponds to a physical system where nutrient can only reach a certain point in the colony at all times. Hence, we have the nutrient concentration $C^j_\tau = 0$ and proliferation probability $p^j_\tau = 0$ for all values of $j > \mathcal{Z}$. As we are assuming a constant nutrient concentration, we also have that $p^j_\tau = p$ for $j \leq \mathcal{Z}$. The evolution of this probability function is illustrated in Figure 3.2.

The average trajectories of the initial cells for the CNCA-Q1 model can be found using Equation (2.4). However, we note that the average trajectories of cells will depend on whether it is in the replicative or quiescent region. We assume that the replicative region is of fixed length $H = \mathcal{Z}\Delta x$. Equation (2.4) simplifies to

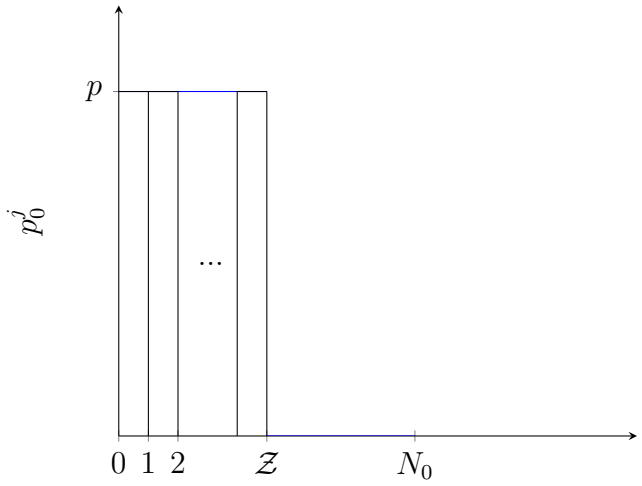

(a) Initial proliferation probabilities for the CNCA-Q1 model. Each of the $\mathcal{Z}$ replicative cells have proliferation probability p. The remaining $N_0 - \mathcal{Z}$ quiescent cells have proliferation probability zero.

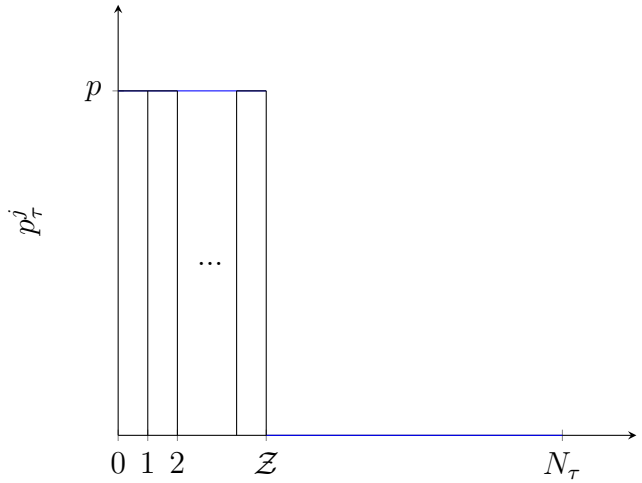

(b) Proliferation probabilities for the CNCA-Q1 model at time step τ. We note that there are now N_τ cells in the colony. However, there are still only $\mathcal{Z}$ replicative cells with proliferation probability p. There are now $N_\tau - \mathcal{Z}$ quiescent cells. We note that the number of quiescent cells has increased.

Figure 3.2: Evolution of the proliferation probabilities over time for the CNCA-Q1 model. Each of the rectangular columns represents the probability of proliferation for a cell. The first rectangle represents the proliferation probability of the first cell, etc. We note that the width of the each of the columns is one and thus the area of the rectangle is also the proliferation probability of the cell.

$$X^j_{\tau+1} = X^j_\tau + pX^j_\tau, \qquad \text{for } X^j_\tau < H. \tag{3.9}$$

Thus the average positions of the initial cells for $X^j_\tau < H$ will be

$$X^j_\tau = X^j_0 (1+p)^\tau . \tag{3.10}$$

We now consider cells in the quiescent region, $X^j_\tau > H$, where the cell proliferation probabilities are zero. In this region, Equation (2.4) simplifies to

$$X^j_{\tau+1} = X^j_\tau + p\mathcal{Z}\Delta x. \tag{3.11}$$

Hence, the average positions for cells in the quiescent region will be

$$X^j_\tau = pH\tau + X^j_0, \qquad \text{for } X^j_0 > H \tag{3.12}$$

where X^j_0 is the initial position of the cell. Lastly, we note that cells may cross over from the replicative to the quiescent quiescent region. Suppose we define the value $\tau^\star_j$ as the time in which the cell with average position X^j_τ crosses from the replicative region to the quiescent region. We note that $\tau^\star_j$ does not have to be a multiple of Δt and is just a way of joining paths up across the two regions. As the cell is initially in the replicative region, its average position for $\tau < \tau^\star_j$ will be given by Equation (3.10). We can find $\tau^\star_j$ by solving

$$X^j_0 (1+p)^{\tau^\star_j} = H, \tag{3.13}$$

where H is the fixed length of the replicative region. This is because H is the location in which the cell with average position X^j_τ crosses into the quiescent region. Solving (3.13), we find that

$$\tau^\star_j = \frac{\log\left(H/X^j_0\right)}{\log(1+p)}. \tag{3.14}$$

For $\tau \geq \tau^\star_j$, the cell will be in the quiescent region. Thus the average trajectory for $\tau \geq \tau^\star_j$ will be of the form

$$X^j_\tau = pH\tau + c_1, \tag{3.15}$$

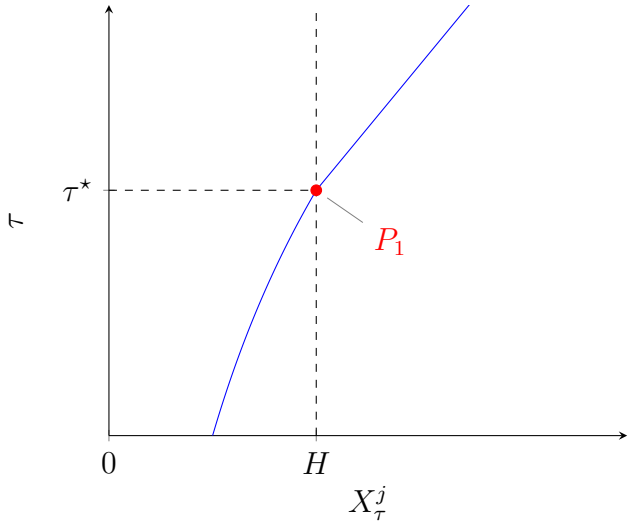

Figure 3.3: An example of the average trajectory of an initially replicative cell. The trajectory of the cell within the replicative region follows the path defined in (3.10). This is until it reaches $X_\tau^j = H$. As H is the length of the replicative region, it is also the point in space where a cell transitions to the quiescent region. Furthermore, we label the time X_τ^j reaches H by $\tau_j^\star$. As we are dealing with an average trajectory, $\tau_j^\star$ may not be an integer. We label the point $\left(X_\tau^j, \tau_j^\star\right)$ by P_1. As the average trajectory must be continuous, the path in the quiescent region must also go through the point P_1. Hence the average trajectory of the cell within the quiescent region follows the path defined in (3.16).

where c_1 is a constant. We note that this is not exactly the same as Equation (3.12). Equation (3.12) is the average trajectory of a cell that starts (and remains for all time) in the quiescent region. We note that the slopes are the same for Equation (3.12) and (3.15) but the intercepts are different. The intercept X_0^j in Equation (3.12) is the initial position of the cell. The constant c_1 is a shift that accounts for the time taken for the cell to leave the replicative region. We can calculate c_1 by considering the point, $P_1 = \left(H, \tau_j^\star\right)$, where the average trajectory transitions from the replicative region to the quiescent region. Substituting $(X_\tau^j, \tau) = \left(H, \tau_j^\star\right)$ into Equation (3.15) and rearranging, we find that $c_1 = H - pH\tau_j^\star$. Thus the average position, for $\tau \geq \tau_j^\star$, of an initially replicative cell that has crossed into the quiescent region at time $\tau = \tau_j^\star$ is

$$X_\tau^j = pH\left(\tau - \tau_j^\star\right) + H. \tag{3.16}$$

An example of the average trajectory of an initially replicative cell that crosses into the quiescent region is illustrated in Figure 3.3. Hence the full expression for the average positions of the tracked cells after τ time steps is

$$X_\tau^j = \begin{cases} X_0^j (1+p)^\tau, & \text{if } X_0^j < H, \tau < \tau_j^\star, \\ pH\left(\tau - \tau_j^\star\right) + H, & \text{if } X_0^j < H, \tau \geq \tau_j^\star, \\ pH\tau + X_0^j, & \text{if } X_0^j \geq H, \end{cases} \tag{3.17}$$

where X_0^j is the initial position of the cell and $\tau_j^\star$ is the time that a cell transitions from the replicative region to the quiescent region given by Equation (3.14). We note that $X_0^j < H$ refers to a cell initially in the replicative region and $X_0^j \geq H$ refers to a cell initially in the quiescent region. We again wish to derive continuum paths for the average trajectories of the initial cells. We recall that $t = \tau\Delta t$, $p = \hat{p}\Delta t$ and that we may find the continuum paths by taking the continuous limit as $\Delta t \to 0$. Applying this limit to (3.17), we find that the average trajectories are given by

$$X^j(t) = \begin{cases} X_0^j \exp\{\hat{p}t\}, & \text{if } X_0^j < H, t < t_j^\star, \\ \hat{p}H\left(t - t_j^\star\right) + H, & \text{if } X_0^j < H, t \geq t_j^\star, \\ \hat{p}Ht + X_0^j, & \text{if } X_0^j \geq H, \end{cases} \tag{3.18}$$

where,

$$t_j^\star = \frac{\log\left(H/X_0^j\right)}{\hat{p}}. \tag{3.19}$$

We note that this is now in terms of the physical proliferation rate $\hat{p}$ instead of the proliferation probability p. We also note that $t_j^\star$ is defined similarly to $\tau_j^\star$ and is found by equating $X^j(t_j^\star) = H$. It is not generally true that $t_j^\star = \tau_j^\star$. Recalling that $L(t) = X^{N_0}(t)$, the length will be given by

$$L_\tau = \hat{p}Ht + L_0, \tag{3.20}$$

where $L_0 = X_0^{N_0}$ is the initial length of the colony. Thus, for the CNCA-Q1 model, the length is growing linearly. 1000 simulations of the CNCA-Q1 are illustrated with the average trajectories (3.18) in Figure 3.4. We observe that there is again a strong agreement between the discrete positions and the continuum paths for the average cell behaviour. We also see that the replicative region exhibits the same uniform growth characteristics as the CNCA model. Specifically, the distances between initially adjacent cells are equal at each time step. We also note that the distances between initially adjacent cells are increasing as the number of time steps increases. In the quiescent region, the distances between initially adjacent cells are not growing as the number of time steps increases. We expect this as the cells within this region are not proliferating. However, we observe that the distances between the adjacent initial cells are not always the same. This is due to the fact that cells are entering the quiescent region at non-constant intervals.

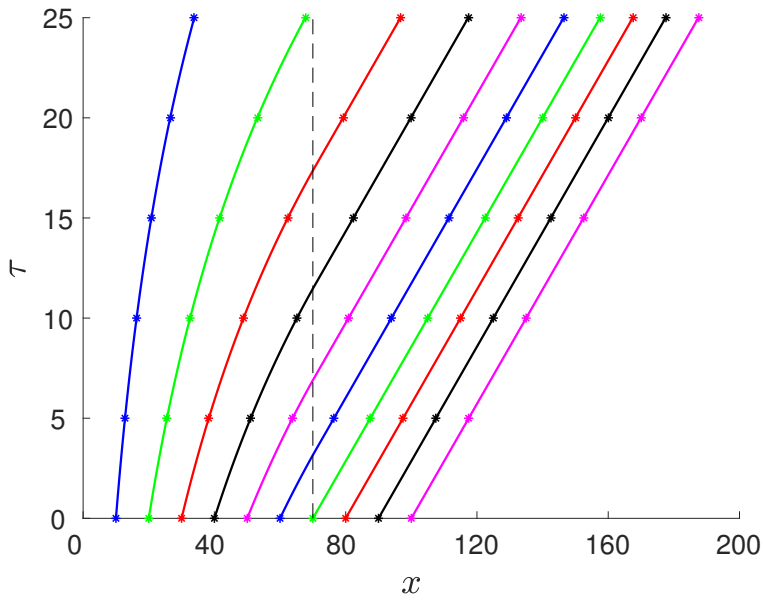

Figure 3.4: Average positions of the initial cells for the CNCA-Q1 model with continuum paths given by Equation (3.18). These are the average results from 1000 simulations and $\mathcal{T} = 25$ time steps. The initial number of cells in the model is $N_0 = 1000$ and the cell width is $\Delta x = 0.1$. Thus the dimensional length of the colony is initially $L_0 = 100$ units. We, again, only chose to plot every 10th cell for brevity. The fixed number of replicative cells is chosen to be $\mathcal{Z} = 70$. Hence the fixed length of the replicative region is $H = 70$. The location of H is the dotted line on the plot. Lastly, we have used a uniform proliferation probability of $p = 0.05$.

We now consider our second specification for the CNCA-Q model. We will refer to this as the CNCA-Q2 model. Suppose we set the number of replicative cells in the region to be $\mathcal{Z}_\tau = hN_\tau$, where h is some fixed scale between 0 and 1. We recall that $h = 0$ implies that there are no replicative cells and thus no growth can occur in the colony. We also recall that $h = 1$ implies all the cells are replicative cells and thus we have the CNCA model. As we are assuming a constant nutrient concentration across the replicative region, the probabilities at time step τ will be

$$p_\tau^i = \begin{cases} p & \text{if } i \leq \mathcal{Z}_\tau, \\ 0 & \text{if } i > \mathcal{Z}_\tau, \end{cases} \tag{3.21}$$

where $i \leq \mathcal{Z}_\tau$ corresponds to the replicative cells and $i > \mathcal{Z}_\tau$ corresponds to the quiescent cells. The evolution of this probability function is illustrated in Figure 3.5.

We may again use Equation (2.4) to derive an expression for the average positions of the initial cells. Similarly to the CNCA-Q1 model, the average positions will depend on whether cells are in the replicative or quiescent region. We firstly note that the length of the replicative region will be given by $H_\tau = \Delta x \mathcal{Z}_\tau = h\Delta x N_\tau$. For the replicative region, we may again use the difference equation (3.2). Hence the average positions in the replicative region will be given by Equation (3.3).

We now consider the cells in the quiescent region. Using the probability function (3.21), we observe that only the first $\mathcal{Z}_\tau$ cells have a non-zero probability of proliferation. Hence, for cells in the quiescent region, the difference equation (2.4) simplifies to

$$\begin{aligned} X_{\tau+1}^j &= X_\tau^j + p\Delta x \mathcal{Z}_\tau, \\ &= X_\tau^j + hpL_\tau. \end{aligned} \tag{3.22}$$

From Equation (3.22), we observe that the average trajectory of a cell depends on the length of the colony. Hence we must first derive an expression for the length of the colony. We recall that $X_\tau^{N_0} = L_\tau$. As $N_0 \geq \mathcal{Z}_0$, we note that this cell is quiescent and thus the length can be derived by solving

$$L_{\tau+1} = L_\tau + hpL_\tau. \tag{3.23}$$

Thus the length of the colony will be

$$L_\tau = L_0 \left(1 + hp\right)^\tau. \tag{3.24}$$

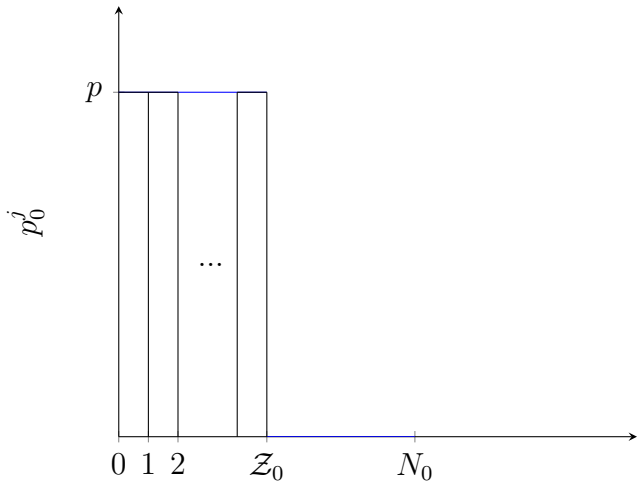

(a) Initial proliferation probabilities for the CNCA-Q2 model. Each of the $\mathcal{Z}_0 = 0.5N_0$ replicative cells have proliferation probability p. The remaining $N_0 - \mathcal{Z}_0$ quiescent cells have proliferation probability zero.

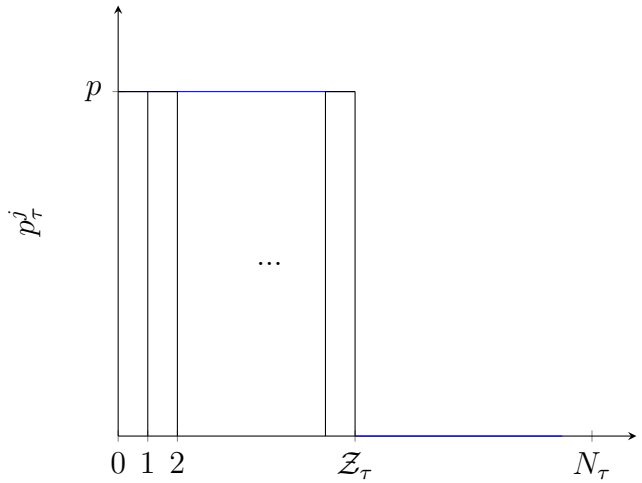

(b) Proliferation probabilities for the CNCA-Q2 model at time step τ. We note that there are now N_τ cells in the colony. Hence, there are now $\mathcal{Z}_\tau = 0.5N_\tau$ replicative cells with proliferation probability p. The remaining quiescent cells have proliferation probability 0. We note that the proportion of replicative and quiescent cells has stayed the same

Figure 3.5: Evolution of the proliferation probabilities over time for the CNCA-Q2 model. We note that the scale in this case is specified to be $h = 0.5$. As with Figure 3.2, each of the rectangular columns represents the probability of proliferation for a cell. The first rectangle represents the proliferation probability of the first cell, etc. We note that the width of the each of the columns is one and thus the area of the rectangle is also the proliferation probability of the cell.

Hence Equation (3.22) becomes the inhomogeneous difference equation

$$X^j_{\tau+1} = X^j_\tau + hpL_0\left(1+hp\right)^\tau . \tag{3.25}$$

We also note that $H_\tau = hL_\tau$ and hence $H_\tau = hL_0\left(1+hp\right)^\tau$. Solving (3.25), we find the average positions for the initially quiescent cells to be

$$X^j_\tau = X^j_0 - L_0 + L_0\left(1+hp\right)^\tau . \tag{3.26}$$

We note the the average positions of the quiescent cells are simply a shift on the average length of the colony. This is exactly as expected as there is no growth in the quiescent region and hence all the cell are being displaced at the same rate due to proliferation in the replicative region. As with the CNCA-Q1 model, the replicative cells will eventually move into the quiescent region. We again refer to the time in which the cell with average trajectory X^j_τ crosses from the replicative region into the quiescent region as $\tau^\star_j$. Using Equation (3.3) for the average positions in the replicative region, we may find $\tau^\star_j$ by equating $X^j_{\tau^\star_j} = H_{\tau^\star_j} = hL_0\left(1+hp\right)^{\tau^\star_j}$. Thus for the CNCA-Q2 model , we find that

$$\tau^\star_j = \frac{\log\left(\frac{X^j_0}{hL_0}\right)}{\log\left(\frac{1+p}{1+hp}\right)}. \tag{3.27}$$

Using a similar argument as illustrated in Figure 3.3, we may find the average trajectories of the initially replicative cells that have crossed into the quiescent region. We know, due to continuity of the cell's path, that the average trajectory in the quiescent region must past through the point $P_1 = (H_{\tau^\star_j}, \tau^\star_j)$. We also know that the form of the average trajectories for $\tau \geq \tau^\star_j$ must be

$$X^j_\tau = c_1 + L_0\left(1+hp\right)^\tau . \tag{3.28}$$

We note that $\tau \geq \tau^\star_j$ refers to time in which the cell is in the quiescent region. We also note that Equation (3.28) follows the paths as (3.26) but with a shift c_1. Similarly to the CNCA-Q1 model, this shift accounts for the time taken to leave the replicative region. Using the fact that the average trajectory of the form (3.28) must pass through point P_1, we may calculate c_1 and find that

$$X^j_\tau = L_0\left(1+hp\right)^\tau - L_0\left(1+hp\right)^{\tau^\star_j} + hL_0\left(1+p\right)^{\tau^\star_j} , \tag{3.29}$$

for $\tau \geq \tau^\star_j$. Thus the average positions for the initial cells of the CNCA-Q2 model are

$$X_\tau^j = \begin{cases} X_0^j (1+p)^\tau, & \text{if } X_0^j < H_0, \tau < \tau_j^\star, \\ L_0 (1+hp)^\tau - L_0 (1+hp)^{\tau_j^\star} + hL_0 (1+p)^{\tau_j^\star}, & \text{if } X_0^j < H_0, \tau \geq \tau_j^\star, \\ X_0^j - L_0 + L_0 (1+hp)^\tau, & \text{if } X_0^j \geq H_0, \end{cases} \tag{3.30}$$

where $\tau_j^\star$ is defined in equation (3.27). We note that $X_0^j < H_0$ coincides with a cell initially in the replicative region and $X_0^j \geq H_0$ coincides with a cell initially in the quiescent region. We again wish to derive continuum paths for the average positions of the initial cells. We recall that $t = \tau\Delta t$, $p = \hat{p}\Delta t$ and that we may find the continuum paths by taking the continuous limit $\Delta t \to 0$. Applying this limit to (3.30), we find that

$$X^j(t) = \begin{cases} X_0^j \exp\{\hat{p}t\}, & \text{if } X_0^j < H_0, t < t_j^\star, \\ L_0 \exp\{\hat{p}t\} - L_0 \exp\{h\hat{p}t_j^\star\} + hL_0 \exp\{h\hat{p}t_j^\star\}, & \text{if } X_0^j < H_0, t \geq t_j^\star, \\ X_0^j - L_0 + L_0 \exp\{h\hat{p}t\}, & \text{if } X_0^j \geq H_0. \end{cases} \tag{3.31}$$

We note that this is now in terms of the physical proliferation rate $\hat{p}$ instead of the proliferation probabilities p. We also note that $t_j^\star$ is defined in the same way as $\tau_j^\star$. However, it is not necessarily the case that $t_j^\star = \tau_j^\star$. By equating $X^j(t_j^\star) = H$, we find that

$$t_j^\star = \frac{\log\left(\frac{X_0^j}{hL_0}\right)}{h\hat{p} - \hat{p}}. \tag{3.32}$$

The average positions over 1000 simulations of the CNCA-Q2 model are illustrated with the average trajectories (3.31) in Figure 3.6. We notice similar cell behaviour to the CNCA-Q model with a fixed number of replicative cells. There is uniform growth within the replicative region and there is no growth within the quiescent region. The most noticeable difference between this model and the CNCA-Q1 model is the length. When the number of replicative cells is increasing, the length is no longer growing linearly. Specifically, in the case where the replicative region is a constant proportion of the length, the length of the colony is growing exponentially.

3.1.3 Depleting Constant Nutrient Cellular Automaton (DC-NCA) Model

In the CNCA and CNCA-Q models, we have assumed that the proliferation probabilities do not decrease as the length of the colony increases. However, with a limited source of the

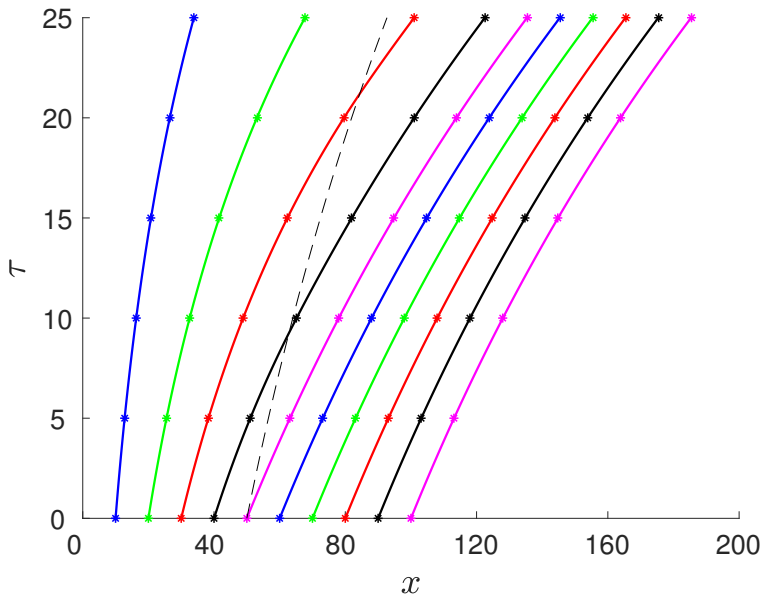

Figure 3.6: Average positions of the initial cells for the CNCA-Q2 model with continuum paths given by Equation (3.31). These are the average results from 1000 simulations and $\mathcal{T} = 25$ time steps. The initial number of cells in the model is $N_0 = 1000$ and the cell width is $\Delta x = 0.1$. Thus the dimensional length of the colony is initially $L_0 = 100$ units. We, again, only chose to plot every 10th cell for brevity. The scale is chosen to be $h = 0.7$. Hence the initial length of the replicative region is $H_0 = 70$. The location of H is the dotted line on the plot. Lastly, we have used a uniform proliferation probability of $p = 0.05$.

nutrient the local nutrient concentration C_τ^j will be decreasing as the length of the colony is increasing. This will result in the proliferation probabilities of the cells also decreasing in time. We assume a uniform nutrient concentration and hence all the probabilities will decrease uniformly. We refer to this model as the depleting constant nutrient cellular automaton (DCNCA) model. We also assume that all cells are replicative cells in the DCNCA model.

The proliferation probabilities for the DCNCA model will not depend on space as they are uniform across the colony but they will depend on time. Thus we observe that $p_\tau^i = p_\tau$. We also impose that the uniform proliferation probabilities will be inversely proportional to the length of the colony. Hence we set

$$p_\tau = \frac{S}{N_\tau}, \tag{3.33}$$

where S is a constant and N_τ is the number of cells in the colony at time step τ. We note that S will be the sum of the proliferation probabilities at any given time step τ. The evolution of the probability function for the DCNCA model, as specified in Equation (3.33), is illustrated in Figure 3.7.

We again use Equation (2.4) to derive an expression for the average positions of the initial cells. Using Equation (3.33) for the proliferation probabilities, we find that

$$X_{\tau+1}^j = X_\tau^j + \Delta x S \frac{X_\tau^j}{L_\tau}, \tag{3.34}$$

noting the fact that $L_\tau = \Delta x N_\tau$. We observe that Equation (3.34) has dependence on L_τ. Thus we must first solve for L_τ before solving for general X_τ^j. Substituting $X_\tau^{N_0} = L_\tau$ into Equation (3.34) , we find that

$$L_\tau = \Delta x S \tau + L_0, \tag{3.35}$$

where L_0 is the initial length of the colony. Hence we may simplify (3.34) to

$$X_{\tau+1}^j = X_\tau^j + \Delta x S \frac{X_\tau^j}{\Delta x S \tau + L_0}. \tag{3.36}$$

By inspection, we note that

$$X_\tau^j = \frac{X_0^j}{L_0} \left(\Delta x S \tau + L_0 \right), \tag{3.37}$$

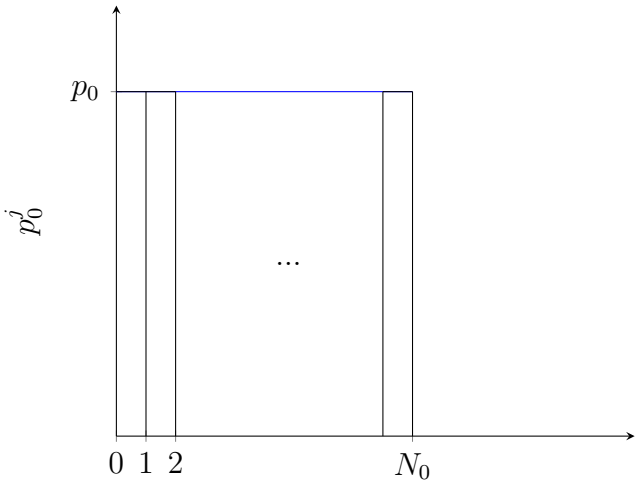

(a) Initial proliferation probabilities for the DCNCA model. Each of the N_0 cells within the colony has proliferation probability $p_0 = S/N_0$.

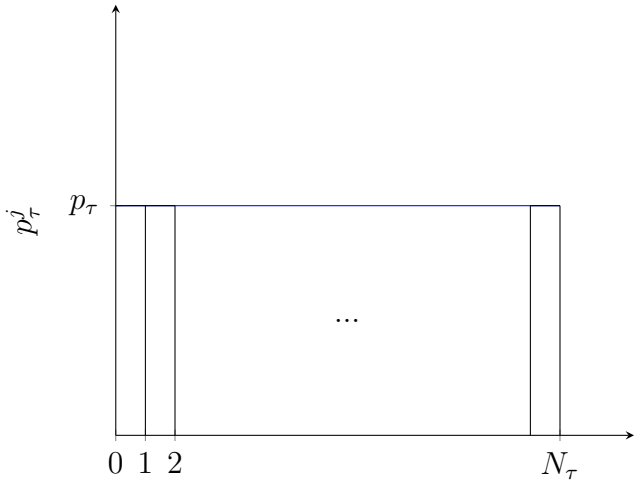

(b) Proliferation probabilities for the DCNCA model at time step τ. We note that there are now N_τ cells in the colony. As $N_\tau > N_0$, the proliferation probability of each of the N_τ cells has decreased. The proliferation probabilities are now $p_\tau = S/N_\tau$.

Figure 3.7: Evolution of the proliferation probabilities over time for the DCNCA model. Each of the rectangular columns represents the probability of proliferation for a cell. The first rectangle represents the proliferation probability of the first cell, etc. We note that the width of the each of the columns is one and thus the area of the rectangle is also the proliferation probability of the cell. Hence the total area of all of the rectangles will be S for all time steps τ.

is a solution to Equation (3.36). We wish to derive a continuous approximation to the average position of the initial cells. We can find the continuum paths to the average positions by taking the continuous limits

$$\lim_{\substack{\Delta t\to 0\\ \Delta x\to 0}} X_\tau^j, \tag{3.38}$$

Substituting $\tau = t/\Delta t$ into Equation (3.37), we may take this limit to find that

$$X^j(t) = \lim_{\substack{\Delta t\to 0\\ \Delta x\to 0}} \frac{X_0^j}{L_0}\left(\frac{\Delta x}{\Delta t}St + L_0\right). \tag{3.39}$$

We note that $X^j(t)$ must be finite as $\Delta x \to 0$ and $\Delta t \to 0$. Noting the term $\Delta x/\Delta t$ in Equation (3.39), we must therefore take the limit such that

$$\Delta x = \mathcal{O}\left(\Delta t\right), \tag{3.40}$$

as $\Delta t, \Delta x \to 0$. This will ensure that $X^j(t)$ is finite. Thus the continuum paths for the average positions of the initial cells for the DCNCA model are

$$X^j(t) = \frac{X_0^j}{L_0}\left(\hat{S}t + L_0\right), \tag{3.41}$$

where

$$\hat{S} = \lim_{\substack{\Delta t\to 0\\ \Delta x\to 0}} \frac{\Delta x}{\Delta t}S. \tag{3.42}$$

Lastly, we recall that S can be interpreted as the expected number of cell proliferation events in each time step. However, when taking the continuous approximation there are no time steps and thus we define $\hat{S}$. The quantity $\hat{S}$ can be expressed in terms of the proliferation rate, $\hat{p}$. Recall that $\hat{p} = p\Delta t$. Thus, for the DCNCA model, we note that

$$\hat{p}_0 = \frac{\Delta x S}{\Delta t L_0}. \tag{3.43}$$

We recall the distinguished limit $\Delta x = \mathcal{O}\left(\Delta t\right)$. Thus we may take the limits for the continuous approximation to find that

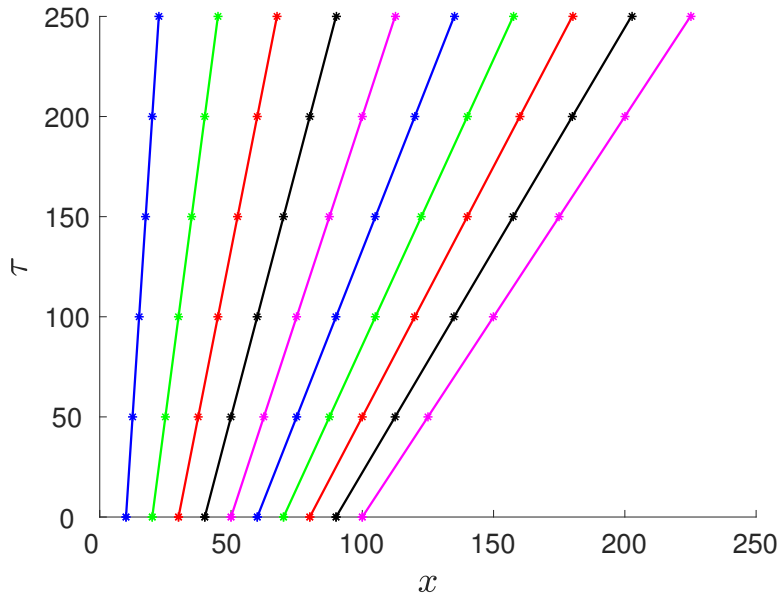

Figure 3.8: Average positions of the initial cells for the DCNCA model with continuum paths (3.45). These are the average results from 1000 simulations and $\mathcal{T} = 250$ time steps. The initial number of cells in the model is $N_0 = 1000$ and the cell width is $\Delta x = 0.1$. Thus the dimensional length of the colony is initially $L_0 = 100$ units. We, again, only chose to plot every 100th cell for brevity. We have set the value $S = 5$. This corresponds to an expected number of 5 cell insertions across the entire colony in each time step.

$$\hat{p}_0 = \lim_{\substack{\Delta x \to 0 \\ \Delta t \to 0}} \frac{\Delta x S}{\Delta t L_0} = \frac{\hat{S}}{L_0}. \tag{3.44}$$

Hence we can simplify Equation (3.41) to find that

$$X^j(t) = X_0^j \hat{p}_0 t + X_0^j. \tag{3.45}$$

Thus we have the continuum paths for the average position of the cells written in terms of physical quantities. The continuum paths are compared with the average results from 1000 simulations of Algorithm 1 in Figure 3.8. We have used $N_0 = 1000$ initial cells and set $S = 5$. We have also increased the number of time steps plotted to $\mathcal{T} = 250$. We have done this as the proliferation probabilities are much smaller than the previous cases and thus less proliferation occurs in a time step.

Observing Figure 3.8, we notice that all of the average trajectories of the initial cells

throughout the colony are linear. We particularly choose to focus the length of the colony. Its average position is given by $L_\tau = \Delta x S\tau + L_0$. We note that at each time the average length of the colony is increasing by $\Delta x S$. This is equivalent to the number of cells in the colony increasing by S. Hence, on average $N_{\tau+1} = N_\tau + S$. Hence S is the expected number of proliferation events that occur within a time step τ. We note that S does not have to be an integer as it is an expected value and not an observed value.

We have shown that our CA model simulated with Algorithm 1 yields similar results to Binder et al. (2008). Thus we conclude that Algorithm 1 and the continuum paths for the average positions derived from Equation (2.4) are accurate for modelling proliferative tissue growth. We have already expanded on the work of Binder et al. (2008) by adding quiescent cells. We now wish to further extend the model by exploring non-uniform growth.

3.2 Non-Uniform Growth

Up to this point we have only explored models with a uniform nutrient concentration. However, we note that many systems do not have a uniform nutrient concentration. An example is the cylindrical yeast colonies grown by Vulin et al. (2014). We note that the nutrient concentration of cylindrical yeast colonies is highest at the base and smallest at the top. Furthermore, the nutrient concentration is monotonically decreasing. Hence we know that $C_\tau^i \geq C_\tau^j$ if $i < j$. Furthermore we assume that the curve for the nutrient concentration is linear. We explore similar models as Section 3.1 with the linearly decreasing nutrient concentration.

3.2.1 Linear Nutrient Cellular Automaton (LNCA) Model

The first linear nutrient concentration model we consider is the LNCA model. The LNCA model is similar to the CNCA model but has a non-uniform linear nutrient concentration instead of a constant nutrient concentration. Thus all the cells in the LNCA model are replicative. As the nutrient concentration C_τ^j is linearly decreasing, the proliferation rates $\hat{p}_\tau^i$ and hence proliferation probabilities p_τ^i will also be linearly decreasing. Hence, for all time steps τ, the maximum proliferation probability will be p_τ^1 and the minimum probability will be $p_\tau^{N_\tau}$.

For the LNCA model we assume nutrient is being injected at the base of the colony from an unlimited source so we assume that the concentration at the base of the colony C_τ^1 is some constant value. Hence the corresponding proliferation probability at the base of the colony p_τ^1 will also be a constant value. As p_τ^i is the maximum probability, we let $p_\tau^1 = p_{\max}$ for all time steps τ. As nutrient is being injected into the colony from an infinite source, we assume there will be sufficient nutrient diffusing to the end of the

colony. Thus, we assume that the nutrient concentration at the end of the colony $C_\tau^{N_\tau}$ will also be constant so let $p_\tau^{N_\tau} = p_{\min}$ for all time steps τ, where $p_{\min} < p_{\max}$. We also define the maximum and minimum proliferation rates $\hat{p}_{\max}$ and $\hat{p}_{\min}$, respectively. It follows that $\hat{p}_\tau^1 = \hat{p}_{\max} = p_{\max}/\Delta t$ and $\hat{p}_\tau^{N_\tau} = \hat{p}_{\min} = p_{\min}/\Delta t$. The evolution of the probability function for the LNCA model is illustrated in Figure 3.9. We know that the function for the proliferation probabilities is linear and passes through the points $(1, p_{\max})$ and $(N_\tau, p_{\min})$. Hence it can be given by

$$p_\tau^i = p_{\max} + \frac{p_{\max} - p_{\min}}{N_\tau - 1} - \frac{p_{\max} - p_{\min}}{N_\tau - 1} i. \tag{3.46}$$

We again wish to calculate the average trajectories of the intial cells for the LNCA model. Substituting the probability function (3.46) into the difference equation (2.4), we find that

$$X_{\tau+1}^j = X_\tau^j + p_{\max} X_\tau^j + \frac{p_{\max} - p_{\min}}{N_\tau - 1} X_\tau^j - \frac{p_{\max} - p_{\min}}{2\Delta x\,(N_\tau - 1)} X_\tau^j \left(X_\tau^j + \Delta x\right). \tag{3.47}$$

We note that $\Delta x\,(N_\tau - 1) = L_\tau - \Delta x$ and hence (3.47) becomes

$$X_{\tau+1}^j = X_\tau^j + p_{\max} X_\tau^j - \left(X_\tau^j - \Delta x\right) \frac{p_{\max} - p_{\min}}{2\,(L_\tau - \Delta x)} X_\tau^j. \tag{3.48}$$

We again note that (3.48) has dependence on the length of the colony L_τ. Hence we again must first solve for L_τ to find a general solution for (3.48). Substituting $X_\tau^{N_0} = L_\tau$ into Equation (3.48), we can simplify to find that

$$L_{\tau+1} = L_\tau \left(1 + \frac{p_{\max} + p_{\min}}{2}\right). \tag{3.49}$$

Hence we may solve Equation (3.49) to find that

$$L_\tau = L_0 \left(1 + \frac{p_{\max} + p_{\min}}{2}\right)^\tau, \tag{3.50}$$

where L_0 is the initial length of the colony. Lastly, we again take the the continuous limit

$$L(t) = \lim_{\substack{\Delta x \to 0 \\ \Delta t \to 0}} L_\tau, \tag{3.51}$$

to find that

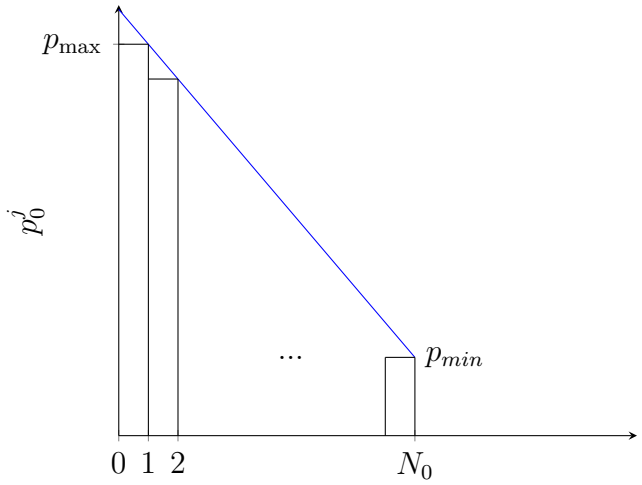

(a) Initial proliferation probabilities for the LNCA model. We note that the function for the probabilities does not pass through the point $(0, p_{\max})$.

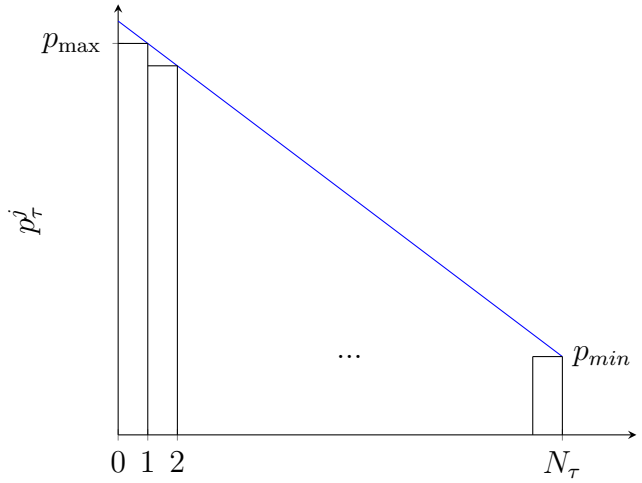

(b) Proliferation probabilities for the CNCA model at time step τ. We note that there are now N_τ cells in the colony.

Figure 3.9: Evolution of the proliferation probabilities over time for the LNCA model. The proliferation probabilities for the LNCA model are given by Equation (3.46). Similarly to the constant nutrient models, the sum of all the probabilities can be found by calculating the area of the reactangles. We also note that probability functions pass through the right of the rectangles. Equivalently, we can define a probability function that passes through the left of the rectangles. However, we note that in the limit $\Delta t \to 0$, the two probability functions would be identical and thus will yield the same results for the continuum paths.

$$L(t) = L_0 \exp\left\{\frac{\hat{p}_{\max} + \hat{p}_{\min}}{2} t\right\}. \tag{3.52}$$

We now wish to solve (3.48) for general X_τ^j. However, we note that the difference equation for the average positions cannot be solved analytically. Thus we choose to take the continuum limit to find a corresponding differential equation to approximate the average trajectories. The solutions to the differential equation can be expressed as the continuum paths or average trajectories of the initial cells. Firstly we rearrange equation (3.48) and divide by Δt to find

$$\frac{X_{\tau+1}^j - X_\tau^j}{\Delta t} = \hat{p}_{\max} X_\tau^j - \left(X_\tau^j - \Delta x\right) \frac{\hat{p}_{\max} - \hat{p}_{\min}}{2\left(L_\tau - \Delta x\right)} X_\tau^j. \tag{3.53}$$

Thus we take the continuum limits $\Delta x \to 0$ and $\Delta t \to 0$ to find that

$$\frac{dX^j}{dt} = \hat{p}_{\max} X^j - \frac{\hat{p}_{\max} - \hat{p}_{\min}}{2} \frac{\left(X^j\right)^2}{L}. \tag{3.54}$$

Thus we may substitute (3.52) into (3.54) to find that

$$\frac{dX^j}{dt} = \hat{p}_{\max} X^j - \frac{\hat{p}_{\max} - \hat{p}_{\min}}{2L_0} \exp\left\{-\frac{\hat{p}_{\max} + \hat{p}_{\min}}{2} t\right\} \left(X^j\right)^2. \tag{3.55}$$

We note that the differential equation (3.55) is a Bernouilli equation. Hence we obtain the closed form solution

$$X^j(t) = \frac{L_0 \exp\left\{\frac{\hat{p}_{\max} + \hat{p}_{\min}}{2} t\right\}}{1 + \left[\frac{L_0}{X_0^j} - 1\right] \exp\left\{-\frac{\hat{p}_{\max} - \hat{p}_{\min}}{2} t\right\}}. \tag{3.56}$$

We note that (3.56) are the average trajectories of the initial cells for the LNCA model. These continuum paths are plotted with 1000 simulations of the LNCA model using Algorithm 1 in Figure 3.10. We note that the length of the colony for the LNCA model is increasing exponentially. We also note the numerator of (3.56) is simply $L(t)$. This implies that $L(t)$ is a limiting value for $X^j(t)$. This is intuitive as the trajectory of a cell cannot cross over the length.

We observe Figure 3.10 to examine the characteristics of non-uniform growth. We recall that uniform growth has occurred when the distance between adjacent cells is equal and increasing at all time steps. We can see that this is not the case for non-uniform growth.

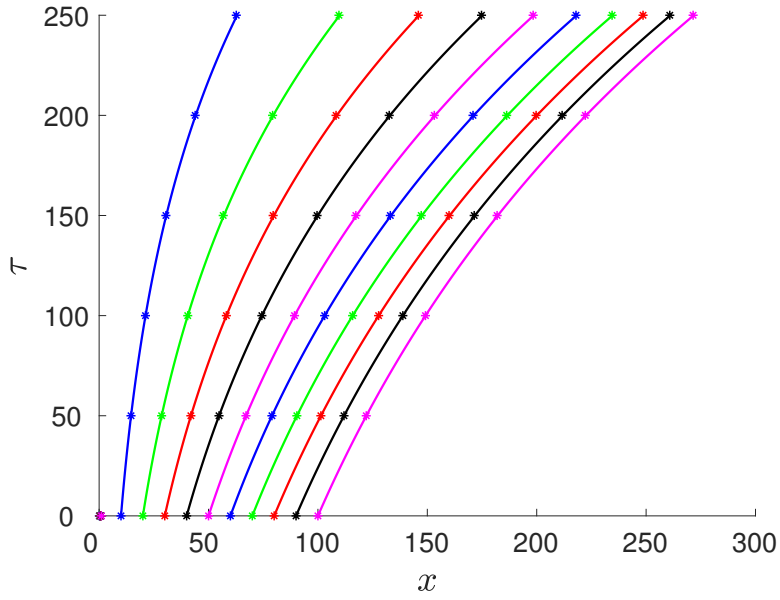

Figure 3.10: Average positions of the initial cells for the LNCA model with continuum paths given by (3.56). These are the average results from 1000 simulations and $\mathcal{T} = 250$ time steps. The initial number of cells in the model is $N_0 = 1000$ and the cell width is $\Delta x = 0.1$. Thus the dimensional length of the colony is initially $L_0 = 100$ units. We again choose to plot every 100th cell for brevity. We have used $p_{\max} = 0.008$ and $p_{\min} = 0$.

We observe that the distance between adjacent cells is increasing as the number of time steps increases. However, the distances across the colony are not equal. We note that the distances between adjacent cells appears to be larger towards the left of the colony. This is because the proliferation probability is larger and thus it is expected that more cells will be born. We now wish to explore how non-uniform growth is affected by adding quiescent cells.

3.2.2 LNCA models with quiescent cells (LNCA-Q Models)

We now consider adding quiescent cells to the LNCA model. Suppose we again have a nutrient source at the base of the colony so that the nutrient concentration will be highest at the base of the colony. However, we assume that the colony readily consumes nutrient. Thus the nutrient concentration hits 0 at some point in the colony. Thus we have a linear decreasing function in the replicative region. We again use $\mathcal{Z}_\tau$ to represent the number of cells in the replicative region after τ time steps and H_τ to represent the physical length of the replicative region after τ time steps. We recall that $H_\tau = \Delta x \mathcal{Z}_\tau$.

We first explore the LNCA-Q model with a fixed number of replicative cells. We refer to this as this LNCA-Q1 model. Thus we set the number of cells in the replicative region to $\mathcal{Z}_\tau = \mathcal{Z}$. Similarly, we have $H_\tau = H$ where $H = \Delta x \mathcal{Z}$. We now wish to define a probability function for the LNCA-Q1 model. We know that the proliferation probability of quiescent cell is zero so $p_\tau^i = 0$ if $i > \mathcal{Z}$. We also again know that the nutrient concentration and thus proliferation probability is largest at the base of the colony. Hence we set $p_\tau^1 = p_{\max}$. We note that the corresponding proliferation rate will be $\hat{p}_{\max}$. Similarly, we know that the nutrient concentration decreases linearly until it hits zero at the end of the replicative region and so we set $p_\tau^{\mathcal{Z}} = p_{\min} = 0$. Thus, as it is assumed to be linear, the proliferation probability function will be

$$p_\tau^i = \begin{cases} p_{\max} + \frac{p_{\max}}{\mathcal{Z}-1} - \frac{p_{\max}}{\mathcal{Z}-1} i & \text{if } i < \mathcal{Z}, \\ 0 & \text{if } i \geq \mathcal{Z}. \end{cases} \tag{3.57}$$

This probability function is plotted in Figure 3.11. We now wish to find the average trajectories for the initial cells using the difference equation (2.4). Substituting the probability function (3.57), we find that

$$X_{\tau+1}^j = X_\tau^j + \Delta x \sum_{i=1}^{X_\tau^j/\Delta x} \left(p_{\max} + \frac{p_{\max}}{\mathcal{Z}-1} - \frac{p_{\max}}{\mathcal{Z}-1} i \right). \tag{3.58}$$

First we wish to solve for the quiescent cells and length of the colony. This corresponds to cells that have index $i \geq \mathcal{Z}$. Hence we can simplify (3.58) to get

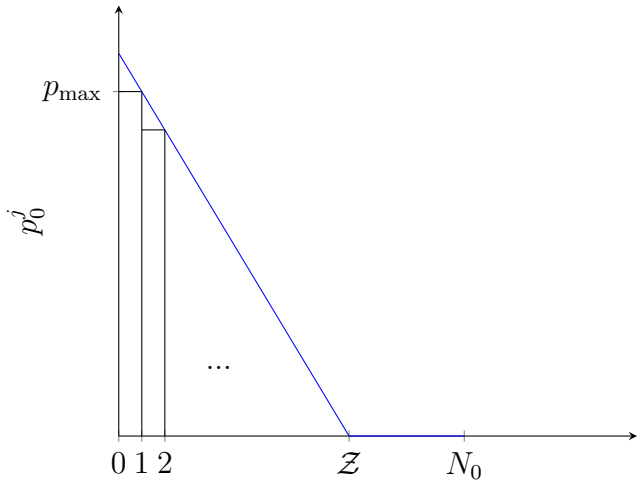

(a) Initial proliferation probabilities for the LNCA-Q model. Each of the $\mathcal{Z}$ replicative cells have proliferation probability p. The remaining $N_0 - \mathcal{Z}$ quiescent cells have proliferation probability zero.

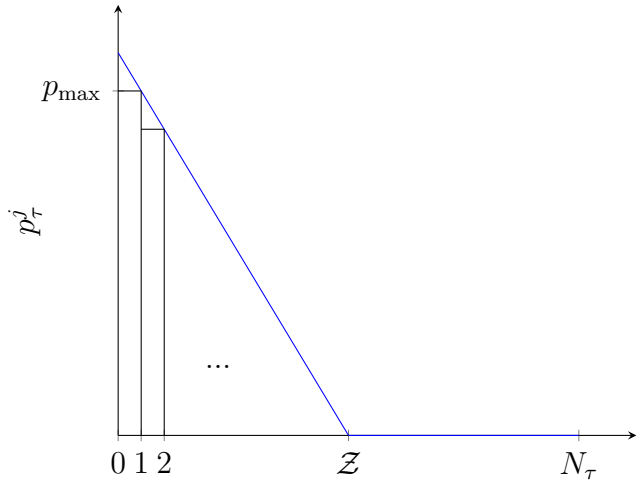

(b) Proliferation probabilities for the LNCA-Q1 model at time step τ. We note that there are now N_τ cells in the colony. However, there are still only $\mathcal{Z}$ replicative cells. There are now $N_\tau - \mathcal{Z}$ quiescent cells. We note that the number of quiescent cells has increased.

Figure 3.11: Evolution of the proliferation probabilities over time for the LNCA-Q1 model. As with Figure 3.9, the probability function does not pass through the point $(0, p_{\max})$ as it passes through the right hand side of the rectangles. Similarly to the LNCA model, this will not affect the accuracy of the derived continuum paths. This probability function is given in Equation (3.57).

$$X_{\tau+1}^{j} = X_{\tau}^{j} + \Delta x \sum_{i=1}^{\mathcal{Z}} \left(p_{\max} + \frac{p_{\max}}{\mathcal{Z}-1} - \frac{p_{\max}}{\mathcal{Z}-1} i \right), \tag{3.59}$$

$$= X_{\tau}^{j} + H\frac{p_{\max}}{2}. \tag{3.60}$$

Solving Equation (3.60), we find the solution to be

$$X_{\tau}^{j} = H\frac{p_{\max}}{2}\tau + X_{0}^{j}. \tag{3.61}$$

Taking the continuum limits as $\Delta t \to 0$ and $\Delta x \to 0$, we find the average trajectory of a cell in the quiescent region to be

$$X^{j}(t) = H\frac{\hat{p}_{\max}}{2}t + X_{0}^{j}. \tag{3.62}$$

We note that the average position for the length and its corresponding continuum path, respectively, are

$$L_{\tau} = H\frac{p_{\max}}{2}\tau + L_{0}, \tag{3.63}$$

and

$$L(t) = H\frac{\hat{p}_{\max}}{2}t + L_{0}. \tag{3.64}$$

We now wish to derive the average trajectories for the replicative cells. Simplifying Equation (3.58), we find that

$$X_{\tau+1}^{j} = X_{\tau}^{j} + X_{\tau}^{j} p_{\max} - \frac{\left(X_{\tau}^{j} - \Delta x\right) p_{\max}}{2\left(H - \Delta x\right)} X_{\tau}^{j}. \tag{3.65}$$

If we apply the scaling

$$Z_{\tau} = \frac{\frac{p_{\max}}{2(H-\Delta x)}}{1 + p_{\max} + \frac{\Delta x p_{\max}}{2(H-\Delta x)}} X_{\tau}^{j}, \tag{3.66}$$

to the difference equation (3.65), then we get the logistic map

$$Z_{\tau+1} = rZ_\tau \left(1 - Z_\tau\right), \tag{3.67}$$

where

$$r = 1 + p_{\max} + \frac{\Delta x p_{\max}}{2(H - \Delta x)} = 1 + p_{\max} + \frac{p_{\max}}{2(\mathcal{Z} - 1)}. \tag{3.68}$$

We note that the logistic map does not have a closed form solution. Thus we must again use the continuous limit to find a continuous approximation to the average trajectories of the initial cells. We also note that the parameter r will be between 1 and 2.5 as $0 < p_{\max} \leq 1$ and $Z \geq 2$. Thus the logistic map will not show any chaotic behaviour. Rearranging Equation (3.65) and dividing by Δt we find that

$$\frac{X^j_{\tau+1} - X^j_\tau}{\Delta t} = X^j_\tau \hat{p}_{\max} - \frac{\left(X^j_\tau - \Delta x\right)\hat{p}_{\max}}{2\left(H - \Delta x\right)} X^j_\tau. \tag{3.69}$$

Thus taking the continuum limits, we find that

$$\frac{dX^j}{dt} = \hat{p}_{\max} X^j - \frac{\hat{p}_{\max}}{2H}\left(X^j\right)^2. \tag{3.70}$$

This is a logistic equation and thus we can solve it to find the closed form solution

$$X^j(t) = \frac{2H}{1 + \left[\frac{2H}{X^j_0} - 1\right]\exp\left\{-\hat{p}_{\max} t\right\}}. \tag{3.71}$$

Similarly to the CNCA-Q models, the replicative cells will eventually cross over into the quiescent region at some time $t^\star_j$ as defined by $X^j(t^\star_j) = H$. Thus, using (3.71), we find that

$$t^\star_j = \frac{-1}{\hat{p}_{\max}} \log\left(\frac{X^j_0}{2H - X^j_0}\right). \tag{3.72}$$

We again note that the path of the initially replicative cells that have crossed over will be of the form

$$X^j(t) = H\frac{\hat{p}_{\max}}{2} t + c_1 \tag{3.73}$$

for $t > t_j^\star$. We can calculate the constant c_1 by again noting that the path must pass through the point $P_1 = \left(H, t_j^\star\right)$. Thus we find that

$$c_1 = H - H\frac{\hat{p}_{\max}}{2}t_j^\star. \tag{3.74}$$

Hence the continuum paths of the initial cells for the LNCA-Q1 model are given by

$$X^j(t) = \begin{cases} \frac{2H}{1+\left(\frac{2H}{X_0^j}-1\right)\exp\{-\hat{p}_{\max}t\}}, & \text{if } X_0^j < H, t < t_j^\star, \\ H\frac{\hat{p}_{\max}}{2}\left(t - t_j^\star\right) + H, & \text{if } X_0^j < H, t \geq t_j^\star, \\ H\frac{\hat{p}_{\max}}{2}t + X_0^j, & \text{if } X_0^j \geq H, \end{cases} \tag{3.75}$$

where $t_j^\star$ is defined in Equation (3.72). These continuum paths are plotted with 1000 simulations of the LNCA-Q model in Figure 3.12. We note that the length of the colony is again growing linearly. We also note that non-uniform growth has occurred in the replicative region as the distances between adjacent cells are increasing unevenly throughout the colony. We also note that the distances between adjacent cells are not changing in the quiescent region. This is characteristic of regions of quiescent cells.

We now consider the LNCA-Q model where the length of the replicative region is some proportion of the length of the colony. We refer to this as the LNCA-Q2 model. Thus we can again specify the number of replicative cells as $\mathcal{Z}_\tau = hN_\tau$, where $0 < h < 1$. We note that $h = 0$ implies that all cells are quiescent and the colony does not grow and $h = 1$ is simply the LNCA model. We again assume a linear nutrient concentration that peaks at the left of the colony and hits 0 at the end of the replicative region. Thus our proliferation probability function will be a straight line from the point $p_\tau^1 = p_{\max}$ to $p_\tau^{\mathcal{Z}_\tau} = 0$. Hence

$$p_\tau^i = \begin{cases} p_{\max} + \frac{p_{\max}}{\mathcal{Z}_\tau - 1} - \frac{p_{\max}}{\mathcal{Z}_\tau - 1}i & \text{if } i < \mathcal{Z}_\tau, \\ 0 & \text{if } i \geq \mathcal{Z}_\tau. \end{cases} \tag{3.76}$$

This probability function is plotted in Figure 3.13. We now wish to find the average trajectories for the initial cells using the difference equation (2.4). Substituting the probability function (3.76), we find that

$$X_{\tau+1}^j = X_\tau^j + \Delta x \sum_{i=1}^{X_\tau^j/\Delta x}\left(p_{\max} + \frac{p_{\max}}{\mathcal{Z}_\tau - 1} - \frac{p_{\max}}{\mathcal{Z}_\tau - 1}i\right). \tag{3.77}$$

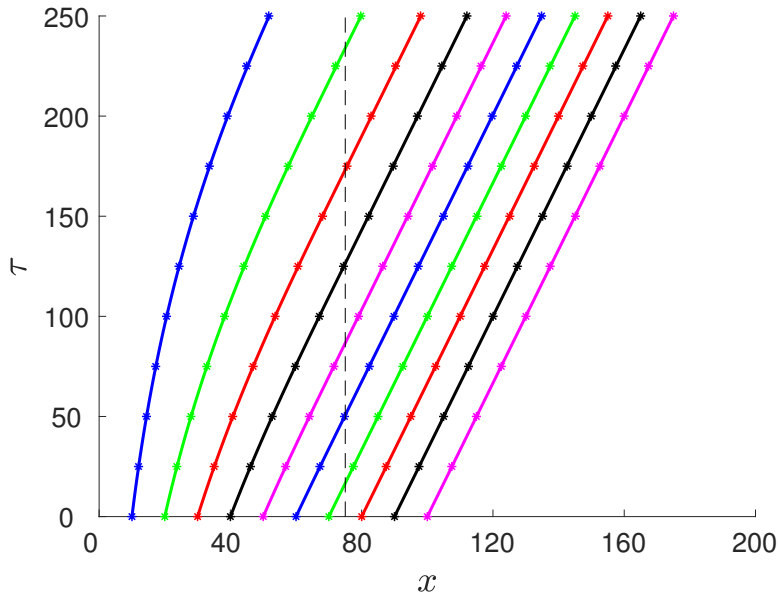

Figure 3.12: Average positions of the initial cells for the LNCA-Q1 model with continuum paths given by (3.75). These are the average results from 1000 simulations and $\mathcal{T} = 250$ time steps. The initial number of cells in the model is $N_0 = 1000$ and the cell width is $\Delta x = 0.1$. Thus the dimensional length of the colony is initially $L_0 = 100$ units. We plot every 100th cell for brevity. We have used $p_{\max} = 0.008$ and $\mathcal{Z} = 750$. Thus the fixed length of the replicative region is $H = 75$.

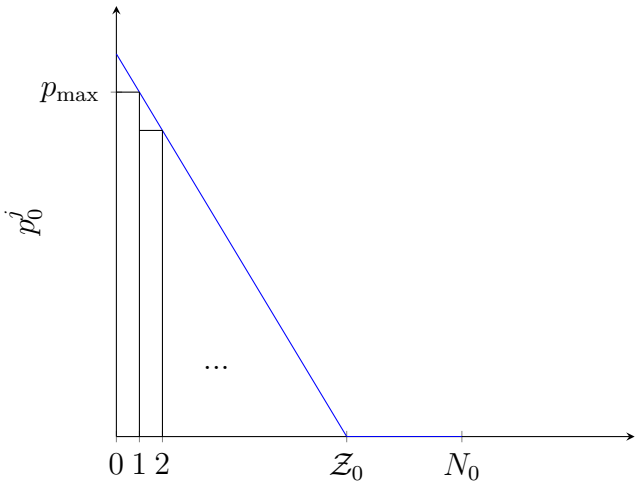

(a) Initial proliferation probabilities for the LNCA-Q2 model. Each of the $\mathcal{Z}_0$ replicative cells have proliferation probability p. The remaining $N_0 - \mathcal{Z}_\prime$ quiescent cells have proliferation probability zero.

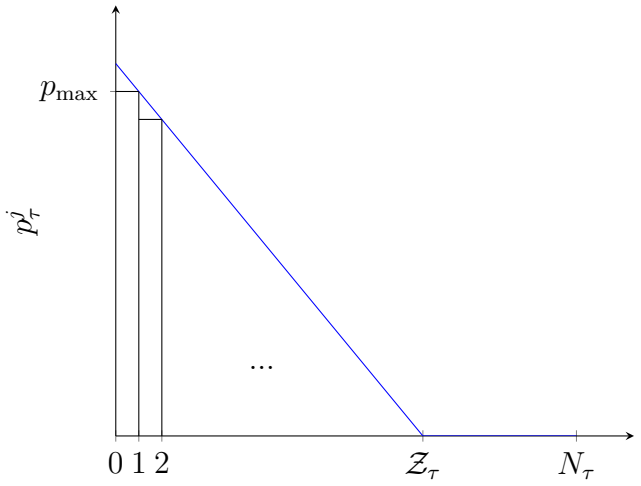

(b) Proliferation probabilities for the LNCA-Q2 model at time step τ. We note that there are now N_τ cells in the colony and hence $\mathcal{Z}_\tau = hN_\tau$ replicative cells. There are now $N_\tau - \mathcal{Z}$ quiescent cells. We note that the number of quiescent cells has increased.

Figure 3.13: Evolution of the proliferation probabilities over time for the LNCA-Q2 model. As with Figure 3.9, the probability function does not pass through the point $(0, p_{\max})$. This probability function is given in Equation (3.57)

First we wish to solve for the quiescent cells and length of the colony. This corresponds to cells that have index $i \geq \mathcal{Z}_\tau$. Hence, noting that $H_\tau = \Delta x \mathcal{Z}_\tau$, we can simplify (3.77) to get

$$X^j_{\tau+1} = X^j_\tau + \Delta x \sum_{i=1}^{\mathcal{Z}_\tau} \left(p_{\max} + \frac{p_{\max}}{\mathcal{Z}_\tau - 1} - \frac{p_{\max}}{\mathcal{Z}_\tau - 1} i \right), \tag{3.78}$$

$$= X^j_\tau + H_\tau \frac{p_{\max}}{2}. \tag{3.79}$$

Noting that $H_\tau = hL_\tau$, we have

$$X^j_{\tau+1} = X^j_\tau + hL_\tau \frac{p_{\max}}{2}. \tag{3.80}$$

Similarly to the previous models, we must first solve for the length L_τ before solving for general X^j_τ. Substituting $X^{N_0}_\tau = L_\tau$ into Equation (3.80), we can solve to find

$$L_\tau = L_0 \left(1 + h \frac{p_{\max}}{2} \right)^\tau. \tag{3.81}$$

Substituting Equation (3.81) into Equation (3.80), we can solve to find that

$$X^j_\tau = X^j_0 - L_0 + L_0 \left(1 + h \frac{p_{\max}}{2} \right)^\tau. \tag{3.82}$$

By taking the continuous limits $\Delta t \to 0$ and $\Delta x \to 0$, we find that the continuum paths are

$$X^j(t) = X^j_0 - L_0 + L_0 \exp\left\{ \frac{h\hat{p}_{\max}}{2} t \right\}, \tag{3.83}$$

and the continuum path for the length is

$$L(t) = L_0 \exp\left\{ \frac{h\hat{p}_{\max}}{2} t \right\}. \tag{3.84}$$

We now wish to derive the average trajectories for the replicative cells. Simplifying Equation (3.77), we find that

$$X^j_{\tau+1} = X^j_\tau + X^j_\tau p_{\max} - \frac{\left(X^j_\tau - \Delta x\right) p_{\max}}{2\left(hL_\tau - \Delta x\right)} X^j_\tau. \tag{3.85}$$

We again note that this difference equation cannot be solved analytically. Thus we must take the continuous limit to find an approximation to the average trajectories. Rearranging Equation (3.85) and dividing by Δt we find that

$$\frac{X^j_{\tau+1} - X^j_\tau}{\Delta t} = X^j_\tau \hat{p}_{\max} - \frac{\left(X^j_\tau - \Delta x\right) \hat{p}_{\max}}{2\left(hL_\tau - \Delta x\right)} X^j_\tau. \tag{3.86}$$

Thus taking the continuous limits, we find that

$$\frac{dX^j}{dt} = \hat{p}_{\max} X^j - \frac{\hat{p}_{\max}}{2hL}\left(X^j\right)^2. \tag{3.87}$$

$$= \hat{p}_{\max} X^j - \frac{\hat{p}_{\max}}{2hL_0} \exp\left\{-\frac{h\hat{p}_{\max}}{2} t\right\}\left(X^j\right)^2 \tag{3.88}$$

This is a Bernoulli equation and thus we can solve it to find the closed form solution

$$X^j(t) = \frac{hL_0 \exp\left\{\frac{h\hat{p}_{\max}}{2} t\right\}}{\frac{1}{2-h} + \left[\frac{hL_0}{X^j_0} - \frac{1}{2-h}\right] \exp\left\{\left(\frac{h}{2} - 1\right) \hat{p}_{\max} t\right\}}. \tag{3.89}$$

Similarly to the previous model, the replicative cells will eventually cross over into the quiescent region at some time $t^\star_j$ defined by

$$X^j(t^\star_j) = hL_0 \exp\left\{h\frac{\hat{p}_{\max}}{2} t^\star_j\right\}. \tag{3.90}$$

We note that the right can side of Equation (3.90) is the continuum path for the value H_τ. This can be found by taking the continuum limits. We find $t^\star_j$ by solving Equation (3.90) numerically. We again note that the path of the initially replicative cells that have crossed over will be of the form

$$X^j(t) = L_0 \exp\left\{h\frac{\hat{p}_{\max}}{2} t\right\} + c_1 \tag{3.91}$$

for $t > t^\star_j$. We can calculate the constant c_1 by again noting that the path must pass through the point $\left(H(t^\star_j), t^\star_j\right)$. Thus we find that

$$C = hL_0 \exp\left\{h\frac{\hat{p}_{\max}}{2}t_j^\star\right\} - L_0 \exp\left\{h\frac{\hat{p}_{\max}}{2}t_j^\star\right\}. \tag{3.92}$$

Hence the continuum paths for the average trajectories of the initial cells for the LNCA-Q2 model with a fixed number of cells in the replicative region are given by

$$X^j(t) = \begin{cases} \frac{hL_0 \exp\left\{\frac{h\hat{p}_{\max}}{2}t\right\}}{\frac{1}{2-h} + \left[\frac{hL_0}{X_0^j} - \frac{1}{2-h}\right]\exp\left\{\left(\frac{h}{2}-1\right)\hat{p}_{\max}t\right\}}, & \text{if } X_0^j < H, t < t_j^\star, \\ L_0 \exp\left\{\frac{\hat{p}_{\max}}{2}t\right\} + hL_0 \exp\left\{\frac{\hat{p}_{\max}}{2}t_j^\star\right\} - L_0 \exp\left\{\frac{\hat{p}_{\max}}{2}t_j^\star\right\}, & \text{if } X_0^j < H, t \geq t_j^\star, \\ X_0^j - L_0 + L_0 \exp\left\{\frac{h\hat{p}_{\max}}{2}t\right\}, & \text{if } X_0^j \geq H, \end{cases} \tag{3.93}$$

where $t_j^\star$ is defined in Equation (3.90). These continuum paths are plotted with 1000 simulations of the LNCA-Q model in Figure 3.14. We note that the length of the colony is again growing exponentially and that non-uniform growth has occurred in the replicative region as the distances between adjacent cells are growing unevenly throughout the colony. We also note that the distances between adjacent cells are not changing in the quiescent region. This is our characteristic for quiescent cells.

3.2.3 Depleting Linear Nutrient Cellular Automaton (DLNCA) Model

The last model we choose to explore is the LNCA model with a depleting nutrient. We refer to this model as the DLNCA model. Similarly to the DCNCA model, we assume we have a finite nutrient source at the base of the colony. Nutrient emitting from this source will diffuse up the colony. However, we again assume that the colony also consumes nutrient. Thus the nutrient concentration will be higher at the base of the colony and lower at the top of the colony. We assume the nutrient concentration will be decreasing linearly so that the proliferation probabilities will be decreasing linearly from the base of the colony to the top of the colony. Hence we again have a maximum probability at p_τ^1 and minimum probability at $p_\tau^{\mathcal{Z}_\tau}$. We assume that $p_\tau^{\mathcal{Z}_\tau} = 0$ for all time steps τ. However, since the nutrient is depleting, these will not be a fixed value in the DLNCA model.

Similarly to the DCNCA model, we assume all of the probabilities sum to a constant value S. Thus we must define a probability function that is linearly decreasing, passes through the point $(N_\tau, 0)$ and sums to S at all time steps τ. The appropriate probability function is

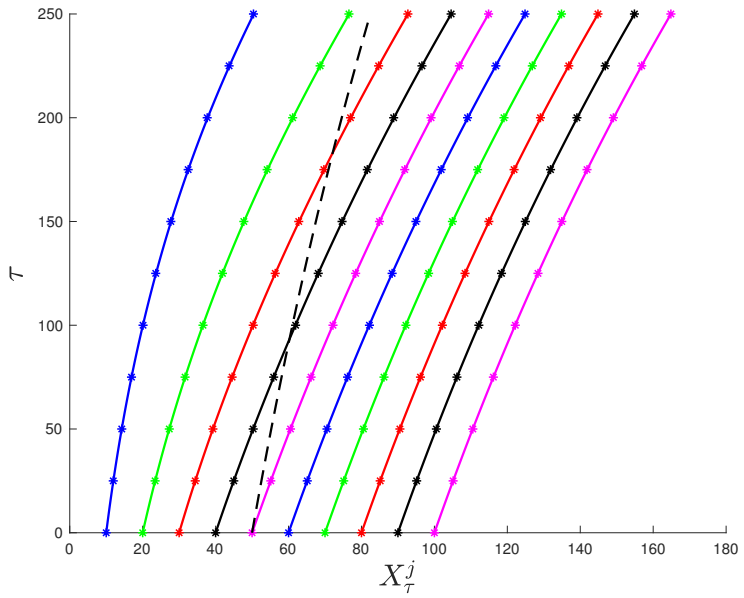

Figure 3.14: Average positions of the initial cells for the LNCA-Q2 with the continuum paths given by (3.93). These are the average results from 1000 simulations and $\mathcal{T} = 250$ time steps. The initial number of cells in the model is $N_0 = 1000$ and the cell width is $\Delta x = 0.1$. Thus the dimensional length of the colony is initially $L_0 = 100$ units. We plot every 100th cell for brevity. We have used $p_{\max} = 0.008$ and $h = 0.5$ as the scale for the replicative region. Thus the initial length of the replicative region is $H_0 = 50$.

$$p_\tau^i = \frac{2S}{N_\tau} - \frac{S\,(2i-1)}{N_\tau^2}. \tag{3.94}$$

This probability function is illustrated in Figure 3.15. From the probability function, we define an average probability, p_τ^{ave} at each time step τ. We recall that the average value will be defined by

$$p_\tau^{\text{ave}} = \frac{1}{N_\tau}\sum_{i=1}^{N_\tau} p_\tau^i. \tag{3.95}$$

Thus we can see that $p_\tau^{\text{ave}} = S/N_\tau$. We also note that we can define the average proliferation rate to be $\hat{p}_\tau^{\text{ave}}$ where $\hat{p}_\tau^{\text{ave}} = p_\tau^{\text{ave}}/\Delta t$. We again wish to find the average trajectories for the DLNCA model by using the difference equation (2.4). We substitute Equation (3.94) into (2.4) to find that

$$X_{\tau+1}^j = X_\tau^j + 2S\Delta x\frac{X_\tau^j}{L_\tau} - S\Delta x\frac{\left(X_\tau^j\right)^2}{L_\tau^2}. \tag{3.96}$$

Again, we must first find the average trajectory for the length of the colony. By substituting $X_\tau^{N_0} = L_\tau$ into Equation (3.96), we find that

$$L_{\tau+1} = L_\tau + S\Delta x. \tag{3.97}$$

Hence the average position for the length is

$$L_\tau = L_0 + S\Delta x\tau \tag{3.98}$$

and that the continuum path for the length is

$$L(t) = L_0 + L_0\hat{p}_0^{\text{ave}}t, \tag{3.99}$$

where $\hat{p}_0^{\text{ave}}$ is the initial average proliferation rate. We note that we have used the fact that

$$\hat{S} = \lim_{\substack{\Delta t\to 0\\ \Delta x\to 0}} \frac{\Delta x S}{\Delta t} = L_0\hat{p}_0^{\text{ave}}. \tag{3.100}$$

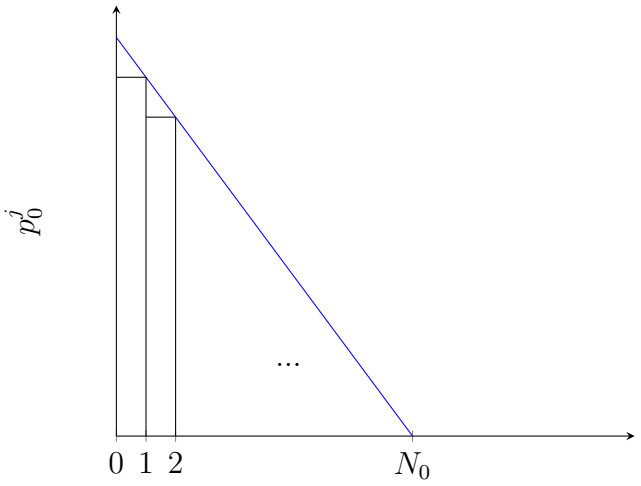

(a) Initial proliferation probabilities for the DLNCA model.

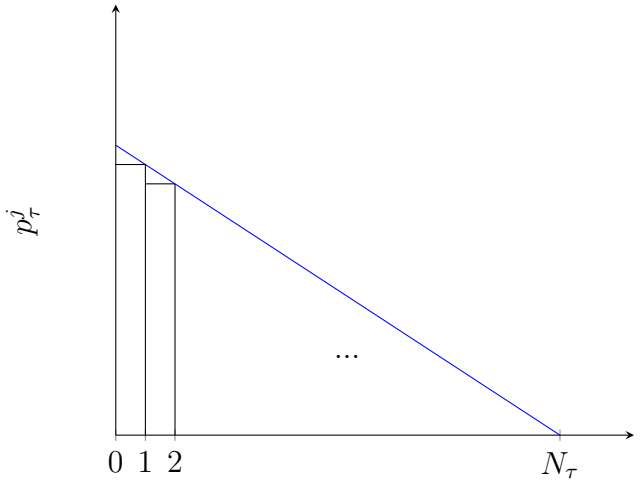

(b) Proliferation probabilities for the DLNCA model at time step τ. We note that there are now N_τ cells in the colony and thus the probabilities at each position have decreased.

Figure 3.15: Evolution of the proliferation probabilities over time for the DLNCA model. The proliferation probabilities for the DLNCA model are given by Equation (3.94).

Suppose we now want to find the average trajectories for all initial cells X_τ^j. Substituting (3.98) into (3.96), we find that

$$X_{\tau+1}^j = X_\tau^j + 2S\Delta x \frac{X_\tau^j}{L_0 + S\Delta x\tau} - S\Delta x \frac{\left(X_\tau^j\right)^2}{\left(L_0 + S\Delta x\tau\right)^2}. \tag{3.101}$$

Rearranging (3.101) and dividing by Δt, we have

$$\frac{X_{\tau+1}^j - X_\tau^j}{\Delta t} = 2S\frac{\Delta x}{\Delta t}\frac{X_\tau^j}{L_0 + S\frac{\Delta x}{\Delta t}t} - S\frac{\Delta x}{\Delta t}\frac{\left(X_\tau^j\right)^2}{\left(L_0 + S\frac{\Delta x}{\Delta t}t\right)^2}. \tag{3.102}$$

We may now take the continuum limits $\Delta t \to 0$ and $\Delta x \to 0$, to derive the ODE

$$\frac{dX^j}{dt} = \frac{2L_0\hat{p}_0^{\text{ave}}}{L_0 + L_0\hat{p}_0^{\text{ave}}t}X^j - \frac{L_0\hat{p}_0^{\text{ave}}}{\left(L_0 + L_0\hat{p}_0^{\text{ave}}t\right)^2}\left(X^j\right)^2. \tag{3.103}$$

Solving the Bernoulli equation (3.103), we find the average trajectories of the initial cells for the DLNCA model to be

$$X^j(t) = \frac{\left(L_0 + L_0\hat{p}_0^{\text{ave}}t\right)^2}{L_0\hat{p}_0^{\text{ave}}t + L_0^2/X_0^j}. \tag{3.104}$$

These continuum paths are plotted with 1000 simulations of the DLNCA model in Figure 3.16. Analysing Figure 3.16 we again observe non-uniform growth throughout the colony, as expected. We also note that the length of the colony is growing linearly.

3.3 Discussion

In this chapter, we have considered a number of generic cell proliferation scenarios applicable to yeast colonies, for which we have developed CA models. We have been able to approximate the continuum paths for the average positions of the initial cells in the colony.

There are many ways in which we can extend our CA models to explore various different cases. There are also many different ways in which we can develop our CA model. Appendix A describes an alternate framework for the CA model which only allows one proliferation event per time step. As the proliferation probability function p_τ^i can be arbitrarily defined, there are infinitely many cases that could be considered. Similarly, using

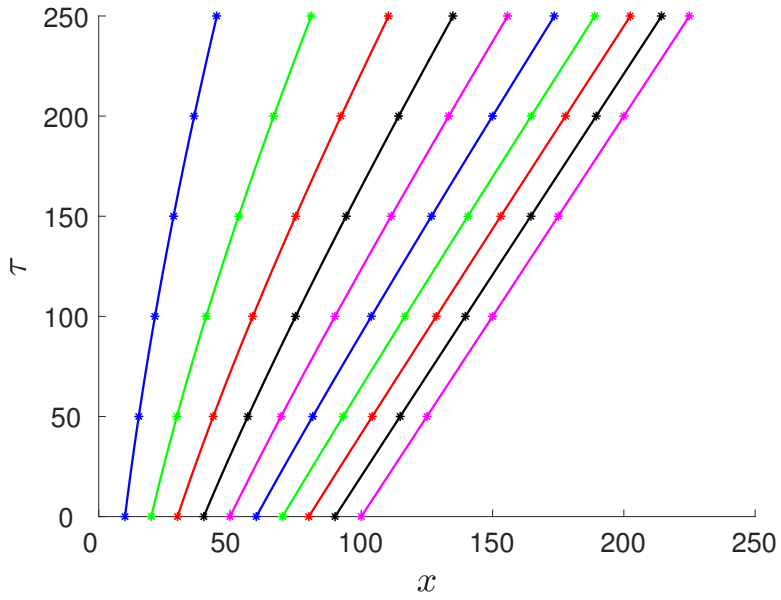

Figure 3.16: Average positions of the initial cells for the DLNCA with the continuum paths given by (3.104). These are the average results from 1000 simulations and $\mathcal{T} = 250$ time steps. The initial number of cells in the model is $N_0 = 1000$ and the cell width is $\Delta x = 0.1$. Thus the dimensional length of the colony is initially $L_0 = 100$ units. We, again, only chose to plot every 100th cell for brevity. We have set the value $S = 5$. This corresponds to an expected number of 5 cell insertions across the entire colony in each time step τ.

the alternate framework described in Appendix A, we can arbitrarily define a pdf $p(x,t)$ for the proliferation probabilities.

We have shown that we can derive a difference equation for any given proliferation probability function and hence we can find a numerical solutions for the average positions of initial cells. Furthermore, we have shown that we can take the continuum limits to derive an ODE and hence find a numerical or analytic solution to the continuum paths for the average trajectories of the initial cells. We may also wish to extend our analysis of quiescent cells to arbitrarily define the number of replicative cells $\mathcal{Z}_\tau$. Furthermore, we may wish to define multiple quiescent and replicative regions.

For the models explored in Sections 3.1 and 3.2, we highlight the accuracy of the continuum approximation for the average positions of the initial cells. For each of the uniform and non-uniform cases, the continuum approximation coincides with the average positions from simulations of the CA models. This is a very important result as it shows that results are accurate when making the continuum approximation if there is a suitably large number of cells. The continuum approximation is also a favourable approach as it takes far less computation time than running simulations of the CA model.

Based on our analysis, we have also identified the characteristics of growth within a colony. Furthermore, we have created a classification system for the type of growth in certain regions of a colony. The first classification is **uniform growth**. There are two conditions to determine whether uniform growth has occurred within a region. Firstly, we require proliferation to occur within the region. Thus, we require the average distances between adjacent initial cells to be increasing. Secondly, we require proliferation to be uniform across the colony. Thus, we expect the average distances between initially adjacent cells to be increasing uniformly across the region. Suppose we define the distance function $d_\tau^{n,i}$ to be the average distance between cells X_τ^i and X_τ^{i+n} at time step τ. Thus we have

$$d_\tau^{n,i} = X_\tau^{i+n} - X_\tau^i. \tag{3.105}$$

We note that the cells X_τ^i and X_τ^{i+n} are initially n cells apart. Thus, it will always be the case that $d_0^{n,i} = n\Delta x$. Hence, for uniform growth, it will be the case that

$$d_\tau^{n,i} = d_\tau^{n,j} \quad \text{for all } i,j,n,\tau, \tag{3.106a}$$

$$d_{\tau+1}^{n,i} > d_\tau^{n,i} \quad \text{for all } i,n,\tau. \tag{3.106b}$$

The second classification is **non-uniform growth**. We again require proliferation to occur within the region and thus require the average distances between adjacent initial cells to be increasing. However, we require proliferation to be non-uniform across the

colony. Thus we expect the average distances between initially adjacent cells to be different as the number of time steps increases. Thus, the conditions for non-uniform growth are

$$d_\tau^{n,i} \neq d_\tau^{n,j} \quad \text{for all } i, j, n, \tau, \tag{3.107a}$$

$$d_{\tau+1}^{n,i} > d_\tau^{n,i} \quad \text{for all } i, n, \tau. \tag{3.107b}$$

The last classification we have is **quiescent growth**. Quiescent 'growth' occurs in quiescent regions within the colony. It is characterised by no proliferation events occurring. Thus we expect the average distances between cells to stay the same for all time steps τ. Hence the condition for quiescent growth is

$$d_{\tau+1}^{n,i} = d_\tau^{n,i} \quad \text{for all } i, n, \tau. \tag{3.108}$$

We can use these to create a classification algorithm. Suppose we have some empirical data for the trajectories of initial cells in some colony exhibiting one-dimensional growth. This data can be obtained by labelling individual cells with unique fluorescent protein colour combinations (Di Talia & Poss 2016). Furthermore, we note that greeen fluorescent proteins (GFP) have previously been used as a marker for tumor cells to detect and predict single-cell behaviour (Zimmer 2002). Lastly, fluorescent ubiquination-based cell cycle indicators (FUCCI) have also been used to track cell progression (Vittadello et al. 2019).

Using the empirical data, we can determine the average distances between adjacent cells $d_\tau^{n,i}$. Hence we can analyse the average distances $d_\tau^{n,i}$ to classify regions of growth. This is outlined in Algorithm 2. This algorithm is purely a classification algorithm. However, we may still make some inference about the proliferation probabilities within the colony. If a region in the colony is classified as having quiescent growth, we know the proliferation probabilities in that region will be $p_\tau^i = 0$. Furthermore, if a region in the colony is classified as having uniform growth, we know the proliferation probabilities in that region will be some constant $p_\tau^i = p$. However, we do not know what the value of p will be. Lastly, we consider when a region in the colony is classified as having non-uniform growth. We cannot make any inference on the proliferation probabilities for these regions without applying further analysis on the empirical data. We may also use statistical analysis to determine the constant proliferation probability p for regions classified as having uniform growth. Algorithm 2 may be extended in the future to also predict the proliferation probabilities using statistical inference.

An alternate method for classifying growth is by analysing the nutrient concentration. If the instantaneous nutrient concentration is known, we can easily determine where quiescent and replicative cells are. If the local nutrient concentration is zero in a region of the

Algorithm 2: Growth Classification Algorithm

input : Import empirical data for trajectories of initial cells
output: Growth Classification for entire colony at all time steps τ

Select appropriate value for n;
// n is the initial number of cells between adjacent trajectories
// It is best to make n as small as possible
Calculate X_τ^j to be the average trajectories of initial cells;
Calculate $d_\tau^{n,i}$ to be the average distances between adjacent cells after τ time steps;
// $d_\tau^{n,i} = X_\tau^{i+n} - X_\tau^i$
Set $\mathcal{T}$ to be the final time step;
for $\tau = 1$ **to** $\mathcal{T}$ **do**
    foreach i **do**
        if $d_\tau^{n,i} = d_{\tau+1}^{n,i}$ **then**
            Set $x_1^\tau = X_\tau^i$;
            Set $x_2^\tau = X_\tau^{i+n}$;
            Classify region $[x_1^\tau, x_2^\tau]$ as quiescent growth;
        else
            if $d_\tau^{n,i} = d_\tau^{n,i+1}$ **then**
                Set $x_1^\tau = X_\tau^i$;
                Set $x_2^\tau = X_\tau^{i+2n}$;
                Classify region $[x_1^\tau, x_2^\tau]$ as uniform growth;
            else
                Set $x_1^\tau = X_\tau^i$;
                Set $x_2^\tau = X_\tau^{i+2n}$;
                Classify region $[x_1^\tau, x_2^\tau]$ as non-uniform growth;
            end
        end
    end
end

colony, the cells in that region will be quiescent and thus we have quiescent growth. Similarly, if the nutrient concentration is a constant across a region within the colony, the cells with in the region will be replicative and exhibit uniform growth. Lastly, if the nutrient concentration is non-constant across a region within the colony, the cells with in the region will be replicative and exhibit non-uniform growth. We may also use the instantaneous nutrient concentration to determine the instantaneous length of the replicative region, H.

The CA model provides an excellent understanding of the macroscopic properties of a cylindrical yeast colony. However, it requires that we specify a nutrient concentration at each time step. We wish to extend the CA model by coupling the nutrient concentration with the length of the colony. As we have shown that the continuum approximation is accurate and more time efficient, we choose to develop continuous models for the remainder of this thesis. Specifically we wish to develop a PDE model to couple nutrient concentration and colony length.

Chapter 4

Derivation of PDE Model for Non-Uniform Growth

In Chapter 2, we developed a CA model to describe non-uniform growth in microorganisms and discussed its applications to cylindrical yeast colonies. We note the assumptions and limitations of the CA model. Firstly, we made the assumption that the cells are incompressible and thus the colony exhibits constant cell density. We also note that the nutrient concentration is not coupled with tissue growth in the CA model. We wish to explore a model in which nutrient concentration is coupled with tissue growth. Furthermore, we wish to develop a model that can be applied to compressible systems.

It is also important to note that the continuum model was found to match the average behaviour of the CA model. This enables us to use techniques based on PDE theory, that cannot be applied to the stochastic model, to analyse the continuum model. Thus we wish to use a continuous partial differential equation (PDE) model for the remainder of this thesis. Specifically, we wish to use reaction–diffusion theory to explore the spatial patterns within biological systems. Crampin et al. (2002) has previously used reaction–diffusion models to predict pattern formation in systems with non-uniform growth. Lastly, we wish to apply the results to the cylindrical yeast colonies.

4.1 Derivation

We assume that we are modelling a system that contains only live cells. Furthermore, we assume that cell proliferation generates a velocity field that relates to domain growth (Neville et al. 2006). Cell proliferation is regulated by the presence of a nutrient diffusing through the colony. We assume that growth is restricted to one spatial dimension, as is the case for the cylindrical yeast colonies. We recall the cylindrical yeast colonies grow

vertically upwards and assume that the effect of gravity on the system is negligible.

As before we let t and x denote time and space, respectively, and let $L(t)$ be the length of the colony where $L(0) = L_0$. As we are only interested in the spatial patterns within the colony, we restrict our spatial variable to the domain $0 \leq x \leq L(t)$. The value $x = 0$ corresponds to the base of the colony and can be interpreted as the spatial position of the surface of the agar plate. Similarly, the value $x = L(t)$ refers to the spatial position of the length (or height) of the colony.

Similarly, the local nutrient concentration is given by $C(x,t)$ and the average trajectories of initial cells are given by $X^j(t)$ (as defined in Chapter 3). Suppose we define the variable $X(t)$ to be the pathlines of the individual cells where $X(0) = X_0$ is the initial position of the cell. This quantity is analogous to the average trajectory of the cell initially in position $X^j(0) = X_0$. We again use this to explore regions of uniform, non-uniform and quiescent growth. Furthermore, we can use the pathlines $X(t)$ to explore the spatial patterns and growth within a biological system. Lastly, we represent the local cell density by $\rho(x,t)$.

When deriving our governing equations, we assume a model in three spatial dimensions. We first consider local cell density ρ and how this is related to the local nutrient concentration C. From conservation of mass, we know the rate of change of the mass must be equal to the total flux of mass. In integral form, over an arbitrary fixed volume V, we write this as

$$\frac{d}{dt}\iiint_V \rho \, dV = -\iint_{\partial V} \boldsymbol{J}_\rho \cdot \hat{\boldsymbol{n}} \, dS + \iiint_V R(\rho, C) \, dV, \tag{4.1}$$

where $\boldsymbol{J}_\rho$ is the local flux of cells, $\hat{\boldsymbol{n}}$ is a unit normal for the surface ∂V and $R(\rho, C)$ is the local cell proliferation rate. We can then use Gauss' Divergence Theorem to show that

$$\frac{d}{dt}\iiint_V \rho \, dV = \iiint_V -\boldsymbol{\nabla} \cdot \boldsymbol{J}_\rho \, dV + \iiint_V R(\rho, C) \, dV. \tag{4.2}$$

As V is not changing in time, we may simplify to

$$\iiint_V \frac{\partial \rho}{\partial t} + \boldsymbol{\nabla} \cdot \boldsymbol{J}_\rho - R(\rho, C) \, dV = 0. \tag{4.3}$$

Since V is arbitrary, we must have that

$$\frac{\partial \rho}{\partial t} + \boldsymbol{\nabla} \cdot \boldsymbol{J}_\rho = R(\rho, C). \tag{4.4}$$

Lastly, we observe that there is both advection and diffusion contributing to the flux of cells. Thus, the flux will be given by

$$\boldsymbol{J}_\rho = \underbrace{\rho \boldsymbol{u}}_{\substack{\text{Flux due to} \\ \text{advection}}} - \underbrace{D_\rho \boldsymbol{\nabla} \rho}_{\substack{\text{Flux due to} \\ \text{diffusion}}}, \tag{4.5}$$

where D_ρ is a coefficient that represents the random motility of a cell and $\boldsymbol{u}$ is the advective cell velocity. The motility coefficient D_ρ is assumed to be constant throughout the colony. Substituting (4.5) into (4.4), we derive the reaction–diffusion–advection equation for cell density,

$$\frac{\partial \rho}{\partial t} + \boldsymbol{\nabla} \cdot [\rho \boldsymbol{u}] = D_\rho \nabla^2 \rho + R(\rho, C). \tag{4.6}$$

We now consider the evolution of local nutrient concentration $C(x,t)$ throughout the colony. We set the nutrient consumption to be $q(\rho, C) = \lambda \rho C$, where λ is the nutrient consumption rate. Then, by using the same arguments as above, we obtain the conservation of mass equation

$$\frac{\partial C}{\partial t} + \boldsymbol{\nabla} \cdot [\boldsymbol{u} C] = D_C \nabla^2 C - \lambda \rho C. \tag{4.7}$$

where D_C is the diffusion coefficient for the nutrient which is assumed to be constant throughout the colony. The reaction–diffusion–advection equations (4.6) and (4.7) have been derived to apply to three dimensions. As the cylindrical yeast colonies are restricted to grow in one dimension, we restrict our model to one spatial dimension. Thus the equations become

$$\frac{\partial C}{\partial t} + \frac{\partial [uC]}{\partial x} = D_C \frac{\partial^2 C}{\partial x^2} - \lambda \rho C, \tag{4.8a}$$

$$\frac{\partial \rho}{\partial t} + \frac{\partial [u\rho]}{\partial x} = D_\rho \frac{\partial^2 \rho}{\partial x^2} + R(\rho, C). \tag{4.8b}$$

Recall that our spatial variable is defined on the domain $0 \leq x \leq L(t)$. We assume that the tissue at the top of the colony $x = L(t)$ moves with the local cell velocity (Neville et al. 2006). Labelling the local velocity by $v(x,t)$, we may write this as

$$\frac{dL}{dt} = v|_{x=L(t)} \tag{4.9}$$

The local cell velocity relates to the flux of cells such that

$$J_\rho = \rho v. \tag{4.10}$$

Equating (4.5) and (4.10), we find that

$$v = u - \frac{D_\rho}{\rho}\frac{\partial \rho}{\partial x}. \tag{4.11}$$

Hence equating (4.9) and (4.11), we find that

$$\frac{dL}{dt} = \left[u - \frac{D_\rho}{\rho}\frac{\partial \rho}{\partial x}\right]\Bigg|_{x=L(t)}. \tag{4.12}$$

We can make a similar argument for the pathlines at $x = X(t)$. Noting that the pathlines move with local cell velocity, we can derive that

$$\frac{dX}{dt} = \left[u - \frac{D_\rho}{\rho}\frac{\partial \rho}{\partial x}\right]\Bigg|_{x=X(t)}. \tag{4.13}$$

We now consider boundary and initial conditions for nutrient concentration. Firstly, we know the cell velocity due to advection at the base of the tower will be zero and thus

$$u|_{x=0} = 0. \tag{4.14}$$

We also assume that there is a constant concentration of nutrient at the base of the tower, say $C|_{x=0} = C_0$, and there is no flux of nutrient at the top of the tower $C_x|_{x=L(t)} = 0$. As the nutrient is initially at the base of the tower and not diffusing throughout it, we impose the initial condition

$$C|_{t=0} = C_I(x) = \begin{cases} C_0 & \text{if } x = 0, \\ 0 & \text{else.} \end{cases}$$

Lastly, we impose an arbitrary initial condition for cell density such that $\rho|_{t=0} = \rho_I(x)$. Thus we have the full model

$$\frac{\partial C}{\partial t} + \frac{\partial \left[uC\right]}{\partial x} = D_C \frac{\partial^2 C}{\partial x^2} - \lambda \rho C, \tag{4.15a}$$

$$\frac{\partial \rho}{\partial t} + \frac{\partial \left[u\rho\right]}{\partial x} = D_\rho \frac{\partial^2 \rho}{\partial x^2} + R(\rho, C), \tag{4.15b}$$

$$\frac{dL}{dt} = \left[u - \frac{D_\rho}{\rho}\frac{\partial \rho}{\partial x}\right]\Bigg|_{x=L(t)}, \tag{4.15c}$$

with boundary and initial conditions

$$u|_{x=0} = 0, \tag{4.15d}$$

$$C|_{x=0} = C_0, \quad \left.\frac{\partial C}{\partial x}\right|_{x=L(t)} = 0, \tag{4.15e}$$

$$C|_{t=0} = C_I(x) = \begin{cases} C_0 & \text{if } x = 0, \\ 0 & \text{else,} \end{cases} \tag{4.15f}$$

$$\rho|_{t=0} = \rho_I(x), \tag{4.15g}$$

$$L|_{t=0} = L_0. \tag{4.15h}$$

where $x \in [0, L(t)]$ and $t \geq 0$. We note that this model is currently underspecified. At this stage, we have four dependent variables and only three equations. To fix this problem, we require a constitutive relation, which specifies the mechanical properties of the system. We follow Byrne & Chaplain (1997) by using Darcy's Law to relate the mechanical pressure, P, and advective cell velocity via,

$$\mathbf{u} = -\alpha \boldsymbol{\nabla} P, \tag{4.16}$$

where α is a constant related to the cell diffusivity. As our system is one-dimensional in space, Darcy's Law will be given by

$$u = -\alpha \frac{\partial P}{\partial x}. \tag{4.17}$$

Secondly, we must also define a pressure law that relates the pressure of the system to cell density, $\rho(x, t)$. For simplicity, we choose the linear relationship

$$P = \frac{\rho - \rho_0}{\beta}, \tag{4.18}$$

where ρ_0 is a constant pressure and β is a compressibility constant. The system is incompressible in the limit $\beta \to 0$. Hence, we note that the pressure law will have a singularity in the incompressible limit. This singularity ensures the cell path lines will not overlap (Hecht & Vauchelet 2017). We explore the incompressible limit further in Chapter 5. Lastly, we must define boundary conditions and initial conditions for the pressure. Our boundary condition for cell velocity (4.21f) now becomes

$$\left.\frac{\partial P}{\partial x}\right|_{x=0} = 0. \tag{4.19}$$

We also assume that the mechanical pressure at the top of the colony will be zero, so that

$$P|_{x=L(t)} = 0. \tag{4.20}$$

The full model can now be given by

$$\frac{\partial C}{\partial t} + \frac{\partial [uC]}{\partial x} = D_C \frac{\partial^2 C}{\partial x^2} - \lambda \rho C, \tag{4.21a}$$

$$\frac{\partial \rho}{\partial t} + \frac{\partial [u\rho]}{\partial x} = D_\rho \frac{\partial^2 \rho}{\partial x^2} + R(\rho, C), \tag{4.21b}$$

$$\frac{dL}{dt} = \left[u - \frac{D_\rho}{\rho}\frac{\partial \rho}{\partial x}\right]\Bigg|_{x=L(t)}, \tag{4.21c}$$

$$u = -\alpha \frac{dP}{dx}, \tag{4.21d}$$

$$\rho = \rho_0 + \beta P, \tag{4.21e}$$

with boundary and initial conditions

$$u|_{x=0} = 0, \tag{4.21f}$$

$$C|_{x=0} = C_0, \quad \left.\frac{\partial C}{\partial x}\right|_{x=L(t)} = 0, \tag{4.21g}$$

$$C|_{t=0} = C_I(x) = \begin{cases} C_0 & \text{if } x = 0, \\ 0 & \text{else,} \end{cases} \tag{4.21h}$$

$$\rho|_{t=0} = \rho_I(x), \tag{4.21i}$$

$$L|_{t=0} = L_0, \tag{4.21j}$$

$$\left.\frac{dP}{dx}\right|_{x=0} = 0, \quad P|_{x=L(t)} = 0. \tag{4.21k}$$

We now have five equations for five dependent variables. We also note our expression for the pathlines is given by Equation (4.13). Thus we are able to solve the system. However, we must first define a proliferation function $R(\rho, C)$. In Chapter 3, we used a proliferation rate defined by $\hat{p} = kC$ where k is a proportionality constant. We recall that for the CA model, there is a constant density assumed. We choose to use the proliferation function $R = k\rho C$, where k is a constant. We note that the rate of proliferation will be higher if the local cell density is higher.

4.1.1 Nondimensionalisation

To solve the model (4.21), we must nondimensionalise it. Firstly, we map the problem to a fixed spatial domain $\xi \in [0, 1]$ (Crank 1984) using the coordinate change

$$(x, t) \to (\xi, T) = \left(\frac{x}{L(t)}, t \right). \tag{4.22}$$

Using the chain rule, we observe that

$$\frac{\partial}{\partial x} = \frac{1}{L}\frac{\partial}{\partial \xi}, \tag{4.23a}$$

$$\frac{\partial^2}{\partial x^2} = \frac{1}{L^2}\frac{\partial^2}{\partial \xi^2}, \tag{4.23b}$$

$$\frac{\partial}{\partial t} = \frac{\partial}{\partial T} - \frac{\xi}{L}\frac{dL}{dT}\frac{\partial}{\partial \xi}, \tag{4.23c}$$

and thus the mapping (4.22) transforms the model (4.21) to

$$\frac{\partial C}{\partial T} + \frac{1}{L}\left(u - \xi\frac{dL}{dT}\right)\frac{\partial C}{\partial \xi} = \frac{D_C}{L^2}\frac{\partial^2 C}{\partial \xi^2} - \lambda\rho C - \frac{1}{L}\frac{\partial u}{\partial \xi}C, \tag{4.24a}$$

$$\frac{\partial \rho}{\partial T} + \frac{1}{L}\left(u - \xi\frac{dL}{dT}\right)\frac{\partial \rho}{\partial \xi} = \frac{D_\rho}{L^2}\frac{\partial^2 \rho}{\partial \xi^2} + k\rho C - \frac{1}{L}\frac{\partial u}{\partial \xi}\rho, \tag{4.24b}$$

$$\frac{dL}{dT} = \left[u - \frac{D_\rho}{\rho L}\frac{\partial \rho}{\partial \xi}\right]\Bigg|_{\xi=1}, \tag{4.24c}$$

$$u = -\frac{\alpha}{L}\frac{dP}{d\xi}, \tag{4.24d}$$

$$\rho = \rho_0 + \beta P, \tag{4.24e}$$

with boundary and initial conditions

$$u|_{\xi=0} = 0, \tag{4.24f}$$

$$C|_{\xi=0} = 1, \quad \left.\frac{\partial C}{\partial \xi}\right|_{\xi=1} = 0, \tag{4.24g}$$

$$C|_{T=0} = C_I(\xi) = \begin{cases} C_0 & \text{if } \xi = 0, \\ 0 & \text{else,} \end{cases} \tag{4.24h}$$

$$L|_{T=0} = L_0, \tag{4.24i}$$

$$\rho|_{T=0} = \rho_I(\xi), \tag{4.24j}$$

$$\left.\frac{dP}{d\xi}\right|_{\xi=0} = 0, \quad P|_{\xi=1} = 0. \tag{4.24k}$$

where $\xi \in [0,1]$ and $T \geq 0$. As the spatial variable has been mapped to the domain $[0,1]$, we require no further rescalings on ξ. We however note that there are two time scales we may use — the advective time scale $\hat{T}_{\text{adv}}$ or the diffusive time scale $\hat{T}_{\text{diff}}$. We define these by

$$\hat{T}_{\text{adv}} = \frac{1}{C_0 k}, \tag{4.25a}$$

$$\hat{T}_{\text{diff}} = \frac{L_0^2}{D_C}. \tag{4.25b}$$

We choose to scale time with the advective timescale. We also define the dimensionless Péclet number Pe by

$$Pe = \frac{\hat{T}_{\text{diff}}}{\hat{T}_{\text{adv}}} = \frac{C_0 k L_0^2}{D_C}. \tag{4.26}$$

We also define three more dimensionless parameters by

$$\hat{\lambda} = \frac{\lambda \rho_0}{C_0 k}, \tag{4.27a}$$

$$D = \frac{D_\rho}{D_C}, \tag{4.27b}$$

$$\hat{\beta} = \frac{\beta L_0^2}{\alpha C_0 k \rho_0}. \tag{4.27c}$$

We choose to scale the temporal variable with the advective timescale and all dependent variables with the scalings

$$T = \hat{T}_{\text{adv}}\tilde{T}, \quad C = C_0\tilde{C}, \quad L = L_0\tilde{L}, \quad X = L_0\tilde{X}, \quad \rho = \rho_0\tilde{\rho}, \quad u = \frac{L_0}{T_{\text{adv}}}\tilde{u}, \quad P = \hat{\pi}\tilde{P}. \tag{4.28}$$

Thus the system becomes

$$\frac{\partial C}{\partial T} + \left[\frac{u}{L} - \frac{\xi}{L}\frac{dL}{dT}\right]\frac{\partial C}{\partial \xi} = \frac{1}{Pe}\frac{1}{L^2}\frac{\partial^2 C}{\partial \xi^2} - \hat{\lambda}\rho C - \frac{1}{L}\frac{\partial u}{\partial \xi}C, \tag{4.29a}$$

$$\frac{\partial \rho}{\partial T} + \left[\frac{u}{L} - \frac{\xi}{L}\frac{dL}{dT}\right]\frac{\partial \rho}{\partial \xi} = \frac{D}{Pe}\frac{1}{L^2}\frac{\partial^2 \rho}{\partial \xi^2} + \rho C - \frac{1}{L}\frac{\partial u}{\partial \xi}\rho, \tag{4.29b}$$

$$\frac{dL}{dT} = \left[u - \frac{D}{Pe}\frac{1}{\rho L}\frac{\partial \rho}{\partial \xi}\right]\Bigg|_{\xi=1}, \tag{4.29c}$$

$$u = -\frac{1}{L}\frac{dP}{d\xi}, \tag{4.29d}$$

$$\rho = 1 + \hat{\beta}P, \tag{4.29e}$$

with boundary and initial conditions

$$u|_{\xi=0} = 0, \tag{4.29f}$$

$$C|_{\xi=0} = C_0, \quad \left.\frac{\partial C}{\partial \xi}\right|_{\xi=1} = 0, \tag{4.29g}$$

$$C|_{T=0} = C_I(\xi) = \begin{cases} 1 & \text{if } \xi = 0, \\ 0 & \text{else,} \end{cases} \tag{4.29h}$$

$$L|_{T=0} = 1, \tag{4.29i}$$

$$\rho|_{T=0} = \rho_I(\xi), \tag{4.29j}$$

$$\left.\frac{dP}{d\xi}\right|_{\xi=0} = 0, \quad P|_{\xi=1} = 0. \tag{4.29k}$$

where $\hat{\lambda} \geq 0$, $Pe \geq 0$, $D \geq 0$ and $\hat{\beta} \geq 0$. Note that all the variables are nondimensional but we have dropped the tildes for brevity. From the nondimensionalisation process, we find that the pressure scale must be given by

$$\hat{\pi} = \frac{L_0^2}{\alpha C_0 k}. \tag{4.30}$$

We also note that the equation for the pathlines will also be affected by the nondimensionalisation process. After performing the coordinate change (4.22) and applying the scalings (4.28) to Equation (4.13), we find the equation for the pathlines to be

$$\frac{dX}{dT} = \left[u - \frac{D}{Pe}\frac{1}{\rho L}\frac{\partial \rho}{\partial \xi}\right]\Bigg|_{\xi=\Xi}. \tag{4.31}$$

We again note that we have dropped the tilde for brevity. Lastly we note that $\Xi = X/L(t)$.

We now have a dimensionless system in terms of two dimensionless independent variables, five dimensionless dependent variables and four non–negative dimensionless parameters. The temporal variable, τ, must be non–negative and the spatial variable is restricted to the domain $0 \leq \xi \leq 1$. We also note that nutrient concentration C must always be non–negative and local cell density must be positive. Using Equation (4.29e), we can see that restricting $\rho > 0$ implies that pressure must satisfy, $p > -1/\hat{\beta}$. Lastly, we note that the cell velocity can be positive or negative. A positive cell velocity implies that the direction of travel is to the right and, conversely, a negative cell velocity implies the direction of travel is to the left.

4.2 Discussion

We have now developed a PDE model for coupled cell proliferation and nutrient concentration which consists of equations and boundary conditions given in (4.29). In general, this model must be solved numerically. We find numerical solutions to the model in Chapters 5 and 6. In Chapter 5, we also find analytic solutions to specific cases that relate to the solutions of the CA model.

The full model (4.29) is quite general and could be applied to a range of physical and biological phenomena. Depending on the application, we may wish to make further assumption on the model. Some systems do not exhibit domain growth and thus we may make the assumption that the length is fixed. Mathematically, we impose this by setting $L(t) \equiv L$. We may also wish to make the assumption that the cells are incompressible. We impose this mathematically by taking the limit $\hat{\beta} \to 0$. An immediate consequence of taking this incompressible limit will be constant cell density across the colony. This is evident from Equation (4.29e). We explore solutions to the model under these assumptions in Chapter 5. We also find solutions to the full model in Chapter 6

We also consider the physical meanings of the dimensionless parameters. The parameter $\hat{\beta}$ can be interpreted as a measure of the compressibility of the system. A large value for $\hat{\beta}$ implies that the system is highly compressible and, as previously discussed, the limit $\hat{\beta} \to 0$ implies that the system is incompressible. The parameter $\hat{\lambda}$ can be interpreted

as a measure of how the cells consume nutrient. A large value for $\hat{\lambda}$ implies that the nutrient consumption rate is high. Similarly, a small value for $\hat{\lambda}$ implies that the nutrient consumption rate is small.

The Péclet number Pe is a ratio between the advective nutrient transport rate and the diffusive nutrient transport rate. If the nutrient advection rate is much higher than the nutrient diffusion rate, the Péclet number will be larger. Conversely, if the nutrient diffusion rate is much higher than the nutrient advection rate, the Péclet number will be small. Lastly, the parameter D can be interpreted as the ratio between diffusion of cells and diffusion of nutrient. If the diffusion of cells is larger than the diffusion of nutrient, we expect D to be large. Conversely, if the diffusion of nutrient is much quicker than the diffusion of cells, we expect D to be small. By altering, these nondimensional parameters, we can find solutions to the model for a wide range of different applications.

For the specific case of the cylindrical yeast colonies, we make the incompressible assumption for simplicity and thus take the incompressible limit $\hat{\beta} \to 0$. Furthermore, an incompressible system implies that there is no diffusion of cells. Thus we set the diffusion scale to $D = 0$. We also expect the yeast cells to consume nutrient at a high rate. Thus we expect the nondimensional parameter $\hat{\lambda}$ to be large. Lastly, We expect the diffusive nutrient transport rate to be much higher than the advective nutrient transport rate. Thus we expect the Péclet number to be small. We explore solutions to this set and other sets of parameters in Chapter 5 and Chapter 6.

Chapter 5

Solutions to the Incompressible System

5.1 Model Assumptions

In this chapter, we consider the model in the case that the cells are incompressible. This corresponds to the limit $\hat{\beta} \to 0$. From Equation (4.29e), the incompressible limit implies that $\rho = 1$ and hence cell density is constant. This constant cell density coincides with the constitutive assumption made by Neville et al. (2006). An immediate consequence of constant density is that all the derivatives of ρ are equal to zero. Thus, we observe that Equation (4.29b) simplifies to

$$\frac{\partial u}{\partial \xi} = LC. \tag{5.1}$$

Using the boundary condition (4.29f), that says the advective cell velocity is zero at the base of the colony, we can rewrite Equation (5.1) as

$$u(\xi, T) = \int_0^{\xi} L(T)C(\xi^\star, T)\, d\xi^\star. \tag{5.2}$$

Equation (5.1) can also be interpreted as a mass conservation or continuity equation for this incompressible system. Typically, the continuity equation in fluid mechanics is $\boldsymbol{\nabla} \cdot \mathbf{u} = 0$. However, in our system mass is being created due to cell proliferation. Thus, the continuity equation for a general proliferation rule will be

$$\boldsymbol{\nabla} \cdot \mathbf{u} = \frac{1}{\rho} R(\rho, C). \tag{5.3}$$

This can be derived by assuming a constant ρ in Equation (4.6). Due to constant density, Equation (4.29c) simplifies to

$$\frac{dL}{dT} = u|_{\xi=1}\,. \tag{5.4}$$

This implies that the length of the colony travels with the advective cell velocity. Furthermore, this implies that the advective cell velocity is equal to the local cell velocity. We also note that Equation (4.31) for the pathlines $X(t)$ simplifies to

$$\frac{dX}{dT} = u|_{\xi=\Xi}\,. \tag{5.5}$$

Lastly, we observe that we now have only four unknown dependent variables. This is because the cell density is known to be constant. We note that it is redundant to calculate pressure in the incompressible model. This is because pressure only appears in one equation and is not used to calculate the other three dependent variables. Thus we choose to drop Equation (4.29d) from the model. Thus the full incompressible model can be written as

$$\frac{\partial C}{\partial T} + \left[\frac{u}{L} - \frac{\xi}{L}\frac{dL}{dT}\right]\frac{\partial C}{\partial \xi} = \frac{1}{Pe}\frac{1}{L^2}\frac{\partial^2 C}{\partial \xi^2} - \hat{\lambda} C - \frac{1}{L}\frac{\partial u}{\partial \xi} C, \tag{5.6a}$$

$$u = L\int_0^{\xi} C(\xi^\star, T)\, d\xi^\star, \tag{5.6b}$$

$$\frac{dL}{dT} = u|_{\xi=1}\,, \tag{5.6c}$$

with boundary and initial conditions

$$u|_{\xi=0} = 0, \tag{5.6d}$$

$$C|_{\xi=0} = 1, \quad \left.\frac{\partial C}{\partial \xi}\right|_{\xi=1} = 0, \tag{5.6e}$$

$$C|_{T=0} = C_I(\xi) = \begin{cases} 1 & \text{if } \xi = 0, \\ 0 & \text{else,} \end{cases} \tag{5.6f}$$

$$L|_{T=0} = 1. \tag{5.6g}$$

5.2 Solving on a Fixed Domain

To understand the dynamics of our nutrient transport problem, we wish to first solve the incompressible model (5.6) on a fixed domain. By restricting the domain to a fixed length, we expect to recover a reaction–diffusion equation. Solving on a fixed domain can also be used as a check to ensure our model is behaving as we expect. We fix the domain by setting $L(T) = 1$ for all values of T. This fixed domain implies that there is no cell proliferation in the colony and thus $R(\rho, C) = 0$. As a result, we use

$$\frac{\partial u}{\partial \xi} = 0. \tag{5.7}$$

in place of (5.6b) when solving on a fixed domain. Solving the continuity equation (5.7), we observe that $u(\xi, T) = c(T)$ where $c(T)$ is an arbitrary function of T. However, we know that $u(0, T) = 0$ from the boundary condition (4.29f) and thus $c(T) = 0$. Hence, the advective cell velocity is equal to 0 across the entire domain. This makes intuitive sense as there is no growth and thus no cell displacement due to advection. The expression $u = 0$ can also be substituted into Equation (5.6c) to derive that $dL/dt = 0$. This is expected as the length of the colony is not increasing nor decreasing. Using the fact that $L = 1$ and $u = 0$, we can simplify equation (5.6a) to find that

$$\frac{\partial C}{\partial T} = \frac{1}{Pe}\frac{\partial^2 C}{\partial \xi^2} - \hat{\lambda} C. \tag{5.8}$$

We recall that the nondimensional temporal variable $\tilde{T}$, used in (5.8), has been scaled by the advective time scale $\hat{T}_{\text{adv}}$. It does not make sense to use an advective time scale for the fixed domain as there is no advection. Thus we wish to rescale time with the diffusive time scale before solving (5.8). We can rescale time by the diffusive timescale by defining a new nondimensional temporal variable by

$$T' = Pe\tilde{T} = \hat{T}_{\text{diff}} T, \tag{5.9}$$

where $\tilde{T}$ is the dimensionless temporal variable scaled by $\hat{T}_{\text{adv}}$, T' is the dimensionless temporal variable scaled by $\hat{T}_{\text{diff}}$ and T is the dimensional temporal variable. Applying the rescaling (5.9) to equation (5.8), we can rescale time to find that

$$\frac{\partial C}{\partial T'} = \frac{\partial^2 C}{\partial \xi^2} - \mu^2 C, \tag{5.10}$$

where μ^2 is a nondimensional constant defined by

$$\mu^2 = Pe\hat{\lambda} = \frac{\lambda L_0^2 \rho_0}{D_C}. \tag{5.11}$$

From here onwards, we drop the apostrophe in our temporal variable T' for brevity. We wish to solve (5.10) subject to the boundary and initial conditions

$$C|_{\xi=0} = 1, \quad \left.\frac{\partial C}{\partial \xi}\right|_{\xi=1} = 0, \tag{5.12a}$$

$$C|_{T=0} = C_I(\xi) = \begin{cases} 1 & \text{if } \xi = 0, \\ 0 & \text{else.} \end{cases} \tag{5.12b}$$

To solve Equation (5.10) we write the nutrient concentration as

$$C(\xi, T) = C_E(\xi) + \bar{C}(\xi, T), \tag{5.13}$$

where $C_E(\xi)$ is the equilibrium solution. The equilibrium solution can be found by setting $\partial C/\partial T = 0$ in Equation (5.10). Thus we find $C_E(\xi)$ by solving the ODE

$$\frac{\partial^2 C_E}{\partial \xi^2} - \mu^2 C_E = 0, \tag{5.14a}$$

subject to the boundary conditions

$$C|_{\xi=0} = 1, \quad \left.\frac{\partial C}{\partial \xi}\right|_{\xi=1} = 0. \tag{5.14b}$$

Hence we find that the equilibrium solution is

$$C_E(\xi) = \frac{1}{\cosh \mu} \cosh\left[\mu\left(1 - \xi\right)\right]. \tag{5.15}$$

By substituting the expression (5.13) into the PDE (5.10) and conditions (5.12), we can derive the PDE

$$\frac{\partial \bar{C}}{\partial T} = \frac{\partial^2 \bar{C}}{\partial \xi^2} - \mu^2 C, \tag{5.16a}$$

and boundary and initial conditions

$$\bar{C}\big|_{\xi=0} = 0, \quad \left.\frac{\partial \bar{C}}{\partial \xi}\right|_{\xi=1} = 0, \tag{5.16b}$$

$$\bar{C}\big|_{T=0} = C_I(\xi) - C_E(\xi). \tag{5.16c}$$

Hence we find the solution for $\bar{C}$ to be

$$\bar{C}(\xi, T) = \sum_{n+1}^{\infty} A_n \sin\left[\left(n - \frac{1}{2}\right)\pi\xi\right] \exp\left\{-\left[\left(n + \frac{1}{2}\right)^2 \pi^2 - \mu^2\right] T\right\} \tag{5.17}$$

where A_n are Fourier coefficients defined by

$$A_n = 2\int_0^1 \left[C_I(\xi^\star) - \frac{1}{\cosh\mu}\cosh\left[\mu\left(1-\xi^\star\right)\right]\right] \sin\left[\left(n - \frac{1}{2}\right)\pi\xi^\star\right] d\xi^\star. \tag{5.18}$$

Thus the nutrient concentration will be given by

$$\begin{aligned} C(\xi, T) =& \frac{1}{\cosh\mu}\cosh\left[\mu\left(1-\xi\right)\right] \\ &+ \sum_{n+1}^{\infty} A_n \sin\left[\left(n - \frac{1}{2}\right)\pi\xi\right] \exp\left\{-\left[\left(n + \frac{1}{2}\right)^2 \pi^2 - \mu^2\right] T\right\} \end{aligned} \tag{5.19}$$

where $0 \leq \xi \leq 1$ and $T \geq 0$. We focus on the equilibrium distribution $C_E(\xi)$ and how the nondimensional parameter μ^2 affects it. The equilibrium distribution is plotted for varying μ^2 in Figure 5.1. Firstly, we consider the case when $\mu^2 \to 0$. This implies that the nutrient diffusion rate D_C is much larger than the nutrient consumption rate λ, the density ρ_0 and the colony length L_0. Equivalently, $\mu^2 \to 0$ implies that $Pe \to 0$ or $\hat{\lambda} \to 0$. Substituting the limit $\mu^2 \to 0$ into (5.15) we find that

$$\lim_{\mu^2 \to 0} C_E = 1. \tag{5.20}$$

Thus a sufficiently large nutrient diffusion rate D_C or sufficiently small nutrient consumption rate λ will result in a constant nutrient concentration across the colony. This is visualised in Figure 5.1. This nutrient concentration coincides with the uniform growth CA models discussed in Chapter 3.1. We now consider the case where the nutrient diffusion rate D_C is much smaller than the nutrient consumption rate λ, the cell density ρ_0

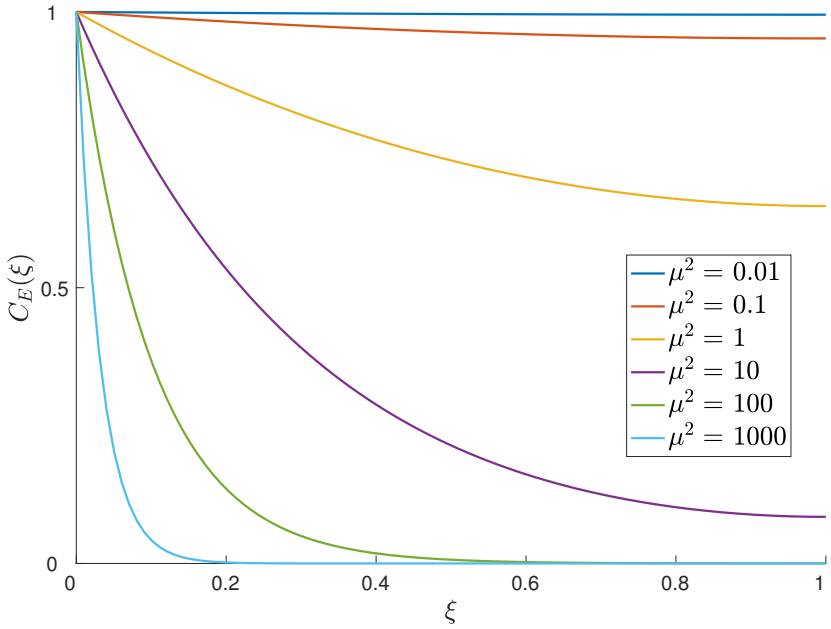

Figure 5.1: Equilibrium distribution of (5.10) subject to (5.12) for varying μ^2. The equilibrium distribution is given by Equation (5.15). In the limit $\mu^2 \to 0$, the equilibrium distribution is given by (5.20) and in the limit $\mu^2 \to \infty$, it is given by (5.22).

and the colony length L_I. We explore this by taking the limit $\mu^2 \to \infty$. We note that $\mu^2 \to \infty$ implies that $Pe \to \infty$ and/or $\hat{\lambda} \to \infty$. Substituting this limit into the ODE (5.14a), we find that

$$\varepsilon \frac{d^2 C_E}{dx^2} - C_E = 0, \tag{5.21}$$

where $\varepsilon = 1/\mu^2 \ll 1$. Hence we have a boundary layer problem. Solving (5.21) subject to the boundary conditions (5.14b) we find that

$$\lim_{\mu^2 \to \infty} C_E = e^{-\mu \xi}. \tag{5.22}$$

We may also interpret this as

$$\lim_{\mu^2 \to \infty} C_E \to \begin{cases} 1 & \text{if } \xi = 0, \\ 0 & \text{otherwise.} \end{cases} \tag{5.23}$$

Thus a sufficiently small nutrient diffusion rate D_C or sufficiently large nutrient consumption rate λ will result in a monotonically decreasing nutrient concentration. Furthermore, as the parameter μ is large, we expect the nutrient concentration to decrease to zero near the bottom of the colony. We observe this in Figure 5.1. Thus there will be a region of quiescent cells at the top of the colony. This is similar to the LNCA-Q models in Chapter 3.2. We also recall the predicted nutrient distribution from the cylindrical yeast colonies (Vulin et al. 2014). This looks similar to our equilibrium distribution when μ^2 is large.

5.3 Solving on a Growing Domain

5.3.1 Solving with Specified Nutrient Concentration

Before solving the full incompressible model (5.6), we wish to relate it back to the CA model. In Chapter 3, we ran simulations of a CA model with a specified nutrient concentration and found the average trajectories of the initial cells. We wish to explore whether we can derive similar pathlines for the initial cells using the PDE model. By substituting Equation (5.6b) into Equation (5.5), the pathlines can be found by solving

$$\frac{dX}{dt} = L \int_0^{\Xi} C(\xi^\star, T)\, d\xi^\star. \tag{5.24}$$

Suppose we specify a constant nutrient concentration $C(\xi, T) = 1$. Upon noting that $\Xi L = X$, we can substitute the constant nutrient concentration into Equation (5.24) to derive

$$\frac{dX}{dt} = X. \tag{5.25}$$

Hence we find that the pathlines are given by

$$X = X_0 e^t, \tag{5.26}$$

where X_0 is the initial location of the cell. We recall that the temporal variable is dimensionless and scaled by the advective time scale $\hat{T}_{\text{adv}} = 1/kC_0$. Hence, converting back into dimensional time, we find that

$$X = X_0 e^{kC_0 t} \tag{5.27}$$

where k is a proliferation rate constant and C_0 is the dimensional concentration at $x = 0$ (or equivalently $\xi = 0$). We also recall that the proliferation rate is defined as $\hat{p} = kC$, where C is the dimensional nutrient concentration. For the constant nutrient concentration we observe that $\hat{p} = kC_0$. Thus the pathlines will be

$$X = X_0 e^{\hat{p}t}. \tag{5.28}$$

This is equivalent to the average trajectories for the CNCA model (Equation (3.7)) derived in Chapter 3. We can also derive the average trajectories for the LNCA model using this PDE model. Suppose we specify the nutrient concentration to be $C(\xi, T) = 1 - \xi$. This is a linearly decreasing function where nutrient concentration is largest at the base of the colony and zero at the top of the colony. Thus we can simplify Equation (5.24) to

$$\frac{dX}{dt} = X - \frac{X^2}{2L}. \tag{5.29}$$

Converting this into dimensional time, we find that

$$\frac{dX}{dt} = kC_0 X - \frac{kC_0}{2}\frac{X^2}{L}. \tag{5.30}$$

Recall that $\hat{p}_{\max}$ is the proliferation rate at the top of the colony and $\hat{p}_{\min}$ is the proliferation rate at the base for the colony. We observe that $\hat{p} = kC_0(1 - \xi)$ for the linearly

decreasing nutrient concentration and thus $\hat{p}_{\max} = kC_0$ and $\hat{p}_{\min} = 0$. Hence we can re-write the ODE as

$$\frac{dX}{dt} = \hat{p}_{\max} X - \frac{\hat{p}_{\max} - \hat{p}_{\min}}{2} \frac{X^2}{L}. \tag{5.31}$$

This is equivalent to the ODE for the average trajectories for the LNCA (Equation (3.54)). We can derive the average trajectories for each of the other CA models by specifying an equivalent nutrient concentration in the PDE model. Furthermore, we have found a link between the CA model and the PDE model.

5.3.2 Solving for Unspecified Nutrient Concentration

We now wish to find solutions to the full incompressible model (5.6) for a general nutrient concentration. Substituting Equation (5.1) into the Reaction–Diffusion–Advection PDE (5.6a), we can re-write it as

$$\frac{\partial C}{\partial T} + \underbrace{\left[\frac{u}{L} - \frac{\xi}{L}\frac{dL}{dT}\right]\frac{\partial C}{\partial \xi}}_{\text{Advection Term}} = \underbrace{\frac{1}{Pe}\frac{1}{L^2}\frac{\partial^2 C}{\partial \xi^2}}_{\text{Diffusion Term}} - \underbrace{\hat{\lambda} C - C^2}_{\substack{\text{Non–Linear} \\ \text{Source Term}}}. \tag{5.32}$$

We wish to numerically solve Equations (5.32), (5.6b) and (5.6c). We use an upwinding scheme to deal with the advection term in Equation (5.32). We also use an implicit Euler method for time stepping with Picard linearisation for the non-linear term. Lastly, we use the cumulative trapezoidal rule for equation (5.6b) and a first order approximation for (5.6c). We can also use a first order approximation for Equation (5.5) to solve for the pathlines. We solve the system (5.6) using Algorithm 3.

The incompressible model has two nondimensional parameters $\hat{\lambda}$ and Pe that may vary. The parameter $\hat{\lambda}$ is similar to the the parameter μ^2 as defined in Section 5.2. A small value for $\hat{\lambda}$ implies that the nutrient consumption rate λ is small. After running simulations of Algorithm 3 for different values of $\hat{\lambda}$, we find that the nutrient travels further up the colony as $\hat{\lambda} \to 0$. However, unlike the fixed domain case with $\mu^2 \to 0$, the nutrient concentration is not necessarily uniform as $T \to \infty$. This is because the length of the domain is growing and the unlimited nutrient supply cannot necessarily reach the end of the domain. The nutrient concentration can only remain approximately uniform if the nutrient spread is sufficiently fast and the consumption rate is sufficiently small. As a result, the nutrient concentration is monotonically decreasing. We also observe that the nutrient concentration is monotonically decreasing at all times when $\hat{\lambda}$ is large. This is because a large value for $\hat{\lambda}$ implies the nutrient consumption rate is large and thus the

Algorithm 3: Numerical Scheme to find solutions for the incompressible system (5.6).

```
Set a fixed number of time steps as 𝒯;
Initialise the nutrient concentration C_I;
Initialise the colony length L_I;
Initialise the pathlines X_I;
Calculate the advective velocity u_I, using L_I and C_I;
for i = 1 to 𝒯 do
    Calculate colony length at next iteration L_i, using u_{i−1};
    Calculate pathlines at next iteration X_i, using u_{i−1};
    Calculate nutrient concentration at next iteration C_i, using L_i and u_{i−1};
    Calculate advective velocity at next iteration u_i, using L_i and C_i;
end
```

nutrient will not be able to travel as far up the colony. These results for a varying $\hat{\lambda}$ are illustrated in Figure 5.2.

From Figure 5.2, we can also see a large difference in the lengths. The length appears to be growing much quicker when $\hat{\lambda}$ is small. This is exactly as expected. We recall that a small value for $\hat{\lambda}$ implies that the nutrient consumption rate is small. When the nutrient consumption rate is small, we expect a larger nutrient concentration. As the proliferation rule is given by $R(\rho, C) = k\rho C$, we expect more cell proliferation events for a larger nutrient concentration. Thus the length L will grow quicker for smaller values of $\hat{\lambda}$. This can also be seen in Figure 5.4.

Lastly, we observe that we have used the value $Pe = 0.01$. A small Péclet number implies that the rate of diffusion is much larger than the rate of advection. Thus we expect our nutrient to diffuse throughout the domain before the length of the domain has drastically increased. From Figure 5.2, we observe the time lapse concentrations for $t = 0.05$ and how these relate to the equilibrium distributions for the fixed domain case (Figure 5.1). We recall that $\mu^2 = Pe\hat{\lambda}$. Thus the values $Pe = 0.01$ and $\hat{\lambda} = 0.01$ correspond to a value of $\mu^2 = 0.0001$ and $Pe = 0.01$ and $\hat{\lambda} = 100$ correspond to a value of $\mu^2 = 1$. For $\mu^2 = 0.0001$, the equilibrium nutrient distribution for the fixed domain will be almost constant. From Figure 5.2, we observe that the nutrient concentration for $Pe = 0.01$ and $\hat{\lambda} = 0.01$ is approximately constant at $t = 0.05$. Similarly we observe that the nutrient concentration for $Pe = 0.01$ and $\hat{\lambda} = 100$ at $t = 0.05$ is similar to the equilibrium nutrient distribution for $\mu^2 = 1$. Hence the nutrient diffuses to approximately the equilibrium distribution before the colony starts to grow. This is what we expect for a small Péclet number.

We now wish to explore the effects of that varying the Péclet number. Figure 5.3 shows time lapse images of the nutrient concentration for a small and large Péclet number. We

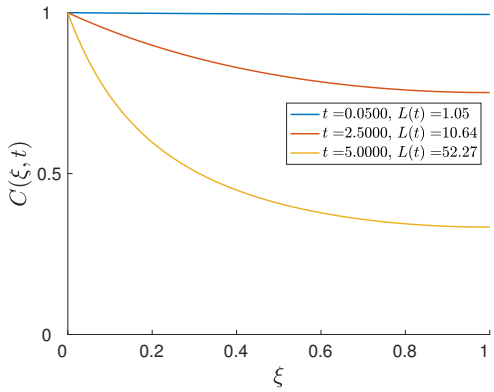

(a) Evolution of nutrient concentration for $\hat{\lambda} = 0.01$.

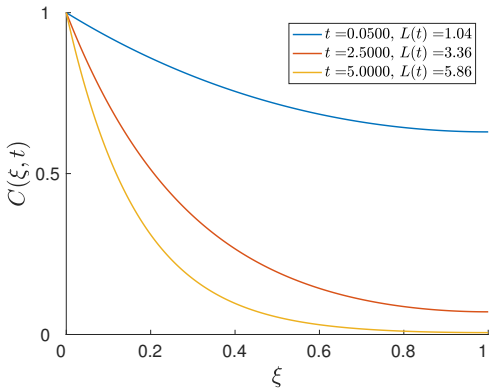

(b) Evolution of nutrient concentration for $\hat{\lambda} = 100$.

Figure 5.2: Numerical solutions of the nutrient concentration for the incompressible case with Péclet number $Pe = 0.01$ and varying $\hat{\lambda}$. These solutions were simulated using Algorithm 3. We recall that the initial condition for the nutrient concentration is given in equation (4.29h).

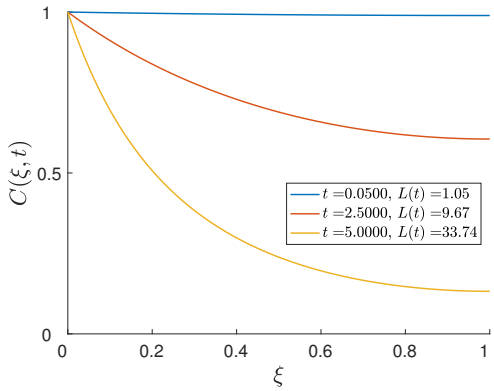

(a) Evolution of nutrient concentration for $Pe = 0.01$.

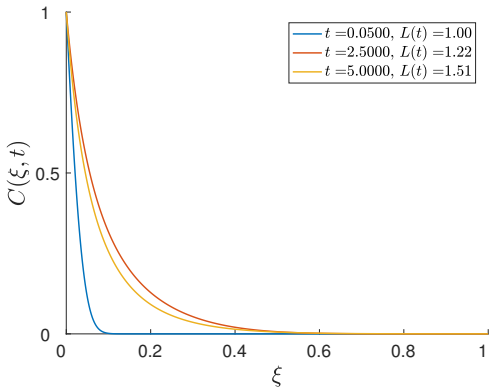

(b) Evolution of nutrient concentration for $Pe = 100$.

Figure 5.3: Numerical solutions of the nutrient concentration for the incompressible case with $\hat{\lambda} = 1$ and varying Pe. These solutions were simulated using Algorithm 3. We recall that the initial condition for the nutrient concentration is given in equation (4.29h).

can see that the nutrient does not travel as far up the colony when the Péclet number is larger. As the nutrient is not travelling as far up the colony, the total nutrient concentration is smaller and thus the cell proliferation rate is smaller. Hence the length of the colony grows faster when the Péclet number is smaller. This can also be seen in Figure 5.4.

We can also numerically simulate the pathlines in the system using Algorithm 3. The pathlines are analogous to the continuum paths for the trajectories of the initial cells. The results for varying Pe and $\hat{\lambda}$ are illustrated in Figure 5.4. We also numerically evaluate the instantaneous size of the replicative region H. In Chapter 2 we assumed that quiescent cells occur when the local nutrient concentration is zero. In the continuum model C may never reach zero, so we impose that quiescent cells occur when the nutrient concentration is below a tolerance, θ. Thus we can determine H by examining when the nutrient concentration C has dropped below the tolerance. The function H is illustrated by a black dotted line in Figure 5.4 and was calculated using a tolerance of $\theta = 10^{-3}$.

Analysing Figure 5.4 we notice that the colonies tend to exhibit non-uniform growth in the replicative region with a majority of proliferation occurring near the base of the colony. This is expected as nutrient concentration is largest at the base of the colony. We also observe that quiescent growth appears to be occurring in the numerically evaluated quiescent region. This confirms that our numerical solution for H is an accurate approximation for the length of the replicative region.

We recall that the evolution of the size of the replicative region H affects the growth of the colony. If the size of the replicative region is growing, we expect to see exponential growth. We also expect to see exponential growth if there are no quiescent cells. Conversely, we expect linear growth if the size of the replicative region is fixed. We observe that there are no quiescent cells in Figures 5.4a, 5.4b, 5.4c and thus approximately exponential growth in the colony. In Figure 5.4f we observe that the size of the replicative region is fixed and thus growth is linear. Figures 5.4d and 5.4e display more unique results. The size of the replicative region H is initially increasing but tends to a fixed value as t gets large. As a result, the colony starts to grow approximately exponentially for early times but appears to be growing approximately linearly as t gets large.

We also observe a small kink in the solution for H in Figure 5.4e. A similar kink occurs in Figures 5.5 and 5.6. The kink occurs when the solution for H transitions from the length of the colony to a fixed value. It can be viewed as a correction as H is transitioning between two solutions. We expect to only see this kink in the mathematical model as there is no experimental evidence of its existence.

Despite the domain growth, we have numerically shown that the size of replicative region remains fixed for some parameter values. This is a useful result for understanding why some biological systems, including the cylindrical yeast colonies, grow linearly. We have

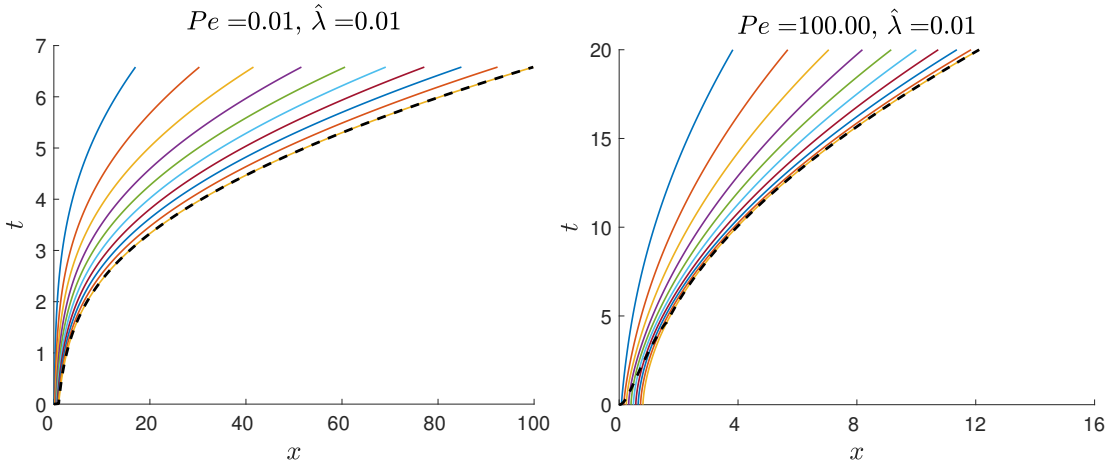

(a) $Pe = 0.01$, $\hat{\lambda} = 0.01$ (b) $Pe = 100$, $\hat{\lambda} = 0.01$

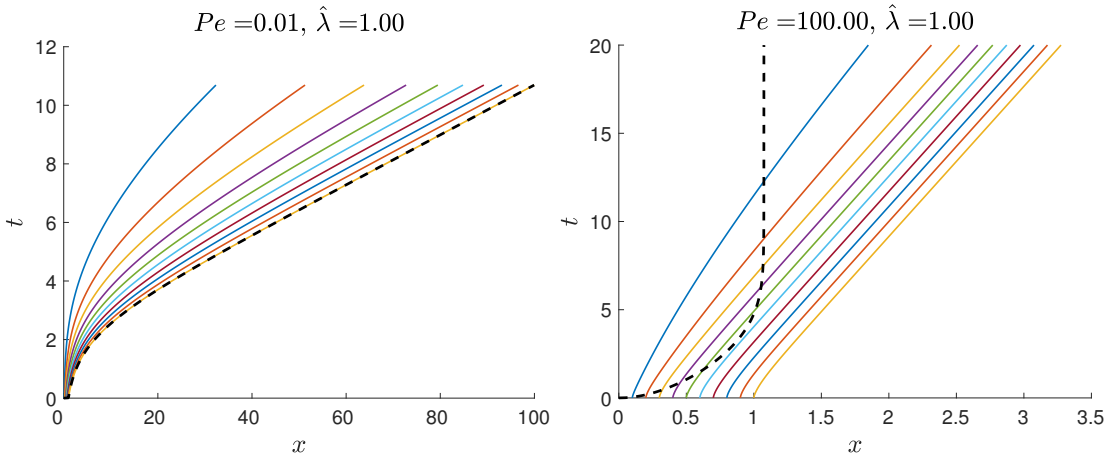

(c) $Pe = 0.01$, $\hat{\lambda} = 1$ (d) $Pe = 100$, $\hat{\lambda} = 1$

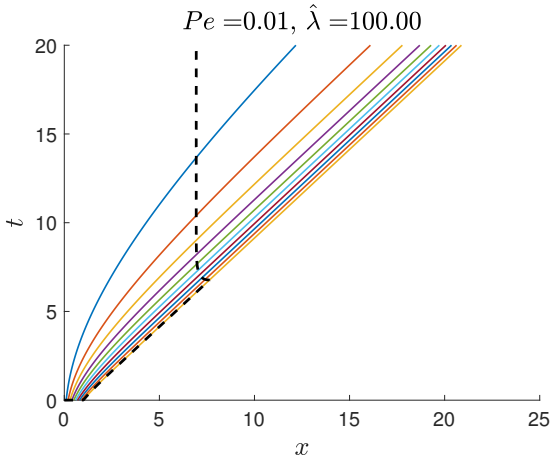

(e) $Pe = 0.01$, $\hat{\lambda} = 100$ (f) $Pe = 100$, $\hat{\lambda} = 100$

Figure 5.4: The Pathlines $X(t)$ of the incompressible system for varying parameter values. These results were numerically simulated using Algorithm 3. We ran these simulations until $t = 20$ or $L = 100$. The dotted line in each plot illustrates the numerical approximation to the function $H(t)$. The cells to the left of the dotted line are replicative and the cells to the right of the dotted line are quiescent. We note the axes are scaled differently for each plot.

noted that there are no quiescent cells for the simulations illustrated in Figures 5.4a, 5.4b, 5.4c. Hence the size of the replicative region is equivalent to the length of the colony. However, we wish to explore the size of the replicative region as $t \to \infty$. We are particularly interested in whether the size of the replicative region will eventually tend to a constant value (similar to Figures 5.4d and 5.4e). Consider the governing equation for nutrient concentration (5.32). If we assume $Pe \to 0$ and write (5.32) in terms of the Eulerian spatial variable x, we find that

$$\frac{\partial^2 C}{\partial x^2} = \mu^2 C, \tag{5.33}$$

where $C = 1$ at $x = 0$, $C_x = 0$ at $x = L(t)$ and $\mu^2 = Pe\hat{\lambda}$. Solving (5.33) subject to these mixed boundary conditions, we find that

$$C(x,t) = \frac{1}{\cosh(\mu L)} \cosh\left[\mu\left(L - x\right)\right]. \tag{5.34}$$

We observe that (5.34) is a monotonically decreasing function on the domain $0 \leq x \leq L(t)$. Recall that we have imposed that cells are replicative when $C > \theta$ and quiescent when $C < \theta$. Hence the value of H will be the spatial position where the nutrient concentration C is equal to the tolerance θ. Setting $C(H,t) = \theta$ in Equation (5.34), we may rearrange to derive that

$$H = L - \frac{1}{\mu} \cosh^{-1}\left(\theta \cosh \lambda L\right). \tag{5.35}$$

There is no explicit time dependence in Equation (5.35). However, as we are solving on a growing domain, the length is a monotonically increasing function and thus $L \to \infty$ as $t \to \infty$. Hence we may take the limit $L \to \infty$ to approximate the behaviour of H as t gets large. Noting for a fixed λ, that

$$\cosh \lambda L \to \frac{1}{2}\lambda L, \tag{5.36}$$

as L gets large and

$$\cosh^{-1} z \to \ln 2z, \tag{5.37}$$

as z gets large, we find that

$$H_A = \lim_{L\to\infty} H = -\frac{1}{\mu}\ln\theta, \tag{5.38}$$

where H_A is the analytic approximation for H. As $\mu^2 = Pe\hat{\lambda}$ and we have used $\theta = 10^{-3}$, we can re-write (5.38) as

$$H_A(Pe,\hat{\lambda}) = \lim_{L\to\infty} H = \frac{3}{\sqrt{Pe\hat{\lambda}}}\ln 10. \tag{5.39}$$

Although we have assumed $Pe \to 0$ in the derivation of (5.39), we may still use it as an approximation for H when Pe is large.

Evaluating Equation (5.39) for $Pe = 0.01$ and $\hat{\lambda} = 100$, we find that $H_A \approx 6.91$. Comparing this approximation with Figure 5.4e, we observe that the numerical solution tends to approximately $H = 6.91$. Thus the analytic approximation $H_A = 6.91$ is accurate for this set of parameters. We further extend our analysis to the numerical solutions for $Pe = 0.01$ & $\hat{\lambda} = 1$ and $Pe = 0.01$ & $\hat{\lambda} = 0.01$. While some of the plots shown in Figure 5.4 have not yet reached a steady state for H, running the simulation further shows that H in Figure 5.4a will tend to $H_A(0.01, 0.01) \approx 690.78$ and H in Figure 5.4c will tend to $H_A(0.01, 1) \approx 69.08$.

5.3.3 Application to Cylindrical Yeast Colonies

As discussed in Chapter 4, we assume that the cells within the cylindrical yeast colonies are incompressible and the nutrient diffuses throughout the colony at a much faster rate than the colony grows. Thus, the advective transport rate is much smaller than the diffusive transport rate. Hence we expect the Péclet number to be small. The yeast cells are also expected to readily consume nutrient. Thus we expect the value for $\hat{\lambda}$ to be large. We approximate this behaviour by setting the parameter values to $Pe = 0.01$ and $\hat{\lambda} = 1000$. We can justify this choice by using the known values from Vulin et al. (2014) for a colony with diameter 1.5mm. We recall that the Péclet number can be written as

$$Pe = \frac{L_0^2}{D_C\hat{T}_{\text{adv}}}, \tag{5.40}$$

where $L_0 = 2\times10^{-4}$ m is the initial length of the colony, $\hat{T}_{\text{adv}}$ is the advective time scale and D_C is the diffusivity of the nutrient. From the supporting material of Vulin et al. (2014), we find that the measured diffusion of glucose (nutrient) through yeast layers is

$$D_C = 1.44\times10^{-10}\text{m}^2\text{s}^{\text{-}1} = 5.184\times10^{-7}\text{m}^2\text{h}^{\text{-}1}. \tag{5.41}$$

We also note that the linear growth rate of the cylindrical yeast colonies was found to be $\gamma = 0.021$ mmh^{-1}. As the length of the nondimensional simulations for $Pe = 0.01$ and $\hat{\lambda} = 1000$ is growing at approximately 0.0633 mm per unit time, we set the advective time scale to be $\hat{T}_{\text{adv}} = 3.014$ h. Thus the Péclet number is evaluated to be

$$Pe = \frac{2 \times 10^{-8}}{3.014 \times 5.184 \times 10^{-7}} = \frac{2 \times 10^{-8}}{1.56 \times 10^{-6}} \approx 10^{-2}. \tag{5.42}$$

Thus $Pe = 0.01$ is an accurate approximation for the Péclet number. We can make a similar argument for $\hat{\lambda}$. Recall that the nondimensional nutrient consumption rate can be given

$$\hat{\lambda} = \lambda \rho_0 \hat{T}_{\text{adv}}, \tag{5.43}$$

where λ is the nutrient consumption rate, ρ_0 is the density scale and $\hat{T}_{\text{adv}}$ is the advective time scale. Recall, from our derivation in Chapter 4, that the nutrient consumption function is given by $q(\rho, C) = \lambda \rho C$. As density is constant in the incompressible model, we have $\rho(x, t) = \rho_0$. Hence we can re write Equation (5.43) as

$$\hat{\lambda} = \frac{q(\rho_0, C_0)\hat{T}_{\text{adv}}}{C_0}. \tag{5.44}$$

We use a value of $q = 5.48$ mol m^{-3}s^{-1}= 19728 mol m^{-3}h^{-1} (Vulin et al. 2014, Youk & van Oudenaarden 2009) and recall that $\hat{T}_{\text{adv}} = 3.014$ h. We also set the nutrient concentration at the base of the colony as $C_0 = 44.4$ mM. This value corresponds to an experiment where the nutrient delivery into the agar gel has a glucose concentration of $C_{\text{del}} = 111$ mM and we assume the concentration at the base is 40% of the agar gel concentration. We choose to use 40% as Vulin et al. (2014) found that the concentration at the base of the colony was in the order of at least 40% of C_{del}. Using these values, we can evaluate Equation (5.44) to find that

$$\hat{\lambda} = 1.34 \times 10^3 \approx 10^3. \tag{5.45}$$

Thus, we use $\hat{\lambda} = 10^3$ as an approximation for the nondimensional nutrient consumption rate. The numerically simulated pathlines for these parameter values are illustrated in Figure 5.5.

We recall that the cylindrical yeast colonies were found to exhibit linear growth in time (Vulin et al. 2014). Observing Figure 5.5, there are initially no quiescent cells in the colony. However, a majority of the nutrient concentration is at the base of the colony. As

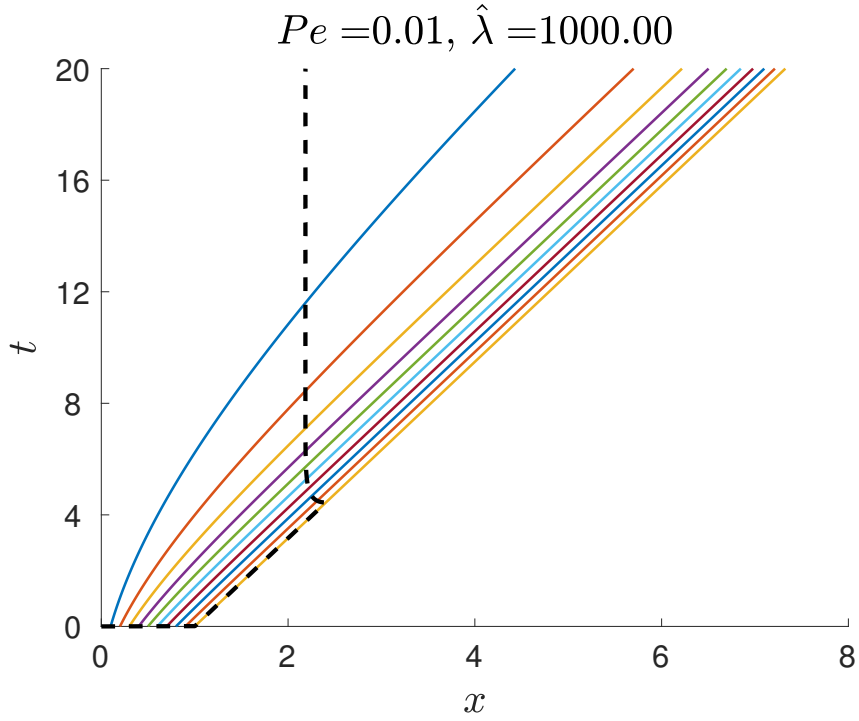

Figure 5.5: The pathlines for the incompressible model with parameters $Pe = 0.01$ and $\hat{\lambda} = 1000$. The dotted line represents the size of the replicative region. This set of parameters is used to predict cell behaviour in the cylindrical yeast colonies.

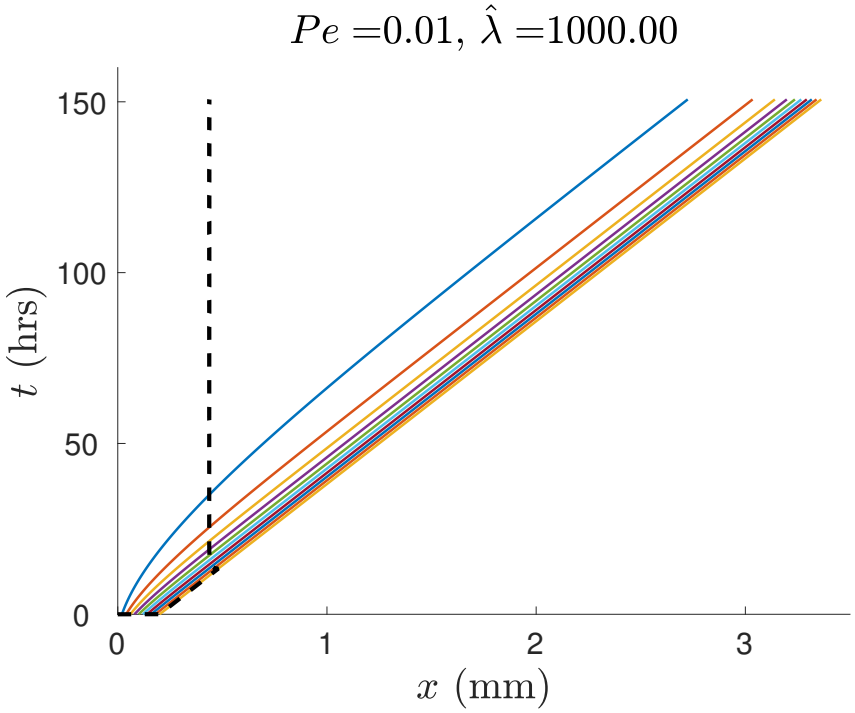

Figure 5.6: The pathlines for the incompressible model with parameters $Pe = 0.01$ and $\hat{\lambda} = 1000$. The pathlines have been plotted in terms of dimensional space and time. We expect the average trajectories of the cells in the cylindrical yeast colonies to behave similarly to these pathlines. The growth rate of the colony is 0.021 mmh^{-1} and the constant nutrient concentration at the base of the colony is 44.4 mM.

a result, a majority of the proliferation is occurring at the base of the colony. Although the cells at the top of the colony are replicative, cell proliferation is highly unlikely. This can be justified by observing the nutrient concentration at early times. Thus the pathlines at the the top of the colony appear to be approximately linear. After some time, the replicative region does eventually remain fixed and thus the colony grows linearly. Hence we dimensionalise the simulations illustrated in Figure 5.5 to approximate the non-uniform growth within the cylindrical yeast colonies.

Using the known values from Vulin et al. (2014) for a colony with diameter 1.5 mm, we can rescale to find results in dimensional form. The pathlines for the cylindrical yeast colonies in terms of dimensional units can be found in Figure 5.6.

From Figure 5.6, we observe that the nutrient cannot travel further than about 0.4 mm up the colony. Thus all of the proliferation is occurring within the first 0.4 mm of the colony, no matter how tall it grows. This is illustrated in Figure 5.7. The nutrient is also monotonically decreasing up the colony. Thus we expect more cell proliferation towards

the base of the colony. This can also be seen from Figure 5.6. The distances between adjacent pathlines are increasing at a higher rate towards the base of the colony. This is because more cells are proliferating between them and the initial cells are being pushed up the colony.

Figure 5.7 illustrates the evolution of the nutrient concentration in terms of dimensional quantities. The chosen time lapse images illustrate the evolution of the nutrient concentration after the size of the replicative region H has tended to a fixed value. We recall that H was determined using a tolerance of $\theta = 0.001$. In terms of a dimensional concentration, this tolerance is equivalent to $\theta = 0.044$ mM. Although the length of the colony is growing, we observe that the curve for nutrient concentration remains steady in the replicative region. This is an important result as it implies the cell proliferation rates across the colony will remain the same as time goes on.

Lastly, we consider the proliferation rate constant k. We recall that the advective timescale is given by $\hat{T}_{\text{adv}} = 1/kC_0$. As we have set $\hat{T}_{\text{adv}} = 3.014$ h and $C_0 = 44.4$ mM, we can calculate the proliferation rate constant to be $k = 0.0075$ $\text{m}^3\text{mol}^{-1}\text{h}^{-1}$. We wish to explore how this proliferation rate constant changes as the radius of the cylindrical yeast colony changes. It was shown by Vulin et al. (2014) that the growth rate of the colony is inversely proportional to the radius of the colony. Hence we know that

$$\gamma = \frac{A}{r}, \tag{5.46}$$

where γ is the linear growth rate of the colony, r is the radius of the colony and A is a proportionality constant. As the the nondimensional simulations for $Pe = 0.01$ & $\hat{\lambda} = 1000$ are growing at approximately 0.0633 mm per unit time, we note that the advective timescale will be given by

$$\hat{T}_{\text{adv}} \approx \frac{0.0633}{\gamma}. \tag{5.47}$$

Thus equating Equations (4.25a), (5.46) and (5.47), we find that

$$k = \frac{B}{rC_0}, \tag{5.48}$$

where B is a constant. As the proliferation rate is given by $R = k\rho C$, we observe that

$$R = \frac{B\rho C}{rC_0}, \tag{5.49}$$

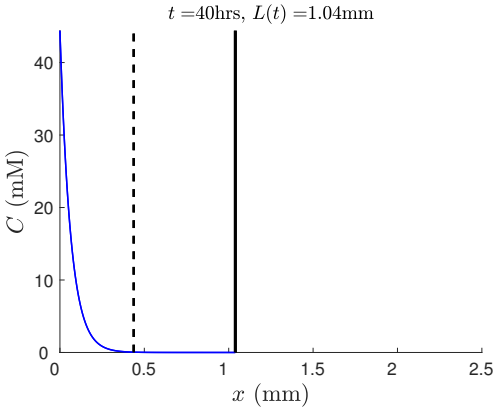

(a)

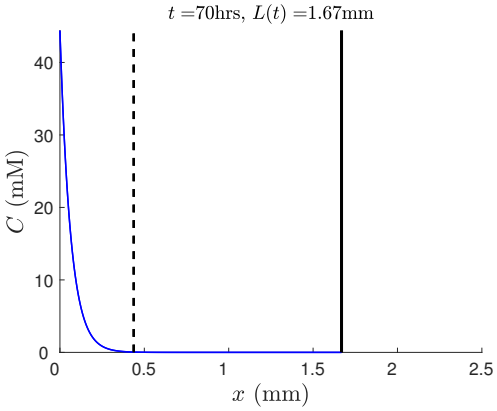

(b)

(c)

Figure 5.7: Plots of the numerical solution for the nutrient concentration C in terms of dimensional quantities. The dotted black line is the numerical approximation for the size of the replicative region H and the fixed black is the length of the colony L. The value of H is evaluated by determining where the nutrient concentration is less than $\theta = 0.044$ mM.

Thus the proliferation rate is also inversely proportional to the radius of the colony. This implies that the one-dimensional proliferation rate will be higher if the radius of the colony is smaller. Furthermore, this implies that the length of the colony will be growing faster if the radius of the colony is smaller. This matches the results found experimentally by Vulin et al. (2014).

5.4 Discussion

In this Chapter, we simulated numerical solutions to the incompressible model (5.6). We found that a replicative region of fixed length occurs when Pe is small and $\hat{\lambda}$ is large. Furthermore, we found that the numerically simulated colony growth is approximately linear when there is a fixed replicative region. This coincides the results from the CA model (Chapter 3).

Using parameters from Vulin et al. (2014), we were able to predict the growth within the cylindrical yeast colonies. For the case in which the colony diameter was 1.5 mm and constant nutrient at the base of the colony was 44.4 mM, we found that nutrient can only reach 0.4 mm up the colony. We note this value was calculated assuming cells cannot proliferate if local nutrient concentration is less than 0.44 mM. Future experiments could be conducted to determine the accuracy of these values for cylindrical yeast colonies.

The cylindrical yeast colonies are just one of the applications of the incompressible model. By altering the values of the nondimensional parameters, Pe and λ, we are able to simulate non-uniform growth in other incompressible systems. However, we recall that our full model, derived in Chapter 4, can also be applied to compressible systems. In Chapter 6, we assume that $\hat{\beta} \neq 0$ and consider methods of solving the full model (4.29) for compressible systems.

Chapter 6

Solutions to the Full Model

6.1 Solving the Compressible Model on a Growing Domain

We wish to find solutions to the full compressible model (4.29) derived in Chapter 3. Before solving this model, we wish to write the reaction–advection–diffusion equation (4.29b) in terms of pressure $P(\xi, T)$. We choose to do this as the boundary conditions (4.29k) are pressure conditions and the advective cell velocity is calculated using pressure (Equation (4.29d)). Substituting (4.29e) into (4.29b), we derive that

$$\frac{\partial P}{\partial T} + \left[\frac{u}{L} - \frac{\xi}{L}\frac{dL}{dT}\right]\frac{\partial P}{\partial \xi} = \frac{D}{Pe}\frac{1}{L^2}\frac{\partial^2 P}{\partial \xi^2} + \left[C - \frac{1}{L}\frac{\partial u}{\partial \xi}\right]P + \frac{1}{\hat{\beta}}\left[C - \frac{1}{L}\frac{\partial u}{\partial \xi}\right]. \tag{6.1}$$

We also note that the equations for the length of the colony and the pathlines can be written as

$$\frac{dL}{dt} = \left[u - \frac{D}{Pe}\frac{\hat{\beta}}{\rho L}\frac{\partial P}{\partial \xi}\right]\Bigg|_{\xi=1}, \tag{6.2}$$

$$\frac{dX}{dt} = \left[u - \frac{D}{Pe}\frac{\hat{\beta}}{\rho L}\frac{\partial P}{\partial \xi}\right]\Bigg|_{\xi=\Xi}. \tag{6.3}$$

Lastly, we chose to set the initial pressure to

$$P_I(\xi) = \frac{\varepsilon}{\hat{\beta}} \cos\left(\frac{\pi\xi}{2}\right), \tag{6.4}$$

where ε is a constant that is assumed to be small. This is equivalent to an initial cell density of

$$\rho_I(\xi) = 1 + \varepsilon \cos\left(\frac{\pi\xi}{2}\right). \tag{6.5}$$

We note that the initial condition for pressure will change as the parameter $\hat{\beta}$ changes. We impose this such that the initial density is the same for all values of $\hat{\beta}$. We may interpret this initial condition as a small perturbation of cell density at the base of the colony. This initial condition also implies that the pressure gradient is zero at the base of the colony and increasing in magnitude up the colony. We wish to numerically evaluate the coupled system

$$\frac{\partial C}{\partial T} + \underbrace{\left[\frac{u}{L} - \frac{\xi}{L}\frac{dL}{dT}\right]\frac{\partial C}{\partial \xi}}_{\text{Advection Term}} = \underbrace{\frac{1}{Pe}\frac{1}{L^2}\frac{\partial^2 C}{\partial \xi^2}}_{\text{Diffusion Term}} - \underbrace{\left[\hat{\lambda}\rho + \frac{1}{L}\frac{\partial u}{\partial \xi}\right]C}_{\text{Source Term}}, \tag{6.6a}$$

$$\frac{\partial P}{\partial T} + \underbrace{\left[\frac{u}{L} - \frac{\xi}{L}\frac{dL}{dT}\right]\frac{\partial P}{\partial \xi}}_{\text{Advection Term}} = \underbrace{\frac{D}{Pe}\frac{1}{L^2}\frac{\partial^2 P}{\partial \xi^2}}_{\text{Diffusion Term}} + \underbrace{\left[C - \frac{1}{L}\frac{\partial u}{\partial \xi}\right]P + \frac{1}{\hat{\beta}}\left[C - \frac{1}{L}\frac{\partial u}{\partial \xi}\right]}_{\text{Source Term}}, \tag{6.6b}$$

$$\frac{dL}{dt} = \left[u - \frac{D}{Pe}\frac{\hat{\beta}}{\rho L}\frac{\partial P}{\partial \xi}\right]\Bigg|_{\xi=1}, \tag{6.6c}$$

$$u = -\frac{1}{L}\frac{\partial P}{\partial \xi}, \tag{6.6d}$$

$$\rho = 1 + \hat{\beta}P, \tag{6.6e}$$

subject to the initial and boundary conditions

$$u|_{\xi=0} = 0, \tag{6.6f}$$

$$C|_{\xi=0} = C_0, \quad \left.\frac{\partial C}{\partial \xi}\right|_{\xi=1} = 0, \tag{6.6g}$$

$$C|_{T=0} = C_I(\xi) = \begin{cases} 1 & \text{if } \xi = 0, \\ 0 & \text{else,} \end{cases} \tag{6.6h}$$

$$L|_{T=0} = 1, \tag{6.6i}$$

$$P|_{T=0} = \frac{\varepsilon}{\hat{\beta}} \cos\left(\frac{\pi\xi}{2}\right), \tag{6.6j}$$

$$\left.\frac{dP}{d\xi}\right|_{\xi=0} = 0, \quad P|_{\xi=1} = 0. \tag{6.6k}$$

We again use an upwinding scheme for the advection terms in equations (6.6a) and (6.6b). We use an implicit Euler method for time stepping with Picard linearisation for the source terms. We use a forward Euler method to solve (6.6c) and (6.3). Lastly, we use a first order centred difference approximation to solve (6.6d). We solve the system (6.6) using Algorithm 4.

Algorithm 4: Numerical Scheme to find solutions for the Compressible system (6.6).

Set a fixed number of time steps as $\mathcal{T}$;
Initialise the nutrient concentration C_I;
Initialise the colony length L_0;
Initialise the pathlines X_I;
Initialise the pressure P_I;
Calculate the advective velocity u_I using P_I;
Calculate the cell density ρ_I;
for $i = 1$ **to** $\mathcal{T}$ **do**
    Calculate colony length at next iteration L_i, using u_{i-1} and P_{i-1};
    Calculate pathlines at next iteration X_i, using u_{i-1} and P_{i-1};
    Calculate nutrient concentration at next iteration C_i, using L_i, u_{i-1} and P_{i-1};
    Calculate pressure at next iteration P_i, using L_i, u_{i-1} and C_{i-1};
    Calculate advective velocity at next iteration u_i, using P_i;
    Calculate the cell density at the next iteration ρ_i, using P_i;
end

We notice one problem when simulating Algorithm 4 with the Picard linearisation in Equation (6.6b). When we are numerically evaluating Equation (6.6b), we use a difference equation of the form

$$\hat{\beta}\frac{P_j^{i+1}-P_j^i}{\Delta t}+\hat{\beta}\underbrace{(\dots)}_{\text{Advection Term}}=\hat{\beta}\underbrace{(\dots)}_{\text{Diffusion Term}}+\hat{\beta}\left[C_j^i-\frac{1}{L^i}\frac{\partial u_j^i}{\partial \xi}\right]P_j^{i+1}+\left[C_j^i-\frac{1}{L^i}\frac{\partial u_j^i}{\partial \xi}\right], \tag{6.7}$$

where j is a spatial index and i is a temporal index. We assume that the values for time with time index i are known and the values with time index $i+1$ need to be calculated. Hence the values for C_j^i, L^i and u_j^i are known for all j and thus can be interpreted in the difference equation (6.7) as constants. Suppose we take the incompressible limit $\hat{\beta} \to 0$. Hence (6.7) will simplify to

$$C_j^i-\frac{1}{L^i}\frac{\partial u_j^i}{\partial \xi}=0. \tag{6.8}$$

However, C_j^i, L^i and u_j^i are all known and thus (6.8) may not be satisfied. As a result, we see instabilities in the numerics if $\hat{\beta}$ is too small. Thus we must be careful when setting a small value for $\hat{\beta}$.

The compressible model has four nondimensional parameters that can vary. We have discussed the Pélet number and nondimensional nutrient consumption rate coefficient in Chapter 5. They will have a similar impact in the compressible model. The other two constants that don't appear in the incompressible model are the diffusion scale D and the nondimensional compressibility coefficient $\hat{\beta}$. As previously discussed, the limit $\hat{\beta} \to 0$ implies that the system is incompressible and thus the density is constant. Hence a large value of $\hat{\beta}$ implies that the system is more compressible. A small perturbation in pressure will result in a larger change in cell density as $\hat{\beta}$ increases. The diffusion scale is defined as the ratio between the diffusion of cells and diffusion of nutrient. Hence, for a small D, we expect the nutrient to diffuse throughout colony at a faster rate than cell diffusion. As a result, the nutrient concentration is expected to reach an equilibrium concentration before the cells diffuse. If D is large, the cells will diffuse throughout the colony before the nutrient has time to diffuse. However, a large D is physically implausible for yeast.

The first case we wish to explore is when D and $\hat{\beta}$ are both small. We set our parameters to $Pe = 0.01$, $\hat{\lambda} = 100$, $\hat{\beta} = 0.125$ and $D = 0.1$ to compare with results in Figure 5.4e. The numerical simulations of the pathlines are illustrated in figure (6.1). We compare this to the pathlines for the incompressible model for parameters $Pe = 0.01$ and $\hat{\lambda} = 100$, illustrated in Figure 5.4e. The pathlines are very similar and thus we can be confident that Algorithm 4 is sufficient for numerically simulating the compressible model (6.6).

We now wish to analyse the impact that changing the values of the parameters D and $\hat{\beta}$ has on the nutrient concentration, cell density, cell pathlines and length of the colony.

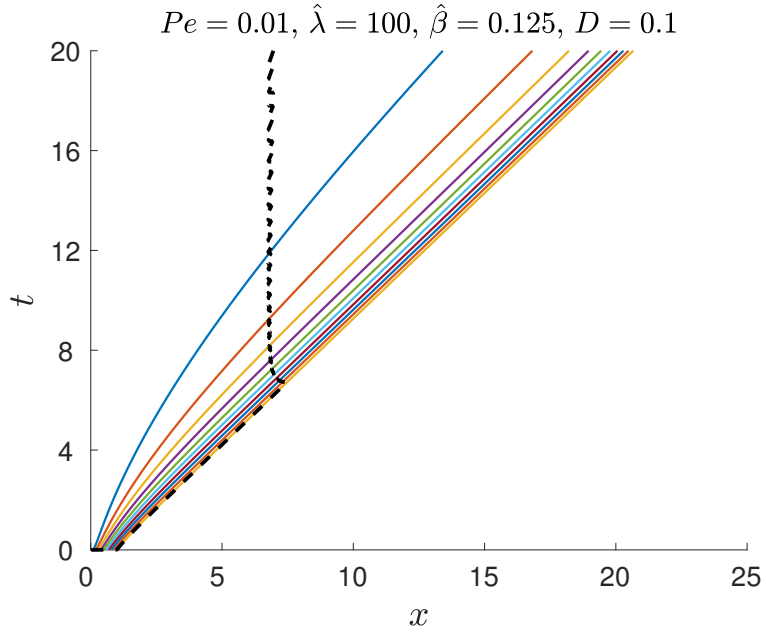

Figure 6.1: The pathlines for the compressible model with parameters $Pe = 0.01$, $\hat{\lambda} = 100$, $\hat{\beta} = 0.125$ and $D = 0.1$. The dotted line represents the size of the replicative region. We have also used a value of $\varepsilon = 1/16$ in the initial condition for pressure. A small value for $\hat{\beta}$ and D imply that the system should behave like the incompressible system where $Pe = 0.01$ and $\hat{\lambda} = 100$ (Figure 5.4e).

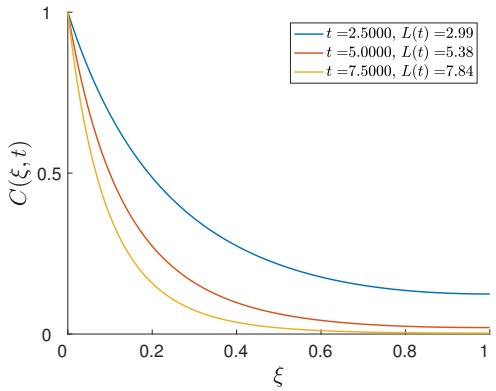

(a) Evolution of nutrient concentration for $\hat{\beta} = 1$ and $D = 0.1$.

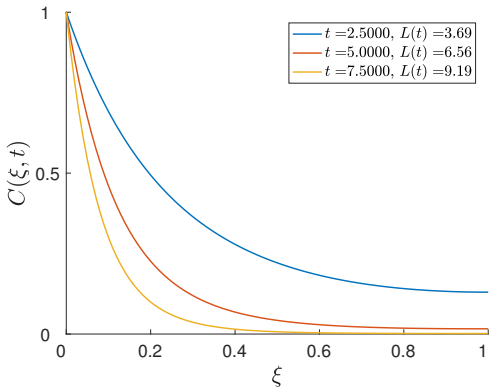

(b) Evolution of nutrient concentration for $\hat{\beta} = 100$ and $D = 10$.

Figure 6.2: Numerical solutions of the nutrient concentration for the incompressible case with $Pe = 1$, $\hat{\lambda} = 1$ and varying $\hat{\beta}$ and D. These solutions were simulated using Algorithm 3. We recall that the initial condition for the nutrient concentration is given in equation (4.29h).

We first wish to explore the impact on nutrient concentration. Figure 6.2 illustrates the evolution of the nutrient concentration for varying D and $\hat{\beta}$. Although the length is different at the same time points for the two parameter sets, we observe that the shape of the concentration curves are similar at the same point in time. Thus we conclude that varying the diffusion scale D and nondimensional compressibility $\hat{\beta}$ will have a negligible effect on the shape of the nutrient concentration. Hence we observe that this nutrient concentration curve is a good approximation for all cases in the compressible model where $Pe = 1$ and $\hat{\lambda} = 1$.

We now extend our analysis to the cell density within the colony. Figure 6.3 illustrates the evolution of the cell density for varying $\hat{\beta}$ and Figure 6.4 illustrates the evolution of the cell density for varying D. We observe that the cell density is growing at the base of the colony much quicker for a larger $\hat{\beta}$. For a large $\hat{\beta}$, a small perturbation in pressure will result in a large perturbation in cell density. However, when the $\hat{\beta}$ is small, a small perturbation in pressure also results in a small perturbation in cell density. The larger cell density for a larger $\hat{\beta}$ can be explained by considering the compressibility. A larger value for $\hat{\beta}$ implies that the compressibility of the system is larger. Hence more cells can be compressed closer together. As there is no flux of cells at the base of the colony, cells are more compressed towards the bottom of the colony and thus cell density is much higher.

We also observe that the length of the colony is shorter when the compressibility is larger. This also makes intuitive sense. When an incompressible cell proliferates, we recall that it will be pushed up the colony and thus increase the length of the colony. However, if the cells are compressible, the additional material created by proliferation can be partly accommodated by cell compression. Thus if $\hat{\beta}$ is larger, the cells will not move as far up the colony when proliferating. As a result, the cell density increases and the length of the colony grows at a slower rate.

We can also see from Figure 6.4 that the length grows faster when D is larger. A large value for D implies that the cell motility is large. Thus the cells are spreading quicker and the length is growing faster. We also observe from Figure 6.4 that the cell density is much higher for a smaller D. Furthermore, most of the cells are concentrated at the base of the colony. Observing the nutrient concentration in Figure 6.2, we expect a majority of the cell proliferation to occur at the base of the colony. When D is large, the newly birthed cells spread out through the colony. However, when D is small the newly birthed cells stay do not spread out as quickly. Hence, the cell density at the base of the colony increases.

Lastly, we compare the pathlines of the plots for varying $\hat{\beta}$ and D. These are plotted in Figure 6.5. We recall that the black dotted line is the numerical approximation for the size of the replicative region. Thus the cells to the left of the dotted line will be the replicative cells that can proliferate. A majority of the proliferation is occurring at the

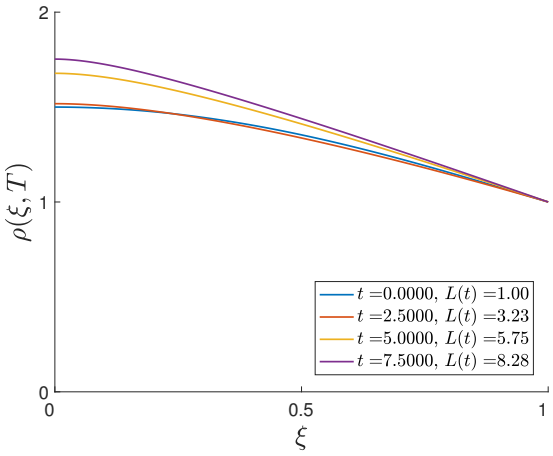

(a) Evolution of cell density for $\hat{\beta} = 1$.

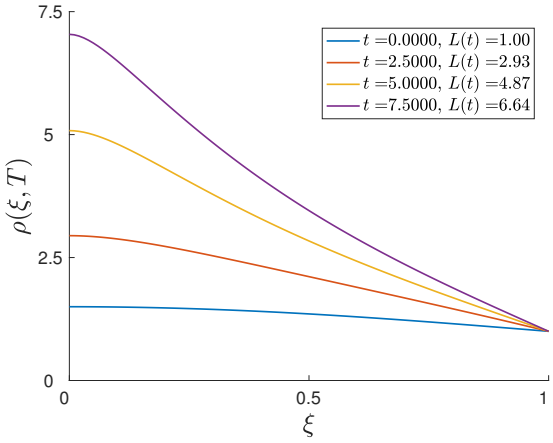

(b) Evolution of cell density for $\hat{\beta} = 100$.

Figure 6.3: Numerical solutions of the nutrient concentration for the incompressible case with $Pe = 1$, $\hat{\lambda} = 1$, $D = 1$ and varying $\hat{\beta}$. These solutions were simulated using Algorithm 4. We note the differing scales on the y-axes between the two figures.

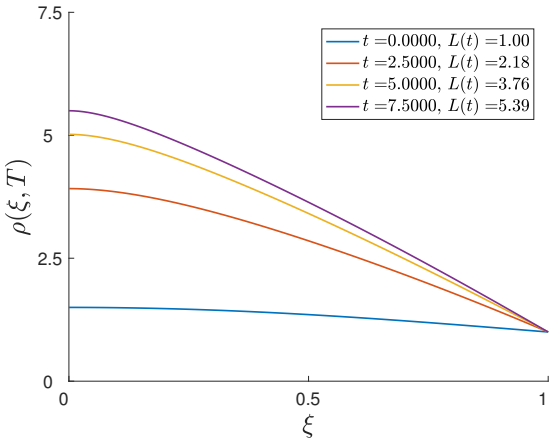

(a) Evolution of cell density for $D = 0.1$.

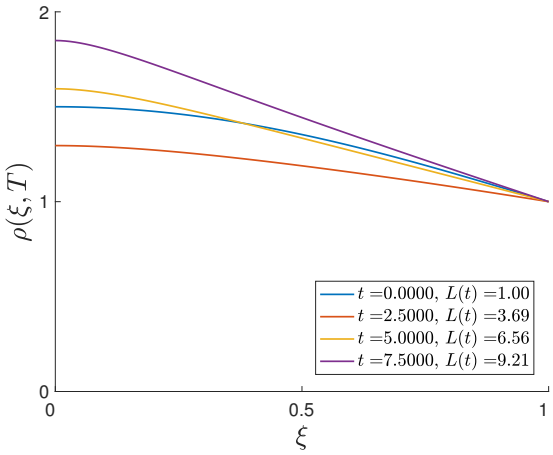

(b) Evolution of cell density for $D = 10$.

Figure 6.4: Numerical solutions of the nutrient concentration for the incompressible case with $Pe = 1$, $\hat{\lambda} = 1$, $\hat{\beta} = 10$ and varying D. These solutions were simulated using Algorithm 4. We note the differing scales on the y-axes between the two figures.

base of the colony and the initial cells are pushed up the colony. This is consistent with the incompressible case. However, we notice a difference for the quiescent region. For the incompressible model, the distances between adjacent initial cells would not increase or decrease in the quiescent region. This corresponds to the advective cell velocity being uniform across the quiescent region. However, due to compressibility, the distances between adjacent initial cells is not constant in the quiescent region.

This is due to a larger cell density and larger pressure at the base of the colony. As proliferation occurs at the base of the colony and the cell density increases, the pressure of the system at the base of the colony increases. However, the pressure at the top of the colony will always remain at zero. Thus the magnitude of the pressure gradient is increases up the colony and thus the advective cell velocity increasing up the colony. Hence the advective cell velocity is not uniform across the quiescent region. This is particularly noticeable when the compressibility is high ($\hat{\beta}$ is large).

We also wish to compare the size of the replicative region in the compressible model to the incompressible model. We recall from Figure 5.4 that the size of the replicative region is a fixed value as $t \to \infty$ for the incompressible case. For the compressible case, however, the size of the replicative region is not fixed but rather tending to a fixed value. This is again due to the compressibility of the system. As cells compress and the cell density increases at the base of the colony, the size of the replicative region gradually decreases. This is why the replicative region appears to tend to a smaller value when $\hat{\beta}$ is large.

6.2 Discussion

We have simulated numerical solutions to the full compressible model (4.21) derived in Chapter 4. We found that cell compressibility does not have a major effect on the nutrient concentration curve but does, however, have an effect on the length of the colony. If the cell compressibility is larger, then the length of the colony will be shorter. This is particularly noticeable when the diffusion scale D is small — as is the case for yeast.

Cell compressibility also affects the distances between initially adjacent cells. In the incompressible model, the distances between initially adjacent cells only increased if cells between them proliferated. However, cells can now move up or down the colony due to compression. As a result, we see distances between initially adjacent cells increasing in the quiescent region.

We note that we have assumed the proliferation rate function is given by $R(\rho, C) = k\rho C$ for the incompressible and compressible models. This function assumes a linear relationship between proliferation and nutrient concentration. Furthermore, it assumes a linear relationship between proliferation and cell density. We may wish to extend our model to consider other relationships between cell proliferation and cell density or nutrient

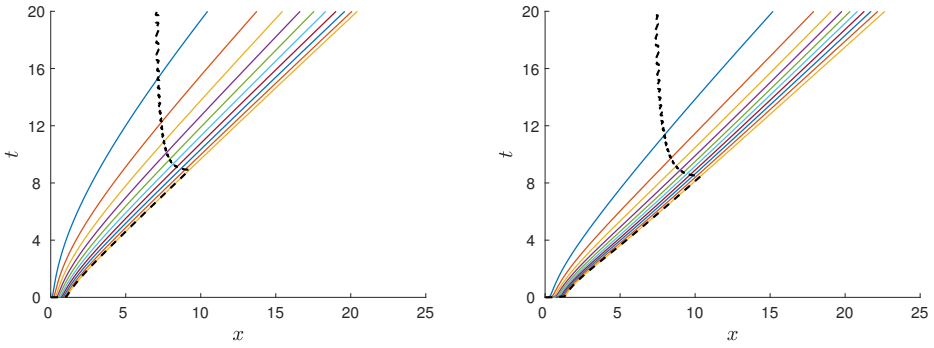

(a) $\hat{\beta} = 1$, $D = 0.1$

(b) $\hat{\beta} = 1$, $D = 10$

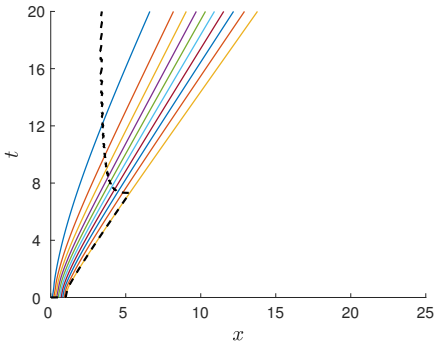

(c) $\hat{\beta} = 10$, $D = 0.1$

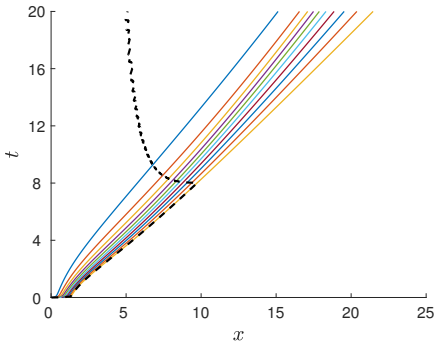

(d) $\hat{\beta} = 10$, $D = 10$

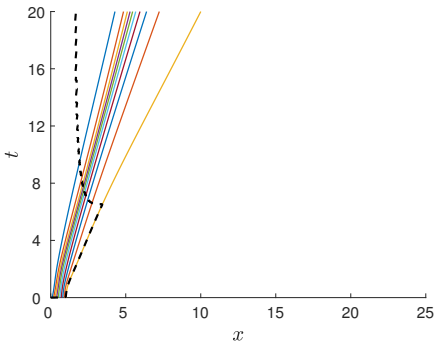

(e) $\hat{\beta} = 100$, $D = 0.1$

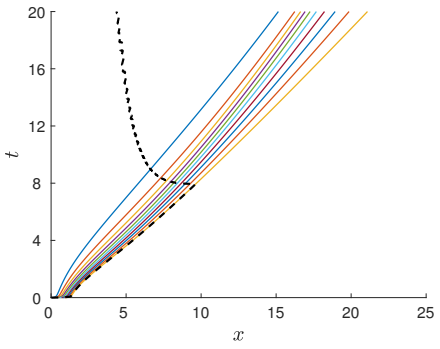

(f) $\hat{\beta} = 100$, $D = 10$

Figure 6.5: The pathlines $X(t)$ of the compressible system for varying $\hat{\beta}$ and D with fixed $Pe = 1$ and $\hat{\lambda} = 1$. These results were numerically simulated using Algorithm 4. We ran these simulations until $t = 20$ with a time step of 0.001 and spatial step 0.01. The dotted line in each plot illustrates the numerical approximation to the function $H(t)$. The cells to the left of the dotted line are replicative and the cells to the right of the dotted line are quiescent. The pathline plots do not capture the local cell density within the compressible colonies.

concentration. We can also extend the model by adding pressure dependence to the proliferation function.

We may also wish to use a different pressure law. A pressure law that has been previously used by Perthame et al. (2014) and Perthame & Vauchelet (2015) is

$$P = \frac{\gamma}{\gamma - 1}\rho^{\gamma-1}, \tag{6.9}$$

where γ is a constant relating to the compressibility of the system. The incompressible limit for this pressure law can be obtained by taking $\gamma \to \infty$. This choice is useful for porous media as it can be used to derive the porous media equation (Hecht & Vauchelet 2017). This, however, does not prevent the cells from overlapping like our selected pressure law. A pressure law that was used by Hecht & Vauchelet (2017) that does not allow for cells to overlap is

$$P = \beta\frac{\rho}{1 - \rho}, \tag{6.10}$$

where β is the compressibility. We may wish to extend our model to use one of these two pressure laws. We choose not to explore these pressure laws in this thesis for simplicity.

Chapter 7

Conclusion

We have developed and solved both a discrete and continuum model to describe and predict the mechanisms in cylindrical yeast growth. Furthermore, we have shown that the average behaviour of the probabilistic CA model matches the results found in the deterministic PDE model. These models were shown to coincide for both uniform and non-uniform growth.

The cylindrical yeast colonies were found to grow linearly and there were two observed cases in which the CA model exhibited linear growth. The first case was when the nutrient supply was depleting at a constant rate as the length of the colony increased. However, the cylindrical yeast colonies were grown with a constant flux of nutrient into an agar plate at the base of the colony. Thus, it is unlikely that the nutrient supply within the colony is depleting and so this scenario would not apply to the cylindrical yeast colonies.

The second case that exhibited linear growth was when only a fixed number of cells at the base of the colony were allowed to proliferate. This is a more appropriate assumption as it is expected that the nutrient can only reach a small distance up the colony. Thus the CA model suggests that there will be a replicative region at the base of the colony where all the cell proliferation occurs. We expect the size of the replicative region to be determined by the height that nutrient reaches up the colony. This will depend on the nutrient transport and consumption by the cells. However, these processes were not modelled explicitly in the CA

In order to address the coupling between nutrient transport, nutrient consumption and cell proliferation, we developed an alternative, PDE-based model. For the cylindrical yeast colonies, the system is assumed to be incompressible and thus cell density is constant. We also assume that nutrient diffusivity is low and the nutrient consumption rate in the yeast is high. The numerical simulations of the incompressible PDE model again showed that the colony growth was linear if there was a fixed replicative region at the base.

Furthermore, if there was not a fixed replicative region at the base of the colony then the colony growth was non-linear. Hence both our incompressible PDE model and CA model predict linear growth if there is a fixed replicative region at the base of the colony. Thus we conclude that the cylindrical yeast colonies grow linearly as the nutrient can only reach a fixed height, determined by nutrient diffusivity and nutrient consumption rate, within the colony.

It was also found in the PDE model that the nutrient concentration is monotonically decreasing within the replicative region. This matches the model originally considered by Vulin et al. (2014). As a result, a majority of the cell proliferation occurs at the base of the colony. Furthermore, the monotonically decreasing nutrient concentration implies that the cell proliferation rate is monotonically decreasing up the colony. This is what leads to non-uniform growth within the colony.

In Chapter 5, our model predicted that the size of the replicative region was approximately 0.4 mm when diameter of the colony was 1.5 mm, the inital height of the colony was 0.2 mm and the concentration at the base of the colony was 44.4 mM. A cylindrical yeast colony with these dimensions was grown by Vulin et al. (2014). The accuracy of this model could be tested experimentally by tracking the initial cells using fluorescent protein. Our model can also be used to predict the growth of cylindrical yeast colonies and the size of their replicative regions in future experiments.

In this thesis, we developed a new model that couples nutrient concentration and colony length. We created a model to explain the non-uniform growth in cylindrical yeast colonies. As yeast is a model organism for other eukaryotic cells, the model may be applied to other problems in cell biology, tumour biology, plant biology or genetics. This may include problems where cells are compressible. Hence we developed a generalised compressible model for one-dimensional non-uniform nutrient-driven growth. The model couples nutrient concentration, cell density, cell velocity and colony length and was developed to explore how cell compressibility affects nutrient driven-growth. The model depends on the Péclet number Pe, the nondimensional nutrient consumption rate $\hat{\lambda}$, the nondimensional compressibility $\hat{\beta}$ and the diffusion scale D. The long term distribution of the nutrient concentration depends on Pe and $\hat{\lambda}$ and the long term distribution of the cell density depends on D and $\hat{\beta}$. However, our numerical approximation was not stable for values of $\hat{\beta} \ll 1$. Future work is to be conducted to find a stable numerical solution for a wider range of parameter values.

We also wish to conduct future research to extend the model and find solutions for three spatial dimensions. We propose that the average behaviour will coincide with our one-dimensional model. However, we have not yet shown this. Lastly, we wish to extend the model to find solutions for different proliferation functions. We have assumed that proliferation is proportional to local cell density and local nutrient concentration. Future

work is to be conducted to explore non-linear relationships with cell density or nutrient concentration and relationships with mechanical pressure.

Appendix A

Alternative Framework for the Depleting Nutrient CA models

If we set $S = 1$ in our DCNCA model, we have a model where the expected number of proliferation events per time step is one. Suppose we create a framework for our DCNCA model where only one cell can proliferate per time step. We aim to derive continuum paths for the average trajectories of the initial cells using the new framework. Algorithm 5 provides an outline for the new framework of the DCNCA model.

We use the same proliferation rule and same definitions that we've used in all previous models. We recall that our previous DCNCA model with $S = 1$ allows for multiple cell proliferations in each time step. However, we impose the rule that one and only one cell must proliferate at each time step τ. Thus, we define a probability mass function (pmf) across the colony rather than defining individual proliferation probabilities. We recall that a pmf must sum to one. We still refer to the proliferation probability of the cell with index i at time time step τ as p_τ^i. However, we must now impose the condition that

$$\sum_{i=1}^{N_\tau} p_\tau^i = 1. \tag{A.1}$$

Furthermore, we can define a cumulative density function (cdf) F_τ^i defined by

$$F_\tau^i = \sum_{j=1}^{i} p_\tau^j. \tag{A.2}$$

We note that F_τ^i refers to the cumulative probability of the cell in position i at time step

τ. From the definition of a cdf, we note that $F_\tau^{N_\tau} = 1$, where N_τ is the number of cells in the colony at time step τ. We note that in the new framework, the time step τ is analogous to the number of cell proliferation events. This is because we impose that one and only one cell must proliferate in each time step.

We note that the pmf p_τ^i and cdf F_τ^i are discrete in space. However, we wish to derive a continuum path for the average trajectories of the initial cells. Thus we must use a continuous probability density function (pdf) and continuous cdf. Hence we must determine a continuous pdf and cdf that are analogous to p_τ^i and F_τ^i. Firstly, we recall our continuous variables x and t. We may use these continuous variables to define the pdf, $p(x;t)$ and cdf, $F(x;t)$. We note that the pdf and cdf are both defined of the domain $[0, L(t)]$. Hence they must satisfy the conditions

$$\int_0^{L(t)} p(x;t)\,dx = 1, \tag{A.3a}$$

$$F(x;t) = \int_0^x p(\tilde{x};t)\,d\tilde{x}. \tag{A.3b}$$

Thus we may link the discrete pmf to the continuous cdf by setting

$$p_\tau^i = F(i\Delta x;t) - F((i-1)\Delta x;t). \tag{A.4}$$

We may view Equation (A.4) as the process of discretising a continuous cdf. Lastly, we specify a method of obtaining the continuum paths for the average trajectories of the initial cells. We know that the displacement of a cell with continuum path $X^j(t)$ will depend on the proliferation probability to the left of it. Hence the rate of displacement will be equal to the cumulative proliferation probability. We note that the cumulative probability will be $F_\tau^{X^j/\Delta x}$. Hence, using Equation (A.4), we find that

$$F_\tau^{X^j/\Delta x} = \sum_{i=1}^{X^j/\Delta x} F(i\Delta x;t) - F((i-1)\Delta x;t) = F(X^j;t) - F(0;t) = \int_0^{X^j} p(\tilde{x};t)\,d\tilde{x}. \tag{A.5}$$

Hence the continuum paths for the average trajectories of the initial cells will be governed by

$$\frac{dX^j}{dt} = \int_0^{X^j} p(\tilde{x},t)\,d\tilde{x}. \tag{A.6}$$

Algorithm 5: Simulating One–Dimensional Growth with Cellular Automata using the new framework. We impose the rule that only one cell can proliferate per time step.

```
Set initial number of cells to N_0;
Initialise a fixed number of time steps as T;
for τ = 1 to T do
    Set pmf for cell proliferation;
    // used to determine which cell proliferates
    for i = 1 to N_{τ−1} do
        Determine which cell proliferates;
        Set j to be the proliferating cell;
        insert new cell at position j;
        if i ≥ j then
            Move cell i to position i + 1;
        end
    end
    Set N_τ = N_{τ+1} + 1 as the new total number of cells in the colony;
end
```

We wish to use a uniform distribution for the pdf $p(x,t)$. Hence

$$p(x,t) = \frac{1}{L(t)}. \tag{A.7}$$

This pdf satisifies the conditions outlined in A.3. Hence we substitute the pdf into Equation (A.6) to find that

$$\frac{dX^j}{dt} = \frac{X^j(t)}{L(t)}. \tag{A.8}$$

Similarly to previous models, we must first find the length to solve for general $X^j(t)$. We solve Equation (A.8) by substituting $X^{N_0}(t) = L(t)$. Thus we find that

$$L(t) = t + L_0, \tag{A.9}$$

where L_0 is the initial length of the colony. Hence (A.8) simplifies to

$$\frac{dX^j}{dt} = \frac{X^j(t)}{t + L_0}. \tag{A.10}$$

Thus we may solve (A.10) to find that the continuum paths for the average trajectories of the initial cells are

$$X^j(t) = \frac{X^j}{L_0}\left(t + X_0^j\right). \tag{A.11}$$

We note that the continuum paths (A.11) are equal to the continuum paths derived for the DCNCA model with $S = 1$. We also note that the differential equation (A.8) can be derived from the difference equation (3.34). We may rearrange (3.34) and divide by Δt to find that

$$\frac{X_{\tau+1}^j - X_\tau^j}{\Delta t} = S\frac{\Delta x}{\Delta t}\frac{X_\tau^j}{L_\tau}. \tag{A.12}$$

We recall that $t = \tau\Delta t$ and

$$\hat{S} = \lim_{\substack{\Delta x\to 0\\ \Delta t\to 0}} S\frac{\Delta x}{\Delta t}. \tag{A.13}$$

We also note that

$$\frac{dX^j}{dt} = \lim_{\Delta t\to 0}\frac{X_{\tau+1}^j - X_\tau^j}{\Delta t}. \tag{A.14}$$

Thus we take the continuum limit as $\Delta t \to 0$ and $\Delta x \to 0$ of (A.12) to find that

$$\frac{dX^j}{dt} = \hat{S}\frac{X^j(t)}{L(t)}. \tag{A.15}$$

Lastly, we note that $\hat{S} = 1$ and hence we have derived Equation (A.8). Thus we have confirmed that the two different methodolgies for producing the model yield similar results. We also wish to use our alternative framework for the DLNCA model. We now use Algorithm 5 to simulate growth. However, as we are assuming a linearly decreasing nutrient concentration, we cannot use the uniform distribution to simulate growth. Instead we use a triangular distribution. In particular, a triangular distribution with its peak at the base of the colony. This is equivalent to a linearly decreasing function. The pdf and cdf for this triangular distribution will be, respectively,

$$p(x,t) = \frac{2\left(L(t)-x\right)}{L^2(t)}, \tag{A.16a}$$

$$F(x,t) = 1 - \frac{\left(L(t)-x\right)^2}{L^2(t)}. \tag{A.16b}$$

Recalling the alternative framework for the uniform case, we can use (A.6) to find the continuum paths for the average trajectories of the initial cells. Substituting (A.16a) into (A.6), we find that

$$\frac{dX^j}{dt} = \frac{2X^j}{L} - \frac{\left(X^j\right)^2}{L^2}. \tag{A.17}$$

Suppose we compare the ODE (A.17) with our ODE for the continuum paths for the DLNCA model (3.103). We recall that

$$L(t) = L_0 + L_0\hat{p}_0^{\text{ave}}t, \tag{A.18}$$

for the DLNCA model and that

$$\hat{S} = \lim_{\substack{\Delta t\to 0\\ \Delta x\to 0}} \frac{\Delta x S}{\Delta t} = L_0\hat{p}_0^{\text{ave}}. \tag{A.19}$$

Thus the ODE (3.103) simplifies to

$$\frac{dX^j}{dt} = \frac{2\hat{S}X^j}{L} - \hat{S}\frac{\left(X^j\right)^2}{L^2}. \tag{A.20}$$

Hence if we set $\hat{S} = 1$ in the DLNCA model, we can derive the ODE (A.17). Hence, similarly to the uniform case, our alternative framework is equivalent to the DLNCA model with $\hat{S} = 1$.

We also consider how our CA model compares to previous one–dimensional non–uniform cellular automata. Lai De Oliveira & Binder (2019) also ran simulations of a CA model similar to Algorithm 5. The pdf used was also linearly decreasing. However, we note that they used a combinatorial approach to find an approximation for the average trajectories. We observe that both the combinatorial formulation and our formulation yield similar and accurate results when approximating the average trajectories of the initial cells. Lastly, we observe that Lai De Oliveira & Binder (2019) has re–scaled time to yield exponential

growth. Thus the combinatorial approach can also yield solutions similar to the LNCA model. We note that we have derived closed form approximations for the continuum paths of the average trajectories to support the combinatorial formulation. This closed form approximation can also be used for further analysis.

We can also extend this alternative framework to explore non–uniform growth from a generalised triangular distribution. The genral triangular distribution again corresponds to a linear nutrient concentration. However, this general distribution also allows for linearly increasing nutrient concentrations. A generalised triangular distribution has pdf

$$p(x) = \begin{cases} 0 & \text{if } x < a; \\ \frac{2(x-a)}{(b-a)(c-a)} & \text{if } a \leq x \leq c; \\ \frac{2(b-x)}{(b-a)(b-c)} & \text{if } c < x \leq b; \\ 0 & \text{if } x > b; \end{cases} \tag{A.21}$$

where a and b are the end points and c peak of the distribution. We may also view c as the x-value at which the probability is maximised. Previously, we have used endpoints $a = 0$ and $b = L(t)$ as this is the domain of the colony. We have also used $c = 0$ as this is where nutrient concentration, and hence proliferation probability, is maximised. In our extension, we assume the endpoints are the same but consider the case where the proliferation probability is not maximised at $c = 0$. Suppose we set $c = \alpha L(t)$, where α is some scale between 0 and 1. Thus the pdf will become

$$p(x,t) = \begin{cases} 0 & \text{if } x < 0; \\ \frac{2x}{\alpha L^2(t)} & \text{if } 0 \leq x \leq \alpha L(t); \\ \frac{2(L(t)-x)}{(1-\alpha)L^2(t)} & \text{if } \alpha L(t) < x \leq L(t); \\ 0 & \text{if } x > L(t). \end{cases} \tag{A.22}$$

Examples of the pdfs of triangular distributions with different values of α are illustrated in Figure A.1. We may substitute (A.22) into the equation (A.6) to derive the ODEs for the continuum paths

$$\frac{dX^j}{dt} = \begin{cases} \frac{\left(X^j(t)\right)^2}{\alpha L^2(t)} & \text{if } 0 < X^j(t) \leq \alpha L(t), \\ \frac{\left(X^j(t)\right)^2}{(\alpha-1)L^2(t)} - \frac{2X^j(t)}{(\alpha-1)L(t)} + \frac{\alpha}{\alpha-1} & \text{if } \alpha L(t) < X^j(t) \leq L(t). \end{cases} \tag{A.23}$$

We first solve for the length by substituting $X^{N_0}(t) = L(t)$. Thus we find that

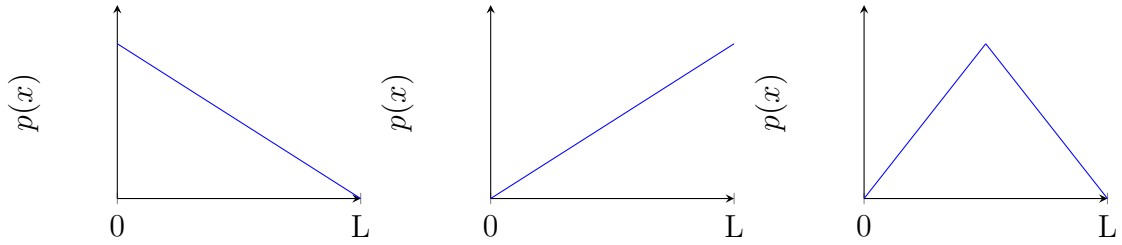

(a) $\alpha = 0$ (b) $\alpha = 1$ (c) $\alpha = 0.5$

Figure A.1: Illustrations of the the pdf of the triangular distribution, as defined in Equation (A.22), with different peaks. The peak of the pdf corresponds to the point in the colony where the nutrient concentration is maximised. The maximum nutrient concentration will correspond to the location of the nutrient source. This may be at the beginning, end or somewhere in the middle of the colony.

$$L(t) = t + L_0. \tag{A.24}$$

Thus we have

$$\frac{dX^j}{dt} = \begin{cases} \frac{\left(X^j(t)\right)^2}{\alpha(t+L_0)^2} & \text{if } 0 < X^j(t) \leq \alpha L(t), \\ \frac{\left(X^j(t)\right)^2}{(\alpha-1)(t+L_0)^2} - \frac{2X^j(t)}{(\alpha-1)(t+L_0)} + \frac{\alpha}{\alpha-1} & \text{if } \alpha L(t) < X^j(t) \leq L(t). \end{cases} \tag{A.25}$$

Hence we can solve (A.25) to find the continuum paths for the average trajectories of the initial cells to be

$$X^j(t) = \begin{cases} \frac{\alpha(t+L_0)}{1+\left(\frac{\alpha}{X_0^j}-\frac{1}{L_0}\right)(t+L_0)}, & \text{if } 0 < X^j(t) \leq \alpha L(t), \\ \left(\frac{1}{(\alpha-1)(t+L_0)} + \frac{1}{X_0^j - L_0} - \frac{1}{(\alpha-1)L_0}\right)^{-1} + t + L_0, & \text{if } \alpha L(t), < X^j(t) \leq L(t). \end{cases} \tag{A.26}$$

This is a particularly interesting extension as we have still made the linear assumption for nutrient concentration and can still write a closed form solution for the continuum paths for the average trajectories of the initial cells. We wish to explore the applications of this model. In previous models we have assumed that the nutrient source is at the base of colony. This corresponds to $\alpha = 0$ as the nutrient concentration will be maximised at $x = 0$. If the nutrient source was at the top of the colony, we would have $\alpha = 1$. We may even have a case where the nutrient source in somewhere in the middle of the

colony. Thus we would set $0 < \alpha < 1$ as appropriate. If the nutrient source is always at the halfway point of the colony, then we would set $\alpha = 0.5$. Lastly, we may even wish to model a situation where the the nutrient source is moving throughout the colony. Thus we may generalise and set $\alpha = \alpha(t)$ where $0 \leq \alpha(t) \leq 1$. We may also wish to extend the model to analyse non-linear nutrient concentrations. Lai De Oliveira & Binder (2019) previously used a binomial distribution for proliferative growth and our formulation can derive continuum paths for that case. Furthermore, any valid pdf can be substituted into Equation (A.6). Thus we can derive an ODE for the continuum path for any pdf we choose. Hence we should be able to find a numerical solution for the continuum paths for the average trajectories of the initial cells for any chosen nutrient concentration.

Bibliography

Alber, M., Chen, N., Glimm, T. & Lushnikov, P. (2006), 'Multiscale dynamics of biological cells with chemotactic interactions: From a discrete stochastic model to a continuous description', *Phys. Rev. E* **73**, 051901.

Baker, R., Yates, C. & Erban, R. (2010), 'From microscopic to macroscopic descriptions of cell migration on growing domains', *Bulletin of Mathematical Biology* **72**(3), 719–762.

Binder, B. J. & Landman, K. A. (2009*a*), 'Exclusion Processes on a Growing Domain', *Journal of Theoretical Biology* **259**, 541–551.

Binder, B. J. & Landman, K. A. (2009*b*), 'Tissue Growth and the Polya Distribution', *Australasian Journal of Engineering Education* **15**, 35–42.

Binder, B. J., Landman, K. A., Simpson, M. J., Mariani, M. & Newgreen, D. F. (2008), 'Modeling proliferative tissue growth: A general approach and an avian case study ', *Physical Review E* **78**(031912).

Botstein, D.and Fink, G. (2011), 'Yeast: An experimental organism for 21st century biology', *Genetics* **189**(3), 695–704.

Britton, N. F. (2003), *Essential Mathematical Biology*, Springer-Verlag London Limited.

Byrne, H. & Chaplain, M. (1995), 'Growth of nonnerotic tutors in the presence and absence of inhibitors', *Math. Biosci.* **130**, 151–181.

Byrne, H. M. & Chaplain, M. A. J. (1997), 'Free boundary value problems associated with the growth and development of multicellular spheroids', *European Journal of Applied Mathematics* **8**(6), 639–658.

Chaplain, M. (1996), 'Avascular growth, angiogenesis and vascular growth in solid tumours: The mathematical modelling of the stages of tumour development', *Mathematical and Computer Modelling* **23**, 47–87.

Chaplain, M., Ganesh, M. & Graham, I. (2001), 'Spatio-temporal pattern formation on spherical surfaces: numerical simulation and application to solid tumour growth', *Journal of Mathematical Biology* **42**(5), 387–423.

Chen, L., Noorbakhsh, J., Adams, R., Samaniego-Evans, J., Agollah, G., Nevozhay, D., Kuzdzal-Fick, J., Mehta, P. & Balazsi, G. (2014), 'Two-dimensionality of yeast colony expansion accompanied by pattern formation', *PLOS Computational Biology* **10**(12), 1–14.

Codling, E., Plank, M. & Benhamou, S. (2008), 'Random walk models in biology', *Royal Society Interface* **5**(25), 813–834.

Crampin, E. J., Gaffney, E. A. & Maini, P. K. (1999), 'Reaction and Diffusion on Growing Domains: Scenarios for Robust Pattern Formation', *Bulletin of Mathematical Biology* **61**, 1093–1120.

Crampin, E. J., Hackborn, W. W. & Maini, P. K. (2002), 'Pattern Formation in Reaction–Diffusion Models with Nonuniform Domain Growth', *Bulletin of Mathematical Biology* **64**, 747–769.

Crank, J. (1984), *Free and Moving Boundary Problems*, 1st edn, Oxford University Press.

Czarnecki, J. S., Jolivet, S., Blackmore, M. E., Lafdi, K. & Tsonis, P. A. (2014), 'Cellular Automata Simulation of Osteoblast Growth on Microfibrous-Carbon-Based Scaffolds', *Tissue Engineering Part A* **20**(23-24), 3176–3188.

Davies, K. (2016), On the derivation and application of closure approximations of cellular automata models, PhD thesis, School of Mathematical Sciences, The University of Adelaide.

Davies, K. J., Green, J. E. F., Bean, N. G., Binder, B. J. & Ross, J. V. (2014), 'On the Derivation of Approximations to Cellular automata models and the assumption of independence', *Mathematical Biosciences* **253**, 63–71.

Deroulers, C., Aubert, M., Badoual, M. & Grammaticos, B. (2009), 'Modeling tumor cell migration: From microscopic to macroscopic models', *Phys. Rev. E* **79**, 031917.

Di Talia, S. & Poss, K. D. (2016), 'Monitoring tissue regeneration at single-cell resolution', *Cell Stem Cell* **19**, 428–431.

Hecht, S. & Vauchelet, N. (2017), 'Incompressible limit of a mechanical model for tissue growth with non-overlapping constraint', *Communications in mathematical sciences* **15**(7), 1913–1932.

Horstmann, D. (2003), 'From 1970 until present : the Keller-Segel model in chemotaxis and its consequences I.', *Jahresbericht der Deutschen Mathematiker-Vereinigung* **105**(3), 103–165.

Hywood, J., Hackett-Jones, E. & Landman, K. (2013), 'Modeling biological tissue growth: Discrete to continuum representations', *Phys. Rev. E* **88**, 032704.

K. Maini, P., J. Painter, K. & Nguyen Phong Chau, H. (1997), 'Spatial pattern formation in chemical and biological systems', *J. Chem. Soc., Faraday Trans.* **93**, 3601–3610.

Kansal, A., Torquato, S., Harsh IV, G., Chiocca, E. & Deisboeck, T. (2000), 'Cellular automaton of idealized brain tumor growth dynamics', *Biosystems* **55**(1–3), 119–127.

Keller, E. & Segel, L. (1970), 'Initiation of slime mold aggregation viewed as an instability', *Journal of Theoretical Biology* **26**, 399–415.

Kondo, S. & Asai, R. (n.d.), 'A reaction–diffusion wave on the skin of the marine angelfish pomacanthus', *Nature* (6543), 765–768.

Lai De Oliveira, A. & Binder, B. J. (2019), 'Modeling uniaxial nonuniform cell proliferation', *Bulletin of Mathematical Biology* **81**(7), 2220–2238.

Matsuura, S. (2000), 'Random Growth of Fungal Colony Model on Diffusive and Non-Diffusive Media', *Forma* **15**, 309–319.

McGillen, J. B., Gaffney, E. A., Martin, N. K. & Maini, P. K. (2014), 'A general reaction–diffusion model of acidity in cancer invasion', *Journal of Mathematical Biology* **68**(5), 1199–1224.

Minarikova, L., Kuthan, M., Ricicova, M., Forstova, J. & Palkova, Z. (2001), 'Differentiated gene expression in cells within yeast colonies', *Experimental Cell Research* **271**(2), 296–304.

Monteagudo, A. & Santos, J. (2015), 'Treatment Analysis in a Cancer Stem Cell Context Using a Tumour Growth model Based on Cellular Automata', *PLOS ONE* **10**(7), e0132306.

Moore-Landecker, E. (1996), *Fundamentals of the fungi*, Prentice Hall.

Mulesa, P., Cruywagen, G., Lubkin, S., Maini, P., Ferguson, M. & Murray, J. (1996), 'On a model mechanism for the spatial patterning of teeth primordia in the alligator', *Journal of Theoretical Biology* **180**, 287–296.

Murray, J. (2003), *Mathematical Biology*, 3rd edn, Springer.

Neville, A. A., Matthews, P. C. & Byrne, H. M. (2006), 'Interaction between Pattern Formation and Domain Growth', *Bulletin of Mathematical Biology* **68**, 1975–2003.

Nguyen, B., Upadhyaya, A., van Oudenaarden, A. & Brenner, M. (2004), 'Elastic instability in growing yeast colonies', *Biophysical Journal* **86**(5), 2740–2747.

Painter, K. (2009), 'Continuous models for cell migration in tissues and applications to cell sorting via differential chemotaxis', *Bulletin of Mathematical Biology* **71**(5), 1117.

Painter, K. J., Maini, P. K. & Othmer, H. G. (1999), 'Stripe formation in juvenile pomacanthus explained by a generalized turing mechanism with chemotaxis', **96**(10), 5549–5554.

Palkova, Z. (2004), 'Multicellular microorganisms: laboratory versus nature', *EMBO Rep* **5**(5), 470–476.

Penington, C., Hughes, B. & Landman, K. (2011), 'Building macroscale models from microscale probabilistic models: A general probabilistic approach for nonlinear diffusion and multispecies phenomena', *Phys. Rev. E* **84**, 041120.

Perthame, B., Quirós, F. & Vázquez, J. (2014), 'The hele–shaw asymptotics for mechanical models of tumor growth', *Archive for Rational Mechanics and Analysis* **212**(1), 93–127.

Perthame, B. & Vauchelet, N. (2015), 'Incompressible limit of a mechanical model of tumour growth with viscosity', *Phil. Trans. R. Soc. A* **373**.

Pirt, S. (1967), 'A kinetic study of the mode of growth of surface colonies of bacteria and fungi', *J. Gen. Microbio.* **47**(2), 181–197.

Priest, F., Stewart, G. & Hardwick, W. (2006), *Handbook of brewing*, 2nd ed. edn, CRC/Taylor & Francis, Boca Raton.

Reynolds, T. & Fink, G. (2001), 'Bakers' yeast, a model for fungal biofilm formation', *Science* **291**(5505), 878–881.

Reynolds, T., Jansen, A., Peng, X. & Fink, G. (2008), 'Mat formation in saccharomyces cerevisiae requires nutrient and ph gradients', *Eukaryotic Cell* **7**(1), 122–130.

Rosa, C. & Peter, G. (2006), *Biodiversity and Ecophysiology of Yeasts*, Springer.

Ross, J. & Binder, B. (2014), 'Approximating spatially exclusive invasion processes', *Phys. Rev. E* **89**, 052709.

Ross, R., Baker, R. & Yates, C. (2016), 'How domain growth is implemented determines the long-term behavior of a cell population through its effect on spatial correlations', *Phys. Rev. E* **94**, 012408.

Ross, R., Yates, C. & Baker, R. (2015), 'Inference of cell?cell interactions from population density characteristics and cell trajectories on static and growing domains', *Mathematical Biosciences* **264**, 108–118.

Simpson, M. J. (2015), 'Exact Solutions of Linear Reaction–Diffusion Processes on a Uniformly Growing Domain: Criteria for Successful Colonization', *PLoS ONE* **10**(2), e0117949.

Tam, A. (2019), Mathematical Modelling of Pattern Formation in Yeast Biofilms, PhD thesis, School of Mathematical Sciences, The University of Adelaide.

Tam, A., Green, E., Balasuriya, S., Tek, E., Gardner, J., Sundstrom, J., Jiranek, V. & Binder, B. (2018), 'Nutrient-limited growth with non-linear cell diffusion as a mechanism for floral pattern formation in yeast biofilms', *Journal of Theoretical Biology* **448**, 122–141.

Teoh, A., Heard, G. & Cox, J. (2004), 'Yeast ecology of kombucha fermentation', *International Journal of Food Microbiology* **95**(2), 119–126.

Tronnolone, H., Gardner, J. M., Sundstrom, J. F., Jiranek, V., Oliver, S. G. & Binder, B. J. (2017), 'Quantifying the dominant growth of mechanisms of dimorphic yeast using a lattice–based model', *J. R. Soc. Interface* **14**, 20170314.

Turing, A. M. (1952), 'The Chemical Basis of Morphogenesis', *Phil. Trans. Roy. Soc. Lond.* **237**(641), 37–72.

Turner, S., Sherratt, J., Painter, K. & Savill, N. (2004), 'From a discrete to a continuous model of biological cell movement', *Phys. Rev. E* **69**, 021910.

Vachova, L., Chernyavskiy, O., Strachotova, D., Bianchini, P., Burdikova, Z., Fercikova, L., Kubinova, L. & Palkova, Z. (2009), 'Architecture of developing multicellular yeast colony: spatio?temporal expression of ato1p ammonium exporter', *Environmental Microbiology* **11**(7), 1866–1877.

Varea, C., Aragón, J. L. & Barrio, R. A. (1997), 'Confined turing patterns in growing systems', *Phys. Rev. E* **56**, 1250–1253.

Vittadello, S. T., McCue, S. W., Gunasingh, G., Haass, N. K. & Simpson, M. J. (2019), 'Mathematical models incorporating a multi-stage cell cycle replicate normally–hidden inherent synchronisation in cell proliferation', *J. R. Soc. Interface* .

Vulin, C., Di Meglio, J., Lidner, A. B., Daerr, A., Murray, A. & Hersen, P. (2014), 'Growing Yeast into Cylindrical Colonies', *Biophysical Journal* **106**(10), 2214–2221.

Ward, J. P. & King, J. R. (1997), 'Mathematical modelling of avascular-tumour growth', *IMA Journal of Mathematics Applied in Medicine and Biology* **14**, 39–69.

Ward, J. P. & King, J. R. (1999), 'Mathematical modelling of avascular-tumour growth II: Modelling growth saturation', *Mathematical Medicine and Biology: A Journal of the IMA* **16**(2), 171–211.

Williams, N. (1996), 'Yeast genome sequence ferments new research', *Science* **272**(5261), 481–481.

Yates, C. (2014), 'Discrete and continuous models for tissue growth and shrinkage', *Journal of Theoretical Biology* **350**, 37–48.

Yates, C., Baker, R., Erban, R. & Maini, P. (2012), 'Going from microscopic to macroscopic on nonuniform growing domains', *Phys. Rev. E* **86**, 021921.

Yates, C., Parker, A. & Baker, R. (2015), 'Incorporating pushing in exclusion-process models of cell migration', *Phys. Rev. E* **91**, 052711.

Youk, H. & van Oudenaarden, A. (2009), 'Growth landscape formed by perception and import of glucose in yeast', *Nature* **462**(7275), 875–879.

Zimmer, M. (2002), 'Green fluorescent protein (gfp): Applications, structure, and related photophysical behaviour', *Chem. Rev.* **102**, 759–782.